



POLITECNICO
MILANO 1863

POLITECNICO DI MILANO

School of Industrial and Information Engineering
Department of Mechanical Engineering

LOADS IDENTIFICATION, DESIGN OPTIMIZATION AND METAL ADDITIVE
MANUFACTURING OF A SAILBOAT PROPELLER'S BLADE

Master Thesis of:
Kakarlapudi V Venkata Satya Surya Nagendra Varma

Supervisor: Prof. Mario Guagliano
Co-supervisor's: Marco Preziosa
Gianluigi Rossi

Academic Year 2019/2020



Abstract

A novel Bound Metal DepositionTM (BMDTM) technology was introduced by Desktop MetalTM which offers an innovative way of manufacturing metal parts. This technology was introduced into the Italian market by Additive Italia Srl (Add-it), which started exploiting DMTM prototype technology, Studio System^{+TM}, for low volume and customized productions in 2019.

This thesis discusses the optimization of a sailboat propeller blade and production feasibility in 316L and 17-4PH stainless steels by using the BMDTM technology.

In this thesis work, the loads acting on the blade are identified with a CFD analysis by using Ansys Fluent. The mass was reduced by creating an internal TPMS diamond lattice structure with nTopology software and then structural rigidity was verified.

The optimization was performed considering the future possible high-volume production by using Binder Jetting technology from DMTM

The optimized blade was produced by BMDTM technology in two different versions with different printing parameters. After sintering cracks are observed on both versions of the blade.

Further parameters optimization should be investigated in future.

Key Words

- Additive Manufacturing
- Bound Metal Deposition™
- CFD analysis
- FEM analysis
- Sailboat propeller's blade
- Stainless Steel
- 3Dprinting

Acknowledgment

I would like to express my special thanks of gratitude to my professor *Mario Guagliano* as well as *Marco Preziosa* who gave me the golden opportunity to do this wonderful thesis on the topic of Loads identification, design Optimization and produced by Additive Manufacturing of an Marine Propeller's Blade which also helped me in doing a lot of Research and I came to know about so many new things I am really thankful to them. Especially I would also like to thank *Gianluigi Rossi* who helped and guided me in this thesis research.

Secondly, I would also like to thank nTopology Inc. for providing software for this thesis work and *S. Moroni*, friends and others who helped me regarding this thesis project.

Contents

Chapter1 Ship Propeller	1
1.1 Introduction:.....	1
1.2 History:	1
1.3 How does a ship propeller work?.....	5
1.4 How does a ship propeller look like?.....	5
1.4.1 Propeller Hub or Boss:.....	5
1.4.2 Propeller Blades:.....	6
1.5 Types of Propeller:.....	7
1.5.1 Classification by Number of Blades Attached:.....	7
1.5.2 Classification By pitch of the blade:	7
1.6 Materials:	8
1.7 Manufacturing of Propeller:.....	8
Chapter2 Additive Manufacturing	10
2.1 Introduction:.....	10
2.2 History of Additive Manufacturing:	10
2.3 Production of 3d object by Additive Manufacturing:	11
2.3.1 3D CAD Model:.....	12
2.3.2 Feed Material:	13
2.3.3 Different types of 3D Printer technologies:	13
Chapter3 Technology Using in Add-It.....	29
3.1 Introduction:.....	29
3.2 3D printer:.....	29
3.3 Debinder:.....	32
3.4 Furnace:.....	34
3.5 BMD™ guidelines:	36
Chapter4 Computational fluid dynamics (CFD).....	42
4.1 Introduction.....	42
4.2 Conservation laws.....	42
4.2.1 Mass conversion in three dimensional:	43
4.2.2 Momentum equation in three dimensional:.....	44
4.3 Navier-Stokes equations for a Newtonian fluid.....	45
4.4 Discretization.....	47
4.4.1 Finite Volume Method:.....	48
4.5 Mesh Quality:.....	49

4.5.1 Cell aspect ratio:.....	49
4.5.2 Skewness:.....	49
4.5.3 Mesh orthogonality:	50
Chapter5 Analysis of the component -Propeller blade	51
5.1 Introduction.....	51
5.2 Identifications of loads subjected by 17” propeller’s blade (CFD analysis):.....	51
5.2.1 Analysis at propeller-speed:1300rpm ,20deg blade orientation.....	52
5.2.1.1.5 Numerical Solution:	60
5.2.2 At 18 deg Blade orientation with different propeller speed:.....	69
5.3 Static analysis of blade:	69
5.3.1 Setup and Analysis:.....	70
5.3.2 Results:.....	72
5.4 Constraints to be maintained for optimization and AM:.....	73
5.5 17-4PH Stainless steel characteristics:.....	74
Chapter6 Optimization and 3Dprinting of Blade	77
6.1 Optimization:	77
6.1.1 First design:.....	77
6.1.2 Second design:	79
6.1.3 Final design:.....	80
6.2 AM the Blade:.....	81
6.2.1 Version1:.....	83
6.2.2 Version2:.....	86
Conclusion:	91
References.....	93

LIST OF FIGURES

Figure 1-1 Robert Hooke’s screw propeller [3].	1
Figure 1-2 Left side Bernoulli’s Propeller Wheel, Right side Archimedean screw of Paucton [3].	2
Figure 1-3 Left side Bramah’s Screw propeller and Right side Shorter’s propulsion system [3].	2
Figure 1-4 Smith's original 1836 patent for a screw propeller of two full turns. He would later revise the patent, reducing the length to one turn [2].	3
Figure 1-5 Ericsson’s screw propeller [3].	4
Figure 1-6 Left side Rim–driven thruster [5] and Right side Screw Propeller [6].	4
Figure 1-7 Ship propeller representation [7].	5
Figure 1-8 Propeller blade face and back [8].	6
Figure 1-9 Rake and skew representation of blade [9].	6
Figure 1-10 Composite Marine Propeller [10].	8
Figure 2-1 Early AM parts by Housholder, Kodama, and Herbert. [12].	11
Figure 2-2 3D Printing Process [22].	12
Figure 2-3 CAD model and their STL formats [12].	12
Figure 2-4 Process Chain of Digital model [12].	12
Figure 2-5 Stereolithography (SLA) [26].	15
Figure 2-6 DLP process. [16].	15
Figure 2-7 CLIP process [28].	16
Figure 2-8 Material jetting [29].	17
Figure 2-9 Representation of Binder jetting machine. [29].	18
Figure 2-10 Representation of Material Extrusion machine [29].	19
Figure 2-11 Representation of Material Extrusion with Plungers and its process schematic representation [30].	20
Figure 2-12 Representation of Material Extrusion with Filaments [30].	24
Figure 2-13 Representation of Material Extrusion with Screws [30].	25
Figure 2-14 Laminated Object Manufacturing (LOM) [26].	26
Figure 2-15 left side representation for Laser engineered net shaping (LENS) process [32] and right side representation for Electron Beam Additive Manufacturing (EBAM) [33].	27
Figure 2-16: Left side shows representation of EBM machine [35] and right side representation for SLS/SLM/DMLS process [29].	28
Figure 3-1 Studio System™ 3D printer [37].	29
Figure 3-2: Fabricate™ software interface [37].	30
Figure 3-3 Toolpath preview [37].	31
Figure 3-4 Changing Material Cartridge and print head [37].	31
Figure 3-5 Feed stock in form rods (metal powder and binder in form of rods) and Cartridge [37].	32
Figure 3-6 Desktop Metal™ debinder [37].	32
Figure 3-7 Loading debinder with green parts [38].	33
Figure 3-8 Studio System+™ furnace by Desktop Metal™ [37].	34
Figure 3-9 Stackable graphite retort box with adjustable shelving and gas channeling [37].	34
Figure 3-10 Desktop Metal™ gas cylinder [23].	35
Figure 3-11 Binder trap for collecting and removing remaining binder of the part [23].	35
Figure 3-12 Furnace heating system with the SiC heating elements positioned on 4 sides [39].	36
Figure 3-13 Left side shows Cross sectional thickness based on wall thickness and internal infill [40] and Right side shows Example of internal infill of a part. Courtesy of Additive Italia Srl.	41
Figure 4-1 Fluid element [42].	42
Figure 4-2 Mass flow in and out of a fluid element [43].	43

Figure 4-3 Stress components on three faces of fluid element [42].	44
Figure 4-4 Stress components in the x-direction [42].	45
Figure 4-5 Structured grid [44].	47
Figure 4-6 Unstructured grid, numbers are marked to individual cells to shows that it doesn't have any particular order as in structured [44].	47
Figure 4-7 Control volume of cell-centered (a) and cell-vertex (b) scheme [44].	48
Figure 4-8 Calculating the Aspect Ratio for a Mesh cell [45].	49
Figure 4-9 Skewness [46].	49
Figure 4-10 A) Vector d and S, on an orthogonal mesh. B) Vector d and S, on a non-orthogonal mesh [47].	50
Figure 5-1 Left side shows modified 17" propeller's blade 3D design and Right side shows 17" propeller assembly 3D design Courtesy by EWOL Srl.	51
Figure 5-2 Experimental data of thrust's at different speed of propeller at 18° blade angle for 16" size propeller, x-axis represents rpm and y-axis represents thrust produced in Newtons courtesy by EWOL Srl.	53
Figure 5-3 Experimental data of thrust's at different speed of propeller at 18° blade angle for 22" size propeller, x-axis represents rpm and y-axis represents thrust produced in Newtons courtesy by EWOL Srl.	53
Figure 5-4 Wireframe representation of fluid domain and blade in geometry model and the names of each faces.	54
Figure 5-5: Quality Range index for Skewness and Orthogonal quality [49].	55
Figure 5-6 Created Mesh for fluid domain.	56
Figure 5-7 Mesh domain as shown in Fluent after launch of the window.	56
Figure 5-8 Solver settings used in this case study in Fluent.	57
Figure 5-9 Shows Model settings for governer equations.	57
Figure 5-10 Material seawater created with properties as mentioned initially.	58
Figure 5-11 Assigned Cell zone condition settings with frame motion	58
Figure 5-12 Defined inlet velocity conditions for the inlet and inlet top faces.	59
Figure 5-13 Assigned outlet settings.	59
Figure 5-14 Assigned Meshinterface settings.	60
Figure 5-15 Assigned solution methods settings	61
Figure 5-16 : Residual Monitors.	61
Figure 5-17 Assigned initializing settings.	62
Figure 5-18 : Residuals graph (propeller-speed:1300rpm, inlet-velocity:4.11m/s,20deg blade orientation).	62
Figure 5-19 Thrust vs iterations Graph.	63
Figure 5-20 Pressure field map on front side of blade	63
Figure 5-21 Pressure field map on back side of blade.	64
Figure 5-22 velocity vectors from the blade.	64
Figure 5-23 Residual graph of refined mesh.	65
Figure 5-24 Thrust vs iterations graph.	65
Figure 5-25 velocity vectors of blade.	66
Figure 5-26 Residuals graph of fine mesh	66
Figure 5-27 Thrust Vs iterations graph	67
Figure 5-28 velocity vectors of Blade.	67
Figure 5-29 Graph for Thrust Vs inlet velocities at 1300 rpm and 20deg orientation of blade.	68

Figure 5-30 Left side shows Pressure field map on front side of blade and Right side shows Pressure field map on back side of blade at 1300rpm,20 deg orientation, inlet velocity 0.5 m/s.....	68
Figure 5-31 Graph between Thrust and rpm for different types of propellers. Black for 22” propeller, Red for 16” propeller (Both velocities zero as mentioned by EWOL). Blue line in graph shows thrust values by CFD analysis for 17” propeller at inlet velocity at 1m/s, Green line shows the estimated values by Average method from given data by EWOL for 17” propeller. For all propellers 18 deg is the blade orientation.....	69
Figure 5-32 Imported Cad body from nTopology (implicit body).	70
Figure 5-33 Pressure field view on blade from nTopology.	70
Figure 5-34: Shows tetrahedral(triangle elements) elements on blade.	71
Figure 5-35 Fixed constraint position for blade at coupling interface.....	71
Figure 5-36: Von Mises stress for both linear and quadratic geometric orders.	72
Figure 5-37 Most stressed locations from blade with 2 plane cross section views.....	72
Figure 5-38 Coupling Interface which should be preserved.	73
Figure 5-39 Outer design of the blade on both side which should be preserved.	73
Figure 5-40 Left side shows Microstructures of water atomized 17-4 PH sample in the as-sintered condition and Right side shows gas atomized 17-4 PH sample in the as-sintered condition [23].	74
Figure 5-41 Infill layers patterns for samples courtesy by Add-it.	76
Figure 6-1 Column type lattice structure in the blade.....	78
Figure 6-2 static analysis results.	78
Figure 6-3 TPMS lattice structure created with blade structure.....	79
Figure 6-4 TPMS lattice structure merged with shell.	79
Figure 6-5 Static analysis results of TPMS lattice structure.	80
Figure 6-6 TPMS lattice structured blade with depowdering channel and reinforced around.....	80
Figure 6-7 static analysis for TPMS reinforced with depowdering channel.....	81
Figure 6-8 Toolpath preview of blade courtesy by Add Italia.	83
Figure 6-9 Final estimated parameters courtesy by Add Italia.	83
Figure 6-10 Left side shows blade while printing and Right side shows final printed part called as green part courtesy by Add Italia.....	84
Figure 6-11 part after sintering process courtesy by Add Italia.....	84
Figure 6-12 separated supporting structures of blade courtesy by Add Italia.....	85
Figure 6-13 Final blade part courtesy by Add Italia.	85
Figure 6-14 Cracks on the blade courtesy by Add Italia.....	86
Figure 6-15 Blade with supports and parameters courtesy by Add Italia.	86
Figure 6-16 Tool Path preview courtesy by Add Italia.....	87
Figure 6-17 Final estimated parameters courtesy by Add Italia.	87
Figure 6-18 Printed part courtesy by Add Italia.	88
Figure 6-19 Part after sintering process with supports courtesy by Add Italia.	88
Figure 6-20 Final part after removing the supports courtesy by Add Italia.....	89
Figure 6-21 Cracks occurred on the final part courtesy by Add Italia.....	89
Figure 6-22 Cracks on support structures courtesy by Add Italia.....	90

LIST OF TABLES

Table 2-1 Examples of binder system compositions used in material extrusion additive manufacturing with highly-filled polymers with filaments [30].	21
Table 2-2 Ceramics and metals investigated for use in MEAM-HP [30].	22
Table 2-3 Feedstocks with powders currently offered by companies; powders in beta phase of development are excluded from the list [30].	22
Table 3-1 Main properties of the principal component of the solvent used in the debinding process [23].	33
Table 3-2 BMD™ guidelines for Studio System+™ 3D printing machine [40].	40
Table 5-1 Chemical composition of 17-4PH certified by Desktop Metal™ [55]	75
Table 5-2 Mechanical properties certified by Desktop Metal™ [55].	75
Table 6-1 Print profiles & settings [58].	82
Table 6-2 Impact on print speed & surface quality [58].	82

Chapter1 Ship Propeller

1.1 Introduction:

Propeller is a rotating device; it looks like a fan which is used to propel the ship by using the power transmitted from the main engine of the ship. The transmitted power is converted to a thrust which imparts momentum to the water from rotational motion which resulting in a force that acts on the ship and pushes it forward. Ship propels based on Bernoulli's principle and Newton's third law. A pressure difference is created on the forward and aft side of the blade and water is accelerated behind the blades. A ship can have with one, two and rarely three propellers depending upon the speed and maneuvering requirements of the vessel [1]. When propeller rotates it performs an action similar to Archimedes' screw.

1.2 History:

Present day Propeller principle originated from sculling. In sculling, a single blade is moved through an arc with an effective angle. Innovation introduced with the screw propeller was the extension of that arc through more than 360° by attaching the blade to a rotating shaft. Propellers can have a single blade, but to balance the forces so it has more than one [2].

The origin of the screw propeller starts with Archimedes' screw invented by Archimedes, which was used to lift water for irrigation and bailing boats. Which was by Egyptians for centuries for irrigation. Later Leonardo da Vinci adopted the principle to drive his famous theoretical helicopter in his sketch book [2]. In 1661, Toogood and Hays proposed waterjet propulsion using screws, although not as a propeller [2]. Robert Hooke in 1681 [3] designed a horizontal watermill which was similar to the Kirsten-Boeing vertical axis propeller designed in 1928 [2]. After two years Hooke modified the design to propel ships through water.

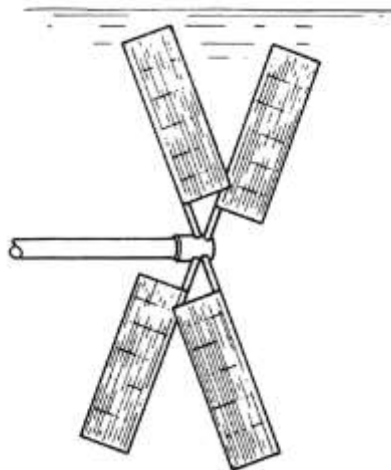


Figure 1-1 Robert Hooke's screw propeller [3].

In 1693 Du Quet invented a screw propeller which was tried initially and later abandoned [2]. In 1752, the Académie des Sciences in Paris presented series of prizes for research in navel architecture which lead to development. In which Bernoulli won a prize for a design of a propeller-wheel [3]. At the same time, the French mathematician Alexis-Jean-Pierre Pauton, proposed a

water propulsion system which was based on the Archimedean screw [3]. In 1771, steam-engine inventor James Watt proposed "spiral oars" to propel boats in a private letter, although he did not implement the idea [2].

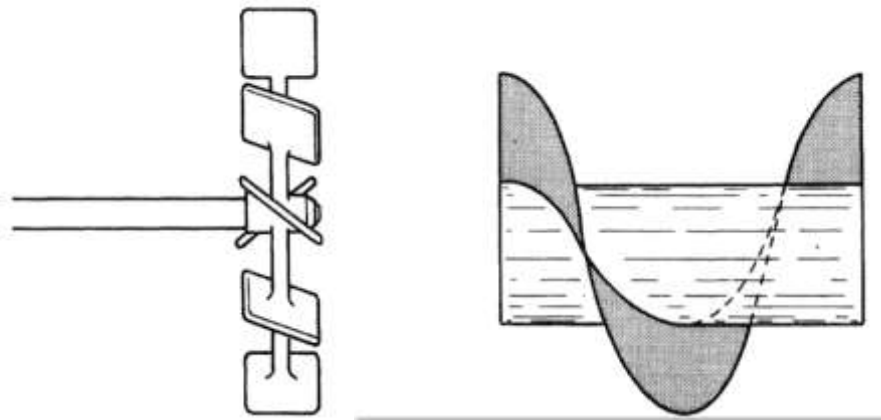


Figure 1-2 Left side Bernoulli's Propeller Wheel, Right side Archimedean screw of Paucton [3].

One of the first practical and applied uses of a propeller was on a submarine dubbed Turtle which was designed in 1775 by David Bushnell, with help of his brother Ezra Bushnell and clock maker, engraver, and brass foundryman Isaac Doolittle, and ship's carpenter and clock maker Phineas Pratt in New Haven, Connecticut, constructing the hull in Saybrook, Connecticut. Aim of the project was to destroy enemy ship from beneath [2, 4].

Joseph Bramah in 1785 proposed a propeller solution of a rod going through the underwater aft of a boat attached to a bladed propeller, which he never built [3]. In 1802, Edward Shorter proposed a similar propeller to Bramah's which was attached to a rod angled down temporarily deployed from the deck above the waterline which led to no need of water seal [3].

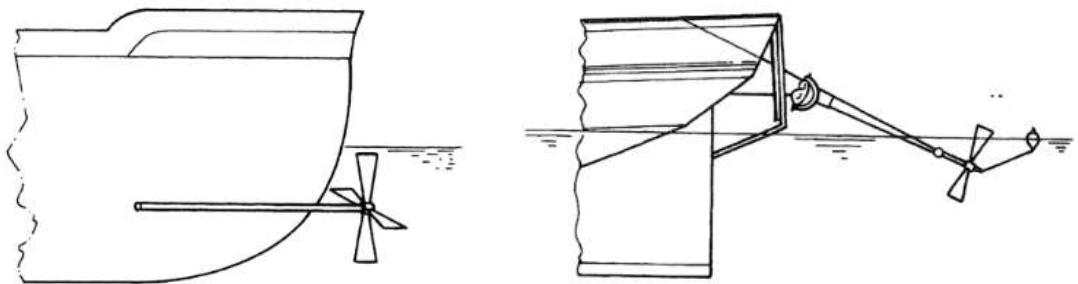


Figure 1-3 Left side Bramah's Screw propeller and Right side Shorter's propulsion system [3].

In 1802, the American lawyer and inventor John Stevens made a 25-foot (7.6 m) boat with a rotary stem engine which was coupled to a four-bladed propeller. Stevens abandoned propellers due to the inherent danger in using the high-pressure steam engines [3]. By 1827, Josef Ressel had invented a screw propeller which had multiple blades fastened around a conical base. In February 1826 he tested his propeller on a small ship which was manually driven. He was successful adapted his bronze screw propeller on a steamboat (1829). His ship, Cavetti of 48 gross register tons, reached a speed of about 6 knots (11 km/h). This was the first successfully driven ship by an

Archimedes screw-type propeller. His experiments were banned due to accident of a new steam engine by the Austro-Hungarian police as dangerous [2].

John Patch developed a two-bladed, fan-shaped propeller in 1832 and in 1833 he demonstrated publicly, propelling a row boat across Yarmouth Harbor and a small coastal schooner at Saint John, New Brunswick. His efficient design got praise in American scientific circles but at the time there were multiple competing versions of the marine propeller [2].

Two inventors John Ericsson and Francis Pettit Smith, in 1835 who began working on the problem separately. Smith was first to take out a patent on screw propeller on 31 May, while Ericsson filed his patent six weeks later. Smith quickly built a small model boat to test his invention, which was demonstrated at his Hendon farm on a pond, and later at the Royal Adelaide Gallery of Practical Science in London, Smith then built a 30-foot (9.1 m), 6-horsepower (4.5 kW) canal boat of six tons burthen called Francis Smith, which was fitted with a wooden propeller of his own design and demonstrated on the Paddington Canal from November 1836 to September 1837 [2]. Smith with an accidental discovery subsequently filed a revised patent. Accident was occurred during a voyage in February 1837 in which wooden propeller of two turns was damaged, and to his surprise the broken propeller, which now consisted of only a single turn, which lead to double the boat's previous speed [2].

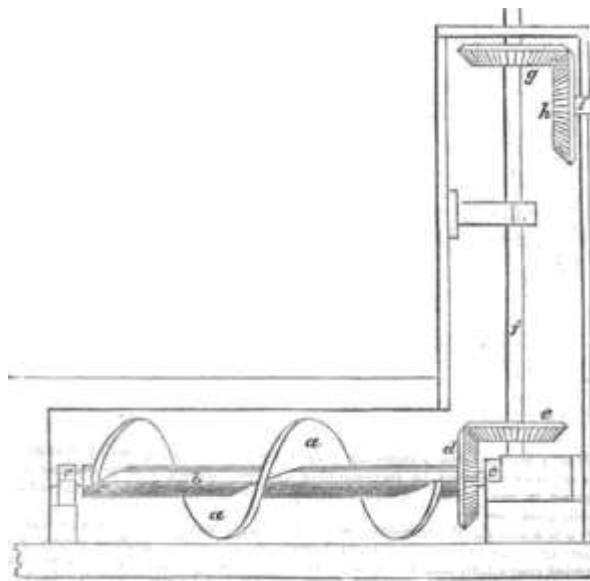


Figure 1-4 Smith's original 1836 patent for a screw propeller of two full turns. He would later revise the patent, reducing the length to one turn [2].

In the meantime, Ericsson built a 45-foot (14 m) screw-propelled steamboat named Francis B. Ogden in 1837, and he demonstrated it on the River Thames to senior members of the British Admiralty, including Surveyor of the Navy Sir William Symonds. In spite of achieving a speed of 10 miles an hour, comparable with other paddle steamers, Symonds and his associates were unimpressed [2]. The Admiralty believed that screw propulsion would be ineffective in ocean-going service could not be steered efficiently [2]. Due to this rejection, he built a second, larger screw-propelled boat named Robert F. Stockton, and sailed it to the United States in 1839, where he gained fame as the designer of the U.S. Navy's first screw-propelled warship, USS Princeton [2].

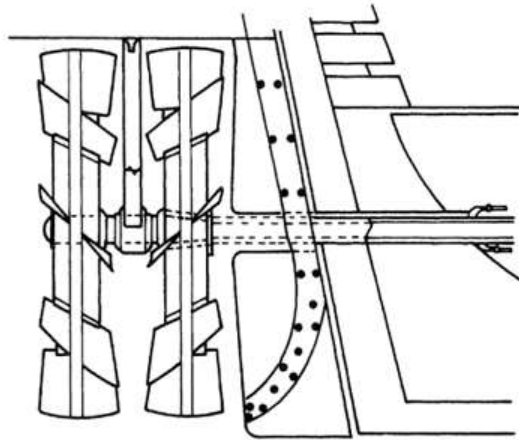


Figure 1-5 Ericsson's screw propeller [3].

Later with more research and development, Screw propeller design stabilized in the 1880s.

A novel type of propulsion unit which was presented at the Shipbuilding, Machinery & Marine Technology 2010 trade fair (SMM) by the companies Voith and Van der Velden is Shaftless Propellers or Rim-driven thruster [5]. It is a marine propeller which does not need a hub for transmission of the driving torque like a conventional propellers. The blades of the rim-driven thruster are mounted on a ring which has the rotor of an electric motor and it is surrounded by the stator which is a ring-shaped which are watertight and the whole unit operates submerged. Required torque is created from rotor and stator like an electric motor [5].

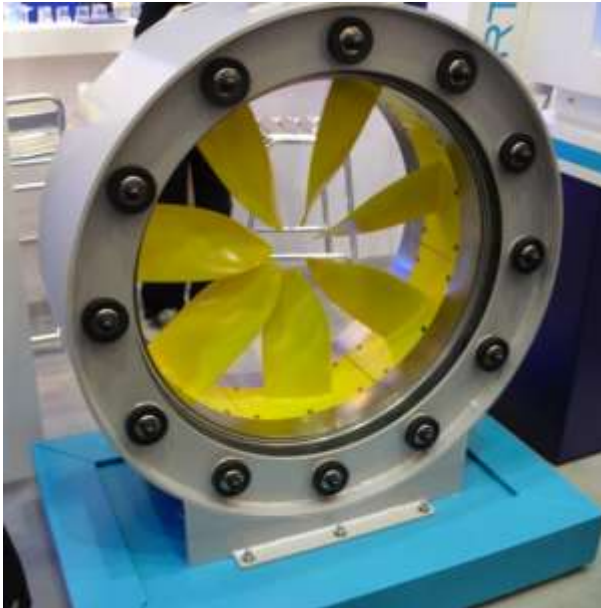


Figure 1-6 Left side Rim-driven thruster [5] and Right side Screw Propeller [6].

1.3 How does a ship propeller work?

Propelling system of vehicles running on land is different, in which engine powers the shaft which is connected to the vehicle tyre to move the vehicle. However, for ships there are no tyres or surfaces where they can ride but are displaced in water. So, the propeller is used to drive the ship forward or backwards, depending upon the direction of rotation or pitch of the propeller. The engine of the ship is connected to the propeller by shaft [1].

As the propeller rotates by the engine, the radiating blades which have a pitch as a helical spiral, like a screw. While in rotation, it transforms the power into thrust which is linear in nature. As the propeller blades rotate, it creates the pressure difference between the surface in front and back of it. Due to this a mass of fluid is accelerated in one direction creating a reactive force which helps the body attached to the propeller (which is the ship) move in the other direction [1]. To move the ship in the reverse direction, the propeller should be rotated in an anti-clockwise direction or opposite direction to the forward one. In general, the engine of the Fixed Pitch-propeller is mostly designed for clockwise rotation when sailing ahead, hence, prolonged operation in astern direction is not efficient [1]. For ships with Controllable Pitch propeller, the engine direction is not affected, hence, the astern efficiency of the ship is better than that of a fixed-pitch propeller [1].

1.4 How does a ship propeller look like?

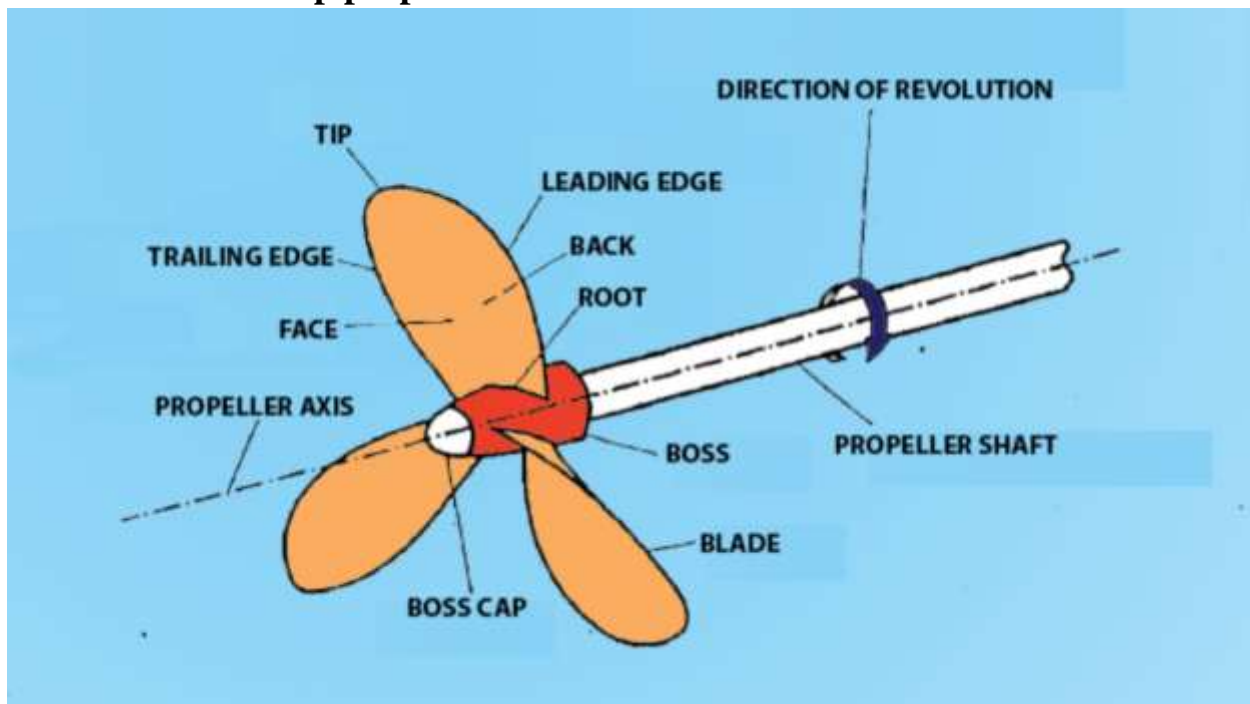


Figure 1-7 Ship propeller representation [7]

1.4.1 Propeller Hub or Boss:

A ship propeller has a boss as shown in figure 1-7, which is a cone-type structure where blades are attached to it and it connects the propeller shaft and blades together. The shaft transmits the power delivered from the engine and in turn, rotates the blades mounted on the hub/boss. Different detailed studies of hydrodynamic behavior of propellers have shown that in different water conditions, the thrust delivered and the resultant efficiency are inversely proportional to the size/diameter of the boss. Thus, modern

designs have evolved with the smaller yet stronger boss to maintain a safety trade-off in terms of strength also [8].

1.4.2 Propeller Blades:

Blades are mounted on the hub, which are like thin airfoil sections as shown in figure 1-7, which creates a hydrodynamic lift for producing thrust. Over the time blades are evolved into innumerable designs with different shapes to satisfy the design and performance requirements for a vessel. Irrespective of the blade design, all propeller has a set of common features they are:

- **Blade Face and Back:** ship propeller blade has two hydrodynamic surfaces: Face and Back. when looked from the behind of the ship the visible blade surface is called the Face, also known as the ‘palm’. The opposite one is called Back [8].

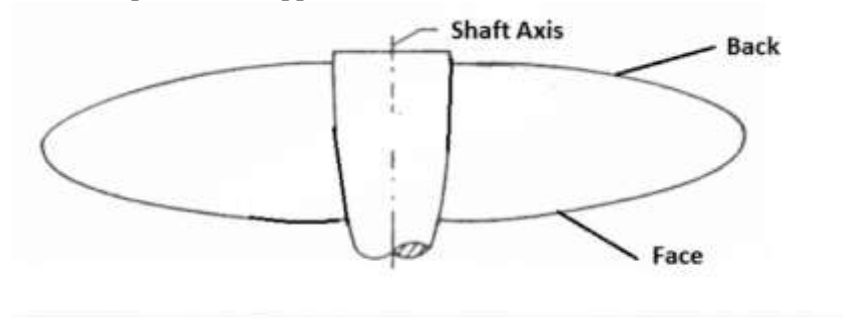


Figure 1-8 Propeller blade face and back [8].

- **Leading Edge and Trailing Edge:** there are two edges for a ship propeller blade. Depending upon the rotation of the propeller the edge which pierces the water surface first is Leading Edge. The other edge, which follows or ‘lags behind’ the leading edge is Trailing Edge [8]. The figure 1-7 shows better.
- **Root and Tip:** The point where the blades are attached with the ship propeller boss or hub is called the root. Tip is the furthest point of the propeller blade from the root. It has the least section width. It joins the leading and trailing edges as well as joins the face and the back [8].figure 1-7 shows the root and tip.
- **Skew:** A blade that is radially symmetrical is said to have zero skew. A blade that is swept back from the direction of rotation is said to be skewed.
- **Rake:** Rake is the angle of a propeller blade face relative to its hub. If the blade face is perpendicular to the hub, the propeller has zero-degree rake.

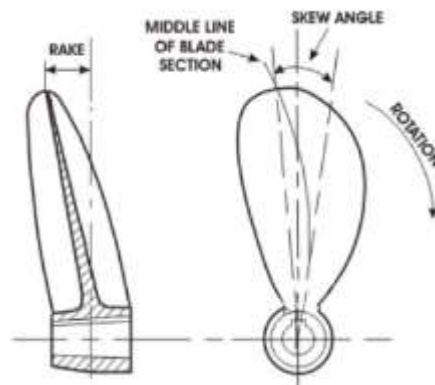


Figure 1-9 Rake and skew representation of blade [9].

1.5 Types of Propeller:

Propellers are classified based on several factors. The classification of different types of propellers is shown below:

1.5.1 Classification by Number of Blades Attached:

Propeller blades may vary from having 3 blades to 4 blades and sometimes even 5 blades. However, the most used are 3 blade and 4 blade propellers [1]. The propeller efficiency will be highest for minimum number of blades i.e. 2 blade propellers. Due to strength factors and the heavy loads subjected by the ship, sea, and weather conditions so they are not used for merchant ships.

3 blade propellers: 3 blade propeller has the following characteristics [1]:

- Manufacturing cost is lower than other types.
- They are normally made up of aluminum alloy.
- They give a good high-speed performance.
- Acceleration is better than other types.
- Low-speed handling is not much efficient.

4 blade propellers: A 4 blade propeller has the following characteristics [1]:

- Manufacturing cost is higher than 3 blade propellers.
- 4 blade propellers are normally made up of stainless-steel alloys.
- It has better strength and durability.
- It gives good low-speed handling and performance.
- It has a better holding power in rough seas.
- 4 blade propeller has better fuel efficiency than all the other types.

5 blade propellers: A 5 blade propeller has the following characteristics [1]:

- Manufacturing cost is higher of all.
- Vibration is minimal from all the other types.
- 5 blade propellers have better holding power in rough seas.

6 blade propellers: A 6 blade propeller has the following characteristics [1]:

- Manufacturing cost is high
- Vibration is minimal from all the other types.
- 6 blade propellers have better holding power in rough seas.
- With six blade propeller, the induced pressure field over the propeller decreases.

Large container ships are mainly fitted with 5 or 6-bladed propellers

1.5.2 Classification By pitch of the blade:

Pitch of a propeller can be defined as the displacement that a propeller makes for a full revolution. Classification of the propellers based on pitch is as follows [1].

Fixed Pitch Propeller

In fixed pitch propeller blades are permanently attached to the hub. Hence pitch of the blade is permanently fixed and cannot be changed during the operation. Fixed pitch propellers are robust and reliable because it does not incorporate any mechanical and hydraulic connections as in Controlled Pitch Propeller (CPP). Manufacturing, installation, and operational costs are lower than controlled pitch propeller (CPP) type. The maneuverability of fixed-pitch propeller is not as good as CPP. So, this type of propeller is fitted in a ship which does not require good maneuverability.

Controllable Pitch Propeller

In this type of propeller, it is possible to change the pitch by rotating the blade about its vertical axis by using mechanical and hydraulic arrangement. This helps in pitch that can be altered to

match the required operating condition. Thus, the maneuverability improves and increases the engine efficiency. It is a complex and expensive system from both installation and operational point. The pitch may get stuck in one position, making it difficult to maneuver the engine. The propeller efficiency of CP propeller is slightly lower than the same size FP propeller due to the larger hub to accommodate the blade pitch mechanism and piping's [1].

1.6 Materials:

Marine propellers are made up of corrosion-resistant materials as they are operating directly in seawater which is a corrosion accelerator. The materials used for making marine propeller are alloys of aluminum and stainless steel. Other popular materials used are alloys of nickel and bronze which are 10~15 % lighter than other materials and have higher strength [1] widely used alloys are NAB and MAB. Recently from last two decades Marine propellers are leaning towards composite materials as an alternative to conventionally used materials. Glass Fiber Composite Material, Carbon/Graphite Fiber Composite, aramid fiber, aluminum, Dry Carbon and Nylon powdered composites [10] are some composite materials.



Figure 1-10 Composite Marine Propeller [10].

1.7 Manufacturing of Propeller:

The manufacturing process of marine propellers mostly unchanged. The propeller is manufactured by sand casting technology. Commonly many components are manufactured by Sand casting. Pattern making, forming the mold cavity, metal pouring, and finishing are the main steps of sand casting. Pattern making technique is different and tedious in propeller manufacturing. Advantage is many metals can be molded in different sizes, shapes and at cheaper cost. But it has poor finish and tolerance [11]. K. Sridhar, Yonas Mitiku Degu et al mentioned about adopting LASER ENGINEERED NET SHAPING (LENS) for manufacturing propeller to reduce the time, cost and increase the mechanical property, quality and productivity [11]. Composite material propellers are manufactured by many researchers by hand layup process, RTM Process and Va-RTM Process [10].

In this case study EWOL tech Srl companies 17” propeller blade design was used for optimization and 3D printing. Originally, they are manufacturing blade by using sheet metal, forging and laser cutting but the details weren't released due to secrecy of manufacturing for competitive reasons.

Chapter2 Additive Manufacturing

2.1 Introduction:

Additive manufacturing (AM) is a technology where the part is built by adding material layer by layer from a 3D CAD model, not like as in traditional way where the part is built by subtractive way (The part is built by removing material from a solid block of metal). Additive manufacturing mimics the nature by style of adding material to its growth. It has different names as “3D Printing (3DP)”, “Rapid prototyping (RP)”, “Solid freeform fabrication (SFF)”, “Layered manufacturing (LM)”. Based on the technology used, the layer thickness ranges from a few microns up to around 0.25mm [12], and a range of materials are now available for the different technologies. In general the popular press continues to refer to additive manufacturing as “3D printing”, as this term can easily be understood by general public. AM can achieve Near net shape. It can be used as an alternative or integrated with traditional manufacturing depending on the requirement.

2.2 History of Additive Manufacturing:

Earliest concepts of additive manufacturing can be seen at end of nineteenth century and early in twentieth century, with the introduction of number of ways to make 3D maps by using paper for representation of topological maps (3D representation of terrain). Photo sculpture also started at the end of the nineteenth century.

We can see modern day additive manufacturing origins in mid of twentieth century from a patent by Otto John Munz in 1951 [13], which can be considered as the origin of modern day stereolithography technique. He developed a technique for selectively exposing a transparent photo emulsion in a layer wise manner in which each layer was exposed with a cross section of an part. The piston where the part was building was gradually lowered, and the next layer was produced by the addition of photo emulsion and fixing agent on top of the old layer. Once the process finished the resulting solid transparent cylinder have a 3D image of the object. Weakness of this system was 3D object need be manually carved or photochemically etched out of the cylinder.

Several new techniques were developed in following decades. One of those Swainson, who proposed a process in 1968 [14] to directly fabricate a plastic pattern by selective, 3D polymerization of a photosensitive polymer at the intersection of two laser beams this process is called Photochemical Machining. This patent was assigned to Formgraphic Engine Corporation and the work, which was undertaken at Battelle Laboratories [15].

Ciraud [16] proposed a powder process in 1971 [12] which can be considered as father of modern-day direct deposition AM techniques. In 1979, Housholder [17] developed the earlier equivalent of a powder laser sintering process. In his patent, he discussed sequentially depositing powder as a layer and selectively solidifying portions of each layer. The solidification could be achieved by using heat and a selected mask or by using a controlled heat scanning process such as a laser.

Hideo Kodama from the Nagoya Municipal Industrial Research Institute where he developed a number of stereolithography-related techniques [18], and in parallel Herbert developed a system in which he engaged a UV laser beam to a photopolymer layer by means of a mirror system on an x - y plotter to scan a layer [19]. The layer was then lowered by 1 mm into a vat of resin and the process repeated until part is made. Examples of Housholder's, Kodama's, and Herbert's parts can be seen in following figure.

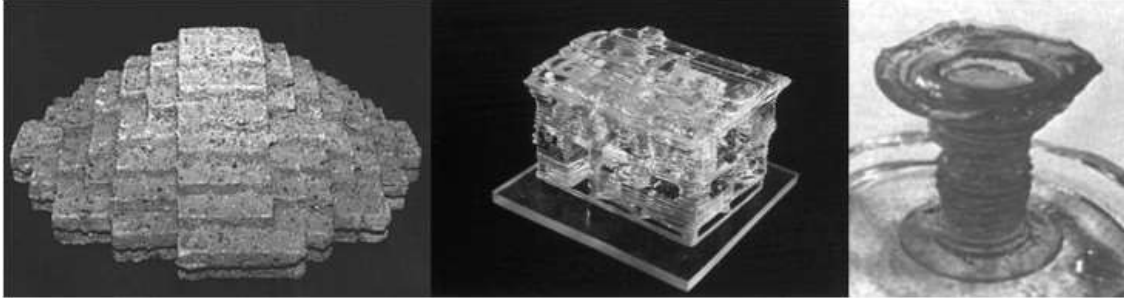


Figure 2-1 Early AM parts by Housholder, Kodama, and Herbert. [12].

The Charles W. Hull's stereolithography patent in 1986 [12] which led to development of commercially available systems as present day. The patent was owned by UVP Inc. and he founded start-up, 3D Systems. This led to the development of first commercial SLA machine which appeared in 1988. Since then every year has seen so much growth in available systems, technologies, and materials.

In 2005 things started changing, when Dr Adrian Bowyer, a Senior Lecturer in mechanical engineering at the University of Bath in England, launched an open-source 3D printer project called the RepRap (self-replicating rapid prototyper) [20]. The technique used for RepRap 3D printers is fused-filament fabrication (FFF) for 3D printing. The process is like same process as fused-deposition modelling (FDM), but it is used to avoid trademark infringement. The aim of the RepRap project is to make a 3D printer that is capable of printing various products as well as replicating itself or printing its own parts. Recent versions of the RepRap printers can print approximately 50 % of their own parts, dramatically reducing costs [21]. Bowyer made the design open source available for free under the GNU General Public License¹. With the open source it is easier for circulation of design and its development due to participation of more innovators, without the concern of intellectual property issues [21]. As soon as the expiration of core patent of RepRap technology in 2009, led to hundreds of derivative innovations by individuals and companies. Number of new companies appeared with open-source printers, and many of them raised funding through crowdsourcing platforms, such as Kickstarter and Indiegogo. In this period the technology improved rapidly, particularly cost of a basic 3D printing also reduced.

2.3 Production of 3d object by Additive Manufacturing:

In this section we will discuss how practically additive manufacturing works for producing a desired 3D object. In Additive Manufacturing we need 3 essential elements to produce the final desired object.

- 3D CAD model
- Feed material
- 3D printer

¹ GNU General Public License (GNU GPL or GPL) is a free software license. It is widely used since it guarantees end users the freedom to run, study, share and modify the software

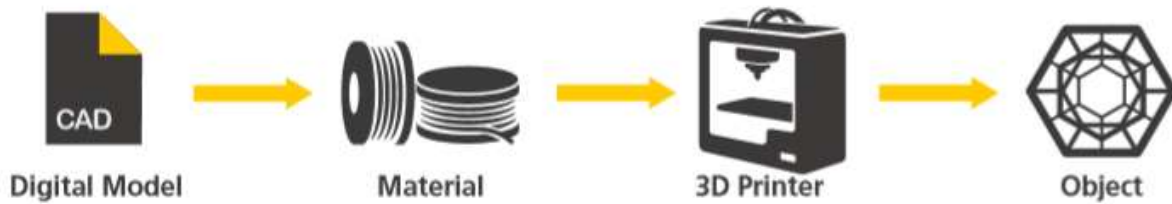


Figure 2-2 3D Printing Process [22]

Next sections explain in detail about each three elements.

2.3.1 3D CAD Model:

3D CAD model is a digital model of our final desired 3D object. Which is in general designed using design software's like SolidWorks, Inventor, Catia etc., then designed is converted into STL (Standard Triangulation Language) format. Better resolution of STL file gives better quality. Figure 2-3 shows the CAD and different resolutions of a STL file. By using Additive Machine's software these STL files are sliced into thin layers.

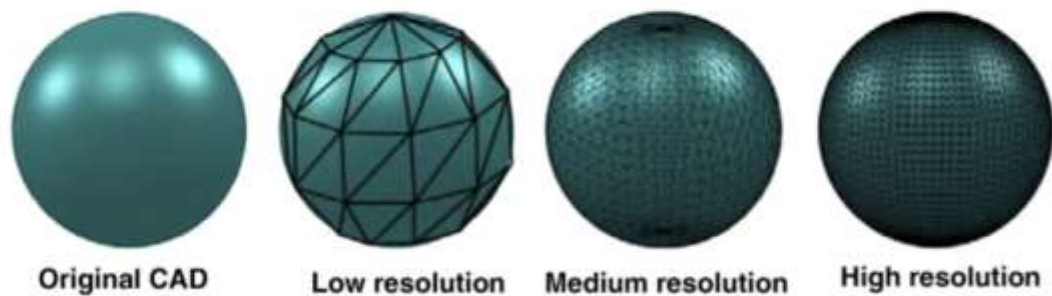


Figure 2-3 CAD model and their STL formats [12]

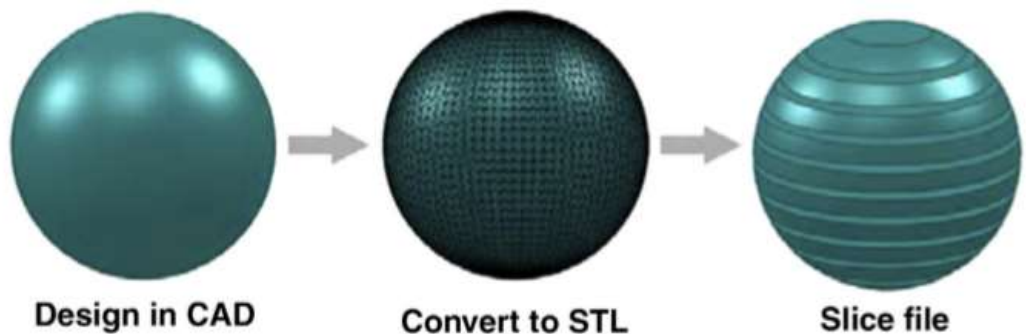


Figure 2-4 Process Chain of Digital model [12]

2.3.2 Feed Material:

In early days, plastic prototypes are made by applying AM technologies. After strong research, AM technology has become capable of producing complex net-shaped or nearly net-shaped parts that can be directly used as functional parts, using different materials including metals, ceramics, and composites. Despite the progress, just a small fraction of materials can be used in 3D printing compared to traditional manufacturing at present. This shows one of the biggest hurdles to a adopt AM technology. However, every year new materials are advanced in AM, resulting in better microstructures, and enhanced material tolerability [23]. The major categories of AM materials are.

- **Polymers** like photosensitive resin, Nylon, elastomer, ABS and wax are can be used to produce parts with 3DP. Nylon, i.e., polyamide (PA), is one of the most widely used polymer because it melts and bonds by laser better than other polymers [23]. Nylon, elastomer, ABS plastic and wax are thermoplastics, which change from a harder structure to a softer structure before finally melting into a viscous flowing liquid when heated to high temperatures. Photosensitive resins are usually thermosetting polymers, which will decompose rather than melt at high temperatures [23]. The parts produced by using polymers through AM technology can be used for prototypes, sacrificial patterns for investment casting, and even functional parts. In addition to industrial polymers, biocompatible polymers, such as poly-ε-caprolactone (PCL) and polyether ether ketone (PEEK) and starch-based polymers, for biomedical applications such as implants and tissue scaffolds [23];
- **Metals** can be used in a “direct” way – by melting metal particles together or an “indirect” way – by bonding the metal with postprocessing. Ti6Al4V, 316SS, IN718, IN625 and 17-4SS are an example of some metallic alloys which are processed with 3DP [23];
- **Ceramics** including alumina, silica, and zirconia. In general, they have great chemical resistance and ability to withstand high temperatures. But these materials are very brittle and hard, which makes them difficult to manufacture, especially for producing parts with complex geometries. AM successfully demonstrated its advantages in producing ceramic parts through both “direct” and “indirect” methods [23].
- **Functionally graded materials** are the outcome of the great flexibility of the technology, especially of AM processes that can deliver different materials (usually through multiple feeding systems) to the building areas. This ability offers the possibility to control the composition and optimize the properties of the built part [23].

Despite growth in the variety and application of AM material inputs and feed stocks, still they are expensive relative to traditional manufacturing materials. For example, powder metals can be 200 times as costly as sheet metal [23] and photopolymers can cost between USD 750 and USD 1,000 per gallon compared to injection molding material, which costs USD 1 per pound [23]. While some manufactures enjoy savings when using AM for custom products and low volume production.

2.3.3 Different types of 3D Printer technologies:

There are different ways to print by AM. Some methods use melting or softening material to extrude layers. Others cure a photo-reactive resin with a UV laser (or another similar light source) layer by layer [24]. According to ISO 17296-2:2016, there are two different categories:

- single-step processes: parts are produced in a single operation where the basic geometric shape and basic material properties of the desired product are achieved simultaneously,

- multi-step processes: parts are produced in two or more operations where the first typically provides the basic geometric shape and the following steps establishes the intended basic material properties for part.

According to the final application of the product, each process may require different post-process treatments to reach the desired properties. Additive Manufacturing processes are classified into 7 categories according to standard terminology for Additive Manufacturing technologies. These seven processes are [24]:

- 1) Vat Photopolymerization
 - a. Stereolithography (SLA)
 - b. Digital Light Processing (DLP)
 - c. Continuous Liquid Interface Production (CLIP)
- 2) Material Jetting
- 3) Binder Jetting
- 4) Material Extrusion
 - a. Fused Deposition Modelling (FDM)/Fused Filament Fabrication (FFF)
- 5) Sheet Lamination
- 6) Directed energy
 - a. Deposition Laser Engineering Net Shaping (LENS)
 - b. Electron Beam Additive Manufacturing (EBAM)
- 7) Powder Bed Fusion
 - a. Selective Laser Sintering (SLS)
 - b. Direct Metal Laser Sintering (DMLS)
 - c. Electron Beam Melting (EBM)

2.3.3.1 Vat photopolymerization:

According to ISO 17296-2 definition of Vat photopolymerization is: “additive manufacturing process in which liquid photopolymer in a vat is selectively cured by light-activated polymerization”. Most of the photopolymers react to radiation in the ultraviolet (UV) range of wavelengths, but other visible light systems are can be used. When irradiation occurs, the liquid material, which fills the container of the 3D printer, undergoes a chemical reaction to become solid [23]. Key features of the process are [25]:

- Feedstock: liquid or paste: photoreactive resin with or without filler.
- Binding mechanism: chemical reaction bonding.
- Source of activation: typically, UV radiation from lasers or lamps.
- Secondary processing: cleaning, support material removal, post-curing by further UV exposure. [25]

The Vat photopolymerization process is performed in three different ways. The most used is Stereolithography (SLA). This technology employs a vat of liquid photopolymer resin which can be ultraviolet curable and an UV laser for building the object layers one at a time. For each layer, the laser beam traces a cross-section of the part pattern on the surface of the liquid resin. Exposure to the ultraviolet laser light cures and solidifies the pattern traced on the resin and joins it to the layer below. After the pattern has been traced, the SLA’s elevator platform descends by a distance equal to the thickness of a single layer, typically 0.05 mm to 0.15 mm [23]. Then, a resin filled blade sweeps across the cross section of the part, re-coating it with fresh material. On this new liquid surface, the subsequent layer pattern is traced, joining the previous layer. The complete three-dimensional object is formed by this project. Stereolithography requires supporting structures which helps to attach the part to the elevator platform and to hold the object because it floats in the

basin filled with liquid resin. Which are removed manually after the object is finished [23]. SLA uses a variety of photosensitive resins which are made by different materials like ABS-like materials, antimony-free liquid photopolymer, nanoparticle filled composites, low viscosity liquid photopolymer, Polycarbonate, hard plastics, polypropylene type, polycarbonate, Polyethylene type and Ceramic type [23].

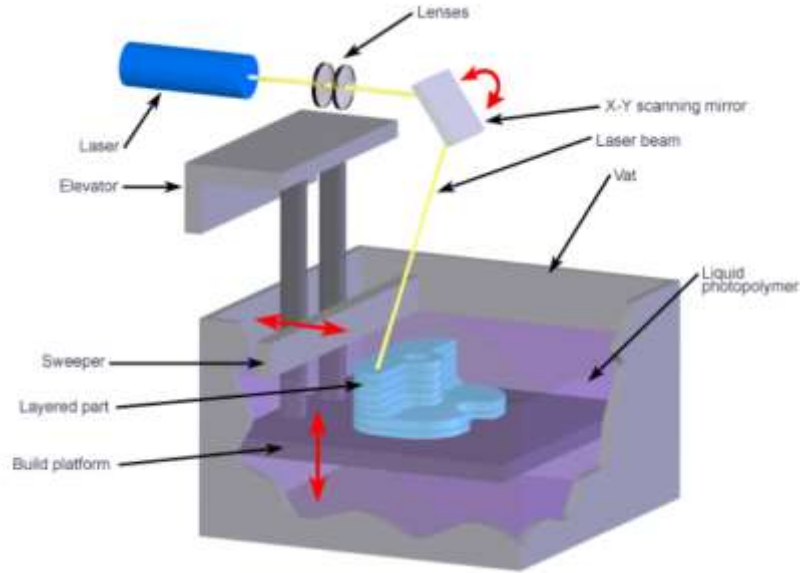


Figure 2-5 Stereolithography (SLA) [26]

Another method is available in the market which is DLP or Digital Light Processing. DLP uses traditional light-sources such as arc lamps to project the desired shape onto a vat of liquid resin. Unlike in SLA, where platforms move downwards after patterns projection, in DLP light projector is located under the platform so that the resin, contained into a tray, is cured from beneath. The platform holding the part will then move up and a new layer of resin will be applied on the tray [16]. This method is quicker than most of the 3D processes due to its light projecting technology that projects a 2D image and not a single spot [16, 27]

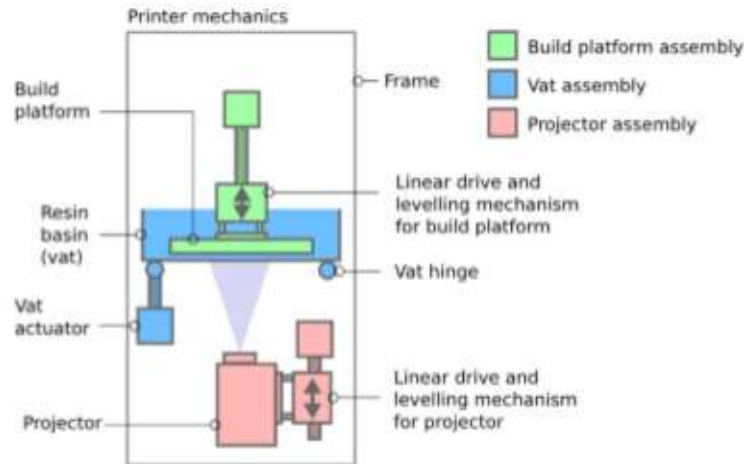


Figure 2-6 DLP process. [16]

CLIP (Continuous Liquid Interface Production) is the newest and fastest process using Vat Photopolymerization. The process begins with a pool of liquid photopolymer resin where some part of pool bottom is transparent (Window). A high-performance LED light engine is projected as a sequence of UV images on printing material (UV curable resin) through window, so that it is partially cured in an accurate and controlled way. The light causes the resin to solidify. The object rises slowly enough to allow the resin to flow under and maintain contact with the bottom of the object. An oxygen-permeable membrane lies below the resin, which creates a “dead zone” (persistent liquid interface) preventing the resin from attaching to the window (photopolymerization is inhibited between the window and the polymerizer). Inventors of CLIP claims that it is 100 times faster than SLA. [28]

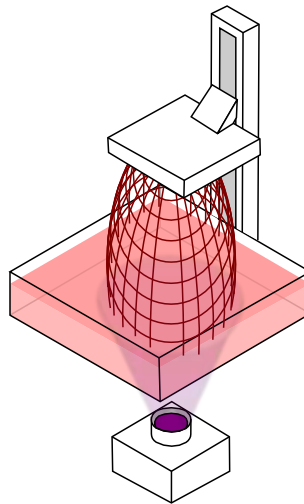


Figure 2-7 CLIP process [28].

2.3.3.2 Material jetting

In this process, droplets of building material is selectively deposited through a small diameter nozzle, similarly to the way a common 2D inkjet paper printer works, but it is applied layer-by-layer to a build platform making a 3D object and then hardened by UV light. According to ISO 17296-2:2016, key features are:

- Feedstock: liquid photopolymer or melted wax, with or without filler.
- Binding mechanism: chemical reaction bonding or adhesion by solidification of melted material.
- Source of activation: radiation light source for chemical reaction bonding.
- Secondary processing: support material removal, post-curing by further radiation light exposure.

In addition to the building material applied by the print head, a wax-based support material is applied to expand the range of geometries achievable by the machine. The support material can be removed using pressurized water [16]. The most common technology associated to material jetting process is Multi-Jet Modelling (MJM), also referred to as Polyjet Matrix (PJM). This technology ensures high speed to the process, because of the

multiple ejection of material from the print head and of the dual UV light system in both sides of the print head. Both attributes enable the production of multiple parts simultaneously and a faster curing process [16].

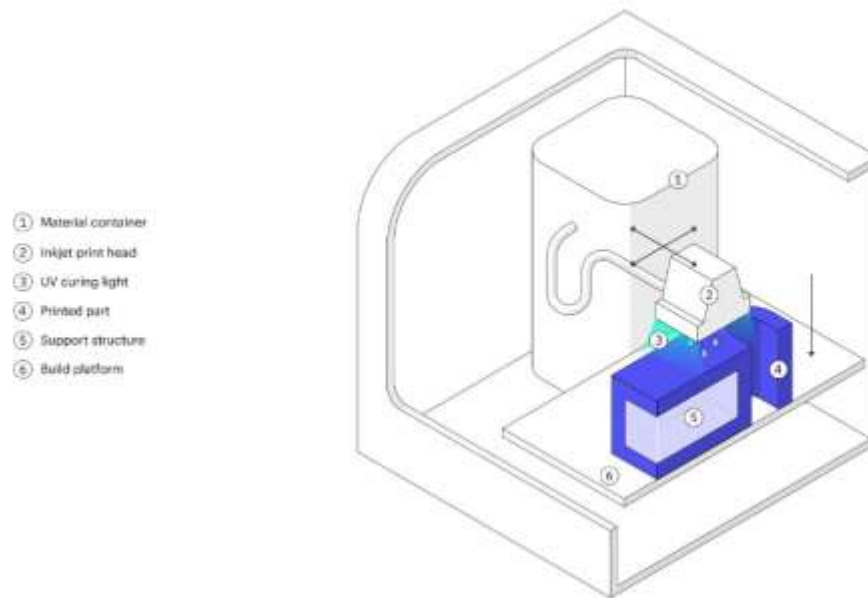


Figure 2-8 Material jetting [29]

2.3.3.3 Binder jetting:

According to ISO 17296-1 definition of binder jetting is “additive manufacturing process in which a liquid bonding agent is selectively deposited to join powder materials”. With binder jetting two materials are used: powder base material and a liquid binder. In the build chamber, powder is spread as a layer and binder is applied through jet nozzles that joins the powder particles together in the required shape as a 2D sliced layer of a 3D object, this process is repeated until part is finished, then the remaining powder is cleaned off and used for further 3D printing process of the next object. features of the process are [23].

- Feedstock: powders, powder blends or particulate materials, and a liquid adhesive/bonding agent.
- Binding mechanism: chemical and/or thermal reaction bonding.
- Source of activation: depending on the bonding agent, chemical reaction.
- Secondary processing: removal of loose powder, impregnation or infiltration of suitable liquid material depending on the powder material and intended application.

Epoxies, waxes, and other adhesives are used for polymer materials, ceramics, and metals. After the printing, the part (which is called as “green part”) is placed in a furnace. Powder particles are bonded by post processing by infiltration with melted material and in sintering initially the binding material is burned off and remaining metal particles sintered together.

After this process the part is reduced about the 20% of volume to diminish this effect the part is printed in large size [29].

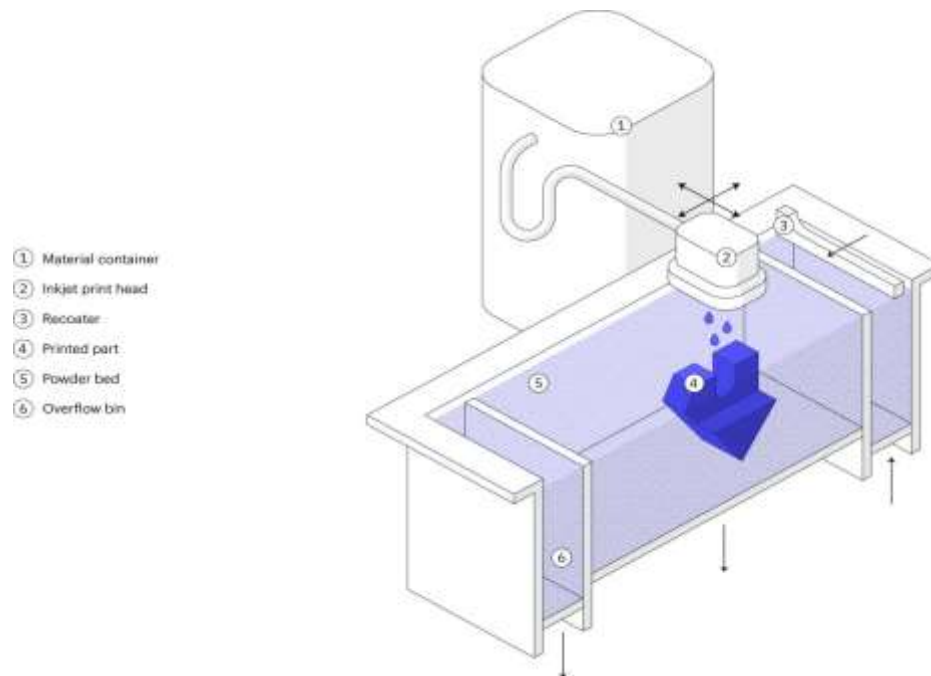


Figure 2-9 Representation of Binder jetting machine. [29]

2.3.3.4 Material extrusion:

According to ISO 17296-1 Material extrusion, is an “AM process in which material is selectively dispensed through a nozzle or orifice”. The key features of this process are [23]:

- Feedstock: filament or paste, typically thermoplastics and structural ceramics.
- Binding mechanism: thermal or chemical reaction bonding.
- Source of activation: heat, ultrasound, or a chemical reaction between components.
- Secondary processing: removal of support structure.

The most used technology in this process is Fused Deposition Modelling (FDM), equivalently referred to as Fused Filament Fabrication (FFF) [16].

Despite other types of additive manufacturing techniques, MEAM is extremely flexible for a large variety of feedstocks. Common materials for MEAM include thermoplastic polymers and composites. Recently new formulations have been produced, with reference to highly filled polymers (HP) which serve as binders for metal or ceramic feedstocks. The majority of MEAM machines are equipped with a single extrusion head, but addition of two or more extrusion units is suitable for multi-material fabrication. Gonzalez-Gutierrez et al. defined and discussed three different classes of MEAM technologies depending on the type of extruder use (plunger, filament and screw material extrusion) [30]

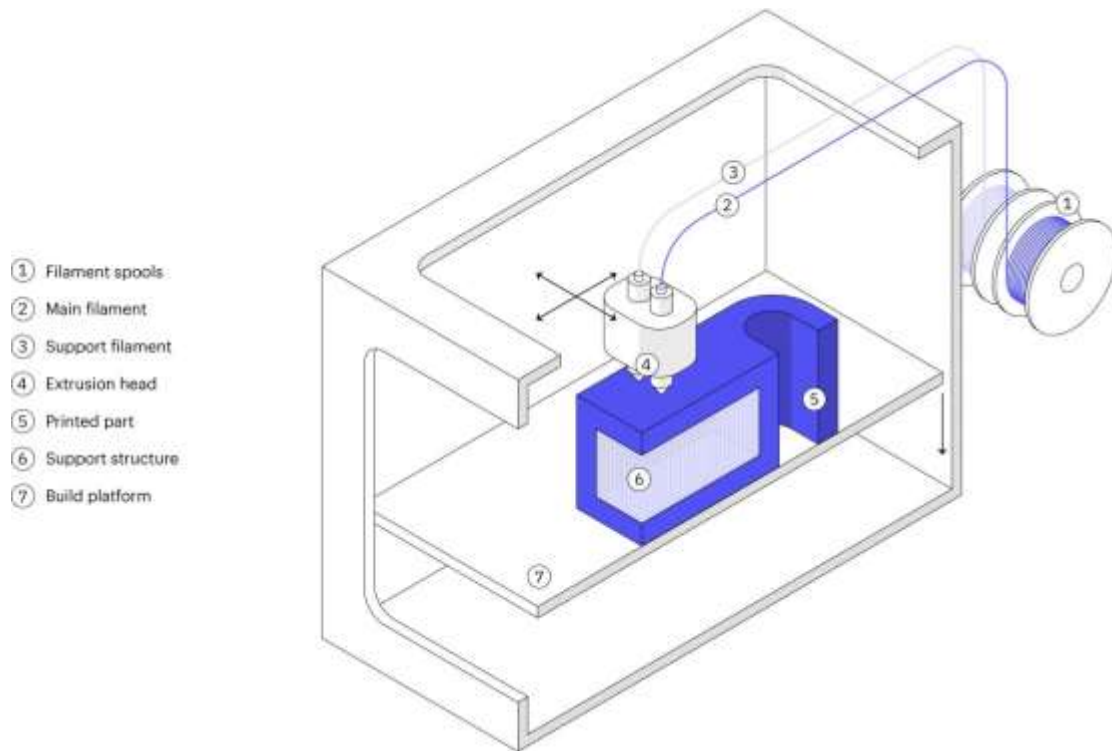


Figure 2-10 Representation of Material Extrusion machine [29].

2.3.3.4.1 Material Extrusion with Plungers:

This Material extrusion technology allows to create 3D objects made of metal or ceramic. At present two American companies, Desktop Metal™ Inc. and Markforged Inc., are providing MEAM machines that use rods which are made up of metal or ceramic powder with a thermoplastic binder system. Desktop Metal™ technology is called Bound Metal Deposition™ (BMD™) and Markforged one is Atomic Diffusion Additive Manufacturing (ADAM). The rods are fitted into cartridges and then they are fed into a plasticizing unit in which highly-filled thermoplastic composite is softened enough for extrusion. Then the soft material accumulates in a reservoir later a plunger pushes the soft material and deposits it onto the building platform in a layer-by-layer manner. Rods can be pushed into the nozzle with higher pressure because of their rigidity. This allows a more consistent and regular deposition [30].

In general, ram extrusion machines with cartridges for shaping parts that will only be made of metal or ceramic, the feedstock rods have a large amount of powder and for obtaining the dense part the printed parts are sintered. Desktop Metal™ rods can contain up to 60 % v/v of metal and 40 % v/v of binder and for Markforged feedstock cannot contain more than 50 % v/v of metal because of higher ductility requirement. The advantage of a feedstock loaded with more metal is to achieve a different density of the printed part while in deposition phase also, having a lower porosity after polymer removal and a higher stability during sintering phase with a lower final porosity from DM™ technology. The binder used by Desktop Metal™ Inc. is partially removed by means of a solvent and then completely removed during sintering [23, 30].

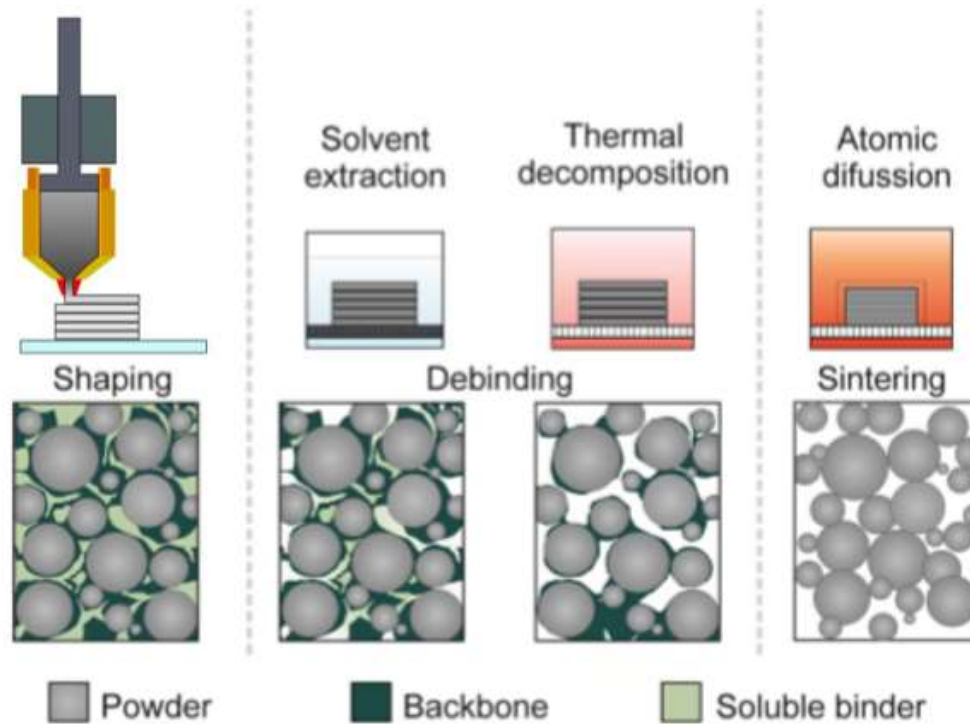


Figure 2-11 Representation of Material Extrusion with Plungers and its process schematic representation [30]

Feedstocks: are multicomponent systems consisting of a polymeric blend, sinterable powder, and additives. All these components are needed to fulfil the requirements at different steps of the overall SDS (shaping, debinding, sintering) process. Details about these different feedstock components are described in the following sections [30].

a) Binder Systems:

The polymeric component is referred as the binder system in feedstock. The production process and the quality of the sintered parts are greatly influenced by the binder system, even though it is completely removed during the debinding step. Usually it contains different types of polymers, waxes, and additives. In general, three main groups in the binder system can be identified:

- i. The main binder component is the largest amount of component present in binder system which is removed during the debinding step. It represents between 50 and 90 vol % of the total binder system.
- ii. The component which will hold together the shape of the part while the main binder component is removed during the first debinding stage is called backbone. It is thermally decomposed prior to sintering. It represents 0 to 50 vol% of the total binder system.
- iii. Additives like dispersant agents, compatibilizers, and stabilizers help to disperse the filler particles in the polymeric binder, preventing agglomeration and phase separation. Additives represent between 0 to 10 vol % of the binder system.

In fact, it is possible to use only one polymeric material for a binder system, but it leads to a very slow process compared to solvent or catalytic debinding due to the debinding step is limited only to thermal degradation.

Main Component (50–90 vol %)	Backbone (0–50 vol %)	Additives (0–10 vol %)
Elastomer and wax	Polymer	Plasticizer, tackifier, oleyl alcohol
Amorphous polyolefin	Amorphous polyolefin	Tackifier, wax, plasticizer, surfactant
Microcrystalline wax	Ethylene Vinyl Acetate (EVA)	None
Thermoplastic elastomer (TPE)	Grafted polyolefin	Unspecified compatibilizer
4 hydroxybenzoic acid-behenylester solid, and 4 hydroxybenzoic acide-thyhexyleste	Co-polyamide (PA) 6/12	None
HDPE	None	Isopropyl tri(dioctyl)pyrophosphato titanate, tri(dioctyl)phosphato zirconate or mixtures thereof
POM	Polyolefin, and other polymer (polyether, polyurethane, polyepoxide, polyamide, etc.)	None
PA	None	Undisclosed
LDPE wax	LDPE	None
Polypropylene	Elastomer	Wax, tackifier, plasticizer

Table 2-1 Examples of binder system compositions used in material extrusion additive manufacturing with highly-filled polymers with filaments [30].

- b) Powder Fillers: Many additive manufacturing technologies use powder as their building material. We use powder in MEAM-HP(material extrusion additive manufacturing with highly-filled polymers), powder is in principle the same metal or ceramic powder as that used in PIM(Powder Injection molding) this gives an advantage compared to other AM techniques that rely on powder bed technology, they require a very specific particle size distribution for the process to work properly. Typical particle sizes used in PIM are fine enough to prevent the plugging of the nozzle (diameter range 0.3 to 0.8 mm) of the MEAM machine [30]. Many metals and ceramics are available for PIM are also works for MEAM-HP, many of them haven't tested yet.

Metal or Ceramic	Type	Powder Content in Feedstock (vol %)
Ceramic	Silicon nitrate (Si ₃ N ₄)	55 and 60
Ceramic	Fused silica (SiO ₂)	56, 60, and 65
Ceramic	Lead zirconium titanate	50 and 52.6
Ceramic	Zirconia	85
Ceramic	Yttria stabilized zirconia	47
Ceramic	Strontium ferrite (SrFe ₁₂ O ₁₉)	53, 55, and 60
Ceramic	Alumina	50
Ceramic	Mullite + Alumina + MgO	47.93 + 6.85 + 0.69 = 55.47
Ceramic	Fused silica + MgO	53 + 3 = 56
Ceramic	Titanium dioxide + MgO	51 + 4 = 55
Metal	Stainless steel (17-4PH)	55 and 60
Metal	Stainless steel (316L)	50 and 55
Metal	Stainless steel (AISI 630)	79
Metal	Tungsten carbide-cobalt	50
Metal	Carbonyl iron	65
Metal	Titanium (Ti6Al4V)	55
Metal	Rare earth magnet (NdFeB)	55

Table 2-2 Ceramics and metals investigated for use in MEAM-HP [30].

Company	Powders
Markforged Inc.	Stainless steels 316L and 17-4PH.
Desktop Metal Inc.	4140 (chrome moly), copper, Kovar F-15, Inconel 625, 316L (austenitic), 17-4 PH, and tool steel H13
AIM3D GmbH	Stainless steels 17-4PH, 316L, 410L, 430 and 440C, tool steel M2, and low-alloy steel 4340
EVO-tech GmbH	Stainless steel 316L

Table 2-3 Feedstocks with powders currently offered by companies; powders in beta phase of development are excluded from the list [30].

Feedstocks preparation: Metal or ceramic powder is mixed with molten binder components to produce a final feedstock, whose composition must be the most homogeneous as possible. Homogeneity is required to minimize segregation of components, which can lead to facial defects, excessive porosity, and cracks in the sintered part. Metal powder is usually produced with one of the following techniques [23]:

- Gas atomization: A metal or alloy is melted through induction or other thermal method. Then the molten metal is forced through a nozzle later a high velocity of gas stream breaks down the melt into fine droplets and while during their falling path droplets are solidify into spherical particles. Usually nitrogen, argon or helium are used as gas. Air is not commonly used because it provokes high surface oxidation, which must be avoided for most materials. The process can produce a wide range distribution of particle sizes.

- Water atomization: It is same as gas atomization. A high-pressure jet stream breaks up the melt material into particles which then solidify. Particles created by this technique will have slightly irregular shapes, this irregularity is useful for shape retention during debinding.
- Thermal decomposition: It is a chemical decomposition caused by heat. The metal is reacted with carbon monoxide to produce metal carbonyl at high temperature and high pressure. The metal carbonyl is purified, cooled, and reheated in presence of a catalyst which leads to vapor decomposition into a powder. Carbon impurities are usually removed by reduction with hydrogen.
- Chemical reduction: Purified oxides are reduced using reducing agent such as carbon to form carbon monoxide or dioxide or with hydrogen. The process can be accelerated at high temperature, even though this leads to diffusion bonds between particles that must be broken by subsequent attrition or milling.

Above the softening point of the binder constituents the powder and the binder are hot mixed to provide a uniform coating to the powder. Mixing processes has both batch and continuous technology. In batch technology has roll mill kneaders and mixers, while in continuous processes has screw extruders and shear rolls. In the case of materials with high tendency to agglomerate, co-rotating screws and shear rolls are preferred because of their high shear obtained. The viscosity of the feedstock determines the shear stress generated during compounding, which in turn determines how well the powder agglomerates are broken and the individual particles are dispersed. Higher temperatures are preferred for feedstocks with a higher viscosity and lower temperatures for feedstocks with low viscosity [30].

2.3.3.4.2 Material Extrusion with Filaments:

Material extrusion of filaments was invented by the company Stratasys [31, 30] and commercialized under the name fused deposition modeling or FDMTM. However, such a name could be applied to other AM techniques that melt materials and deposit them onto a platform or onto previously deposited layers of material so an alternative terminology was introduced as fused filament fabrication or FFF [30]. Fused filament fabrication (FFF) is the most widely used Material extrusion technique. The main reasons for its popularity due to its safe and simple fabrication process (i.e., no powders, lasers, solvents, nor volatile compounds are needed), the low cost of the equipment, and the availability of a great variety of filaments for printing. Process in the FFF is that the filament is extruded through a nozzle and deposited on a building platform one layer at a time, where it solidifies. When a heated chamber and/or heated building platform are available, they kept at temperatures below the material's melting point, but higher than room temperature to reduce thermally induced stresses and to promote adhesion to the printed bed. Without a heated building platform and/or chamber it is still possible to perform MEAM with certain materials at room temperature [30].

FFF machines are ram extruders, where the filament pushes the softened material out of the printing head like ram. In conventional FFF machines the filament is first pulled by the driving wheels and then it is pushed by the same wheels into a liquefier and later into a nozzle. So sufficient mechanical strength is required for the filament for retaining its shape after forced through the drive wheels to transfer the force into the liquefier [30]. This force can be altered by several factors. First, the motors must generate sufficient torque. Next, the wheels must have enough friction with the filament to transfer the force from the wheels to the filament. At the same time, the filament must be strong enough to avoid shearing due to the pinching from the wheels. Finally, the filament must not buckle between the drive wheels and the entrance to the liquefier. In addition to these

requirements, the filament should also be flexible enough to be spooled, so that it can be easily stored in a compact place and fed in a continuous manner into the liquefier [30]. As all materials cannot fulfill all these conditions, yet numerous thermoplastics-based materials are available as filaments for FFF.

Besides positive characteristics there are some limit like surface finish and accuracy because the filament material is extruded through the circular hole so deposited material is round, and build speed is slow because of single model tip which deposit material as each layer of the part and high viscosity of the material restricts the flow rate of the material through the model tip, so low build speed. Due to anisotropic mechanical properties are not the same in all directions [23].



Figure 2-12 Representation of Material Extrusion with Filaments [30]

2.3.3.4.3 Material Extrusion with Screws:

For producing filaments and rods needs additional processes such as extrusion lines and proper machines which can produce filaments or rods of constant cross-sectional area with minimum ovality, which are necessary for a correct deposition in material extrusion machines. In general, not all materials will have the properties for being handled as filaments or as spooled, but at the same times they are rigid enough, so they can be pushed by feeding mechanism. Because of this restrictions, new companies are developing screw extrusion AM systems that utilize pellets instead of filaments. Screw extruders are made up by different zones, solid conveying zone where pellets are transported to the melting zone, in melting zone pellets are softened under heat and friction and the molten material is exposed to high pressure before passing through the nozzle. The rotating screw performs the role of pushing the material from the feeding zone to the nozzle. Several parameters including temperature, pellet size must be controlled to obtain a uniform flow of the extruded material [30].



Figure 2-13 Representation of Material Extrusion with Screws [30].

2.3.3.5 Sheet lamination:

According to ISO 17296-1 defines sheet lamination process as: “AM process in which sheets of material are bonded to form an object”. The process can be done in two ways, using rolls to have a continuous flow or using discontinued sheets subsequently deposited one on another to feed the process [23]. Key features of this process are

- Feedstock: typically sheets of paper, metal foil, polymers or composite sheets formed by metal or ceramic powder material held together by a binder.
- Binding mechanism: thermal reaction, or chemical reaction bonding, ultrasound.
- Source of activation: localized or large-scale heating, chemical reaction, and ultrasonic transducers.
- Secondary processing: removal of waste material, and optionally sintering, infiltration, heat treatment, sanding, or machining to improve surface finish.

Sheets can be metal, paper or a form of polymer. Metal sheets are welded together by ultrasonic welding in layers and then CNC milled into a proper shape (Laminated Object Manufacturing (LOM)). Paper sheets can be used also, but they are glued by adhesive glue and cut in shape by precise blades [29].

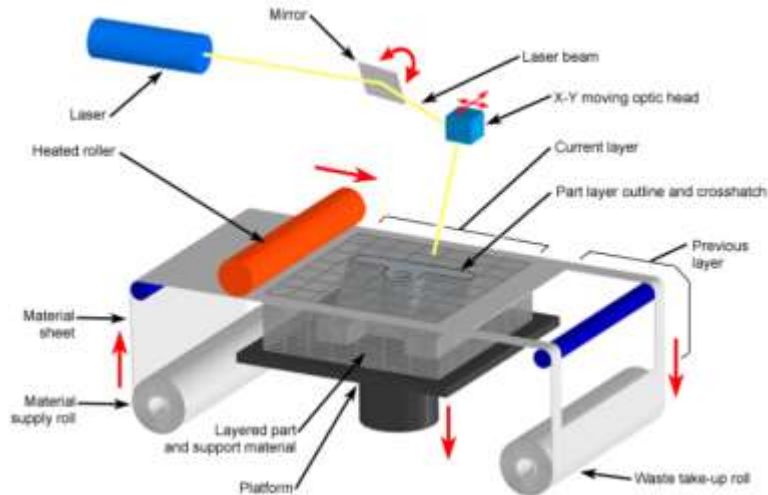


Figure 2-14 Laminated Object Manufacturing (LOM) [26].

2.3.3.6 Directed energy deposition:

According to ISO 17296-1 definition of directed energy deposition is: “AM process in which focused thermal energy is used to fuse materials by melting as they are being deposited”. It is mainly used with metal powders or wire and is often referred to as metal deposition. The 3D printing device is usually attached to a multi-axis robotic arm and consists of a nozzle that deposits metal powder or wire on a surface and an energy source (laser, electron beam or plasma arc) that melts it, forming a solid object [16]. Key features of the process are:

- Feedstock: powder or wire, typically metal, for certain applications ceramic particles can be added to the base material.
- Binding mechanism: thermal reaction bonding via melting and solidification.
- Source of activation: laser, electron beam or plasma transferred arc.
- Secondary processing: surface finish treatments such as machining, micro blasting, laser re-melting, grinding, or polishing and improving material properties (e.g. heat treatments).

This is the only process which is considered “hybrid” among those studied, which means in the same device there are both the additive and the subtractive specific tools. Technologies associated to direct energy deposition are Laser Engineering Net Shape (LENS) and Electron Beam Additive Manufacturing (EBAM). LENS utilizes a deposition head, which contains a laser head, powder dispensing nozzles, and inert gas tubing, to melt powder as it is ejected from the powder dispensing nozzles to build a solid part layer-by-layer. The laser creates a melt pool on the build area and powder is sprayed into the pool, where it is melted and then solidified. The substrate is typically a flat metal plate or an existing part that material is added on (for example for repair). EBAM is used to create metal parts using metal powder or wire, welded together using an electron beam as the heat source. Producing parts in a similar fashion to LENS, electron beams are more efficient than lasers and operate under a vacuum with the technology originally being designed for use in space [23, 16].

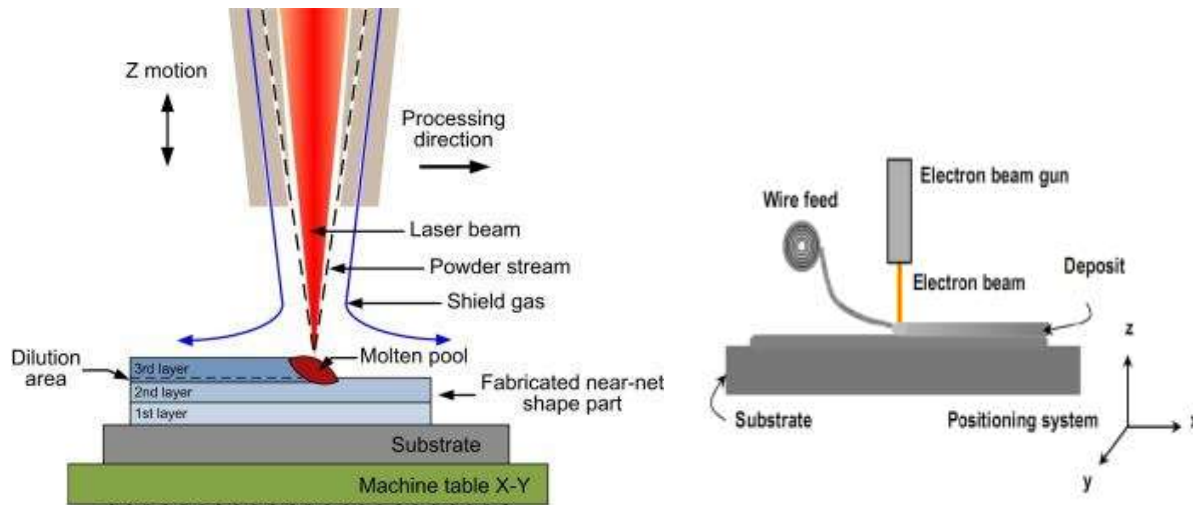


Figure 2-15 left side representation for Laser engineered net shaping (LENS) process [32] and right side representation for Electron Beam Additive Manufacturing (EBAM) [33]

2.3.3.7 Powder bed fusion:

According to ISO 17296-1 defines powder bed fusion as: “AM process in which thermal energy selectively fuses regions of a powder bed”. In this process a container is filled with material powder, that is processed using an energy source, commonly a scanning laser or electron beam. Key features of the process are [23]

- Feedstock: various powders such as thermoplastic polymers, pure metals, or metal alloys, structural or industrial ceramics.
- Binding mechanism: thermal reaction bonding.
- Source of activation: thermal energy, typically transferred from laser, electron beam, and/or infrared lamps.
- Secondary processing: removal of loose powder and, if applicable, support material, and post-process operations to improve surface finish, dimensional accuracy, and material properties.

Powder bed fusion processes were the first commercialized AM processes, among others. The most used technologies are Selective Laser Sintering (SLS), Selective Laser Melting (SLM) or Direct Metal Laser Sintering (DMLS) and the Electron Beam Melting (EBM) [16].

In SLS, a laser selectively sinters the particles of a polymer powder, fusing them together and building a part layer-by-layer. The materials used in SLS are thermoplastic polymers that come in a granular form. Which is used for producing prototypes and for small production runs. Direct Metal Laser Sintering (DMLS) and Selective Laser Melting (SLM) produce parts same as SLS, a laser source selectively bonds together powder particles layer-by-layer. The main difference between the DMLS and SLM processes is, SLM achieves a full melt of the powder particles, while DMLS heats the metal particles to a point that they fuse together on a molecular level. [29]

The Electron Beam Melting (EBM) is like SLM. The most significant difference is that the energy source comes from an electron beam instead of a laser. This process is done in vacuum chamber. The higher power achieved by the heat source (electron beam) enables the machine to process high melting powders. [34].

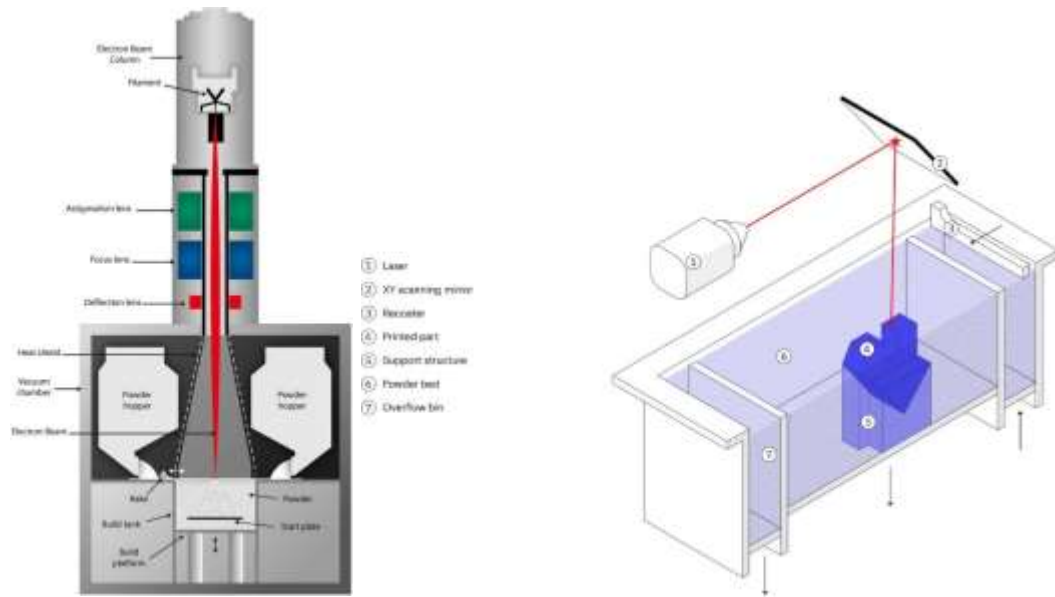


Figure 2-16: Left side shows representation of EBM machine [35] and right side representation for SLS/SLM/DMLS process [29].

Chapter3 Technology Using in Add-It

3.1 Introduction:

Additive Italia Srl (Add-it) is a start-up founded on April 16th, 2018, by Marco Preziosa, which is specialized in simulation driven engineering, generative design, and additive manufacturing. Their collaboration with this project is related to their business in additive manufacturing of metallic parts. As the propeller blade design was provided by EWOL Srl, Desktop Metal's additive manufacturing machine has been chosen for producing of the part. The machine used is Studio System+™ which is an office friendly machine from Desktop Metal™, machine tailored for the machine shop and industrial production are not yet available on the market. Consequently, this machine cannot satisfy large volume demands. For prototyping this machine is perfect fit.

The method which is used for metal printing by Desktop Metal™ is Bound Metal Deposition™ (BMD), which is an “extrusion-based metal additive manufacturing (AM) process where metal components are constructed by extrusion of a powder-filled thermoplastic media. Bound metal rods—metal powder held together by wax and polymer binder—are heated and extruded onto the build plate, shaping a part layer-by-layer. Once printed, the binder is removed via the debind process, and then sintered—causing the metal particles to densify” [36].

This method is discussed in chapter two Additive Manufacturing under Material Extrusion section.

3.2 3D printer:

The Studio System+™ is a 95x83x53 cm printer [37] with glass doors and polycarbonate siding, which allows us 360° view of the build chamber. The machine has an internal camera for the process monitoring, and 7-inch touchscreen display UI for step-by-step guidance and for showing internal elements temperatures and processing time estimation.

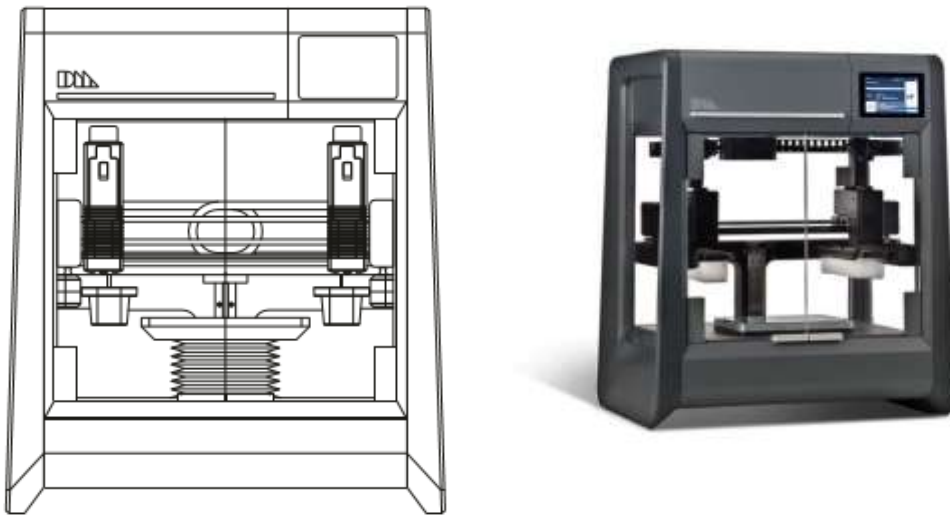


Figure 3-1 Studio System™ 3D printer [37].

The printer is integrated with Fabricate™ software, it is a secure, web-based software constructs build plans from STL or CAD files, automatically generating supports and control parameters based on part geometry and material. Supporting file formats are STL, IGES, JT, STEP, VDA-FS, U3D,

VRML and native file types (SolidWorks, ProE, etc), the interface of the program is customer friendly [37].

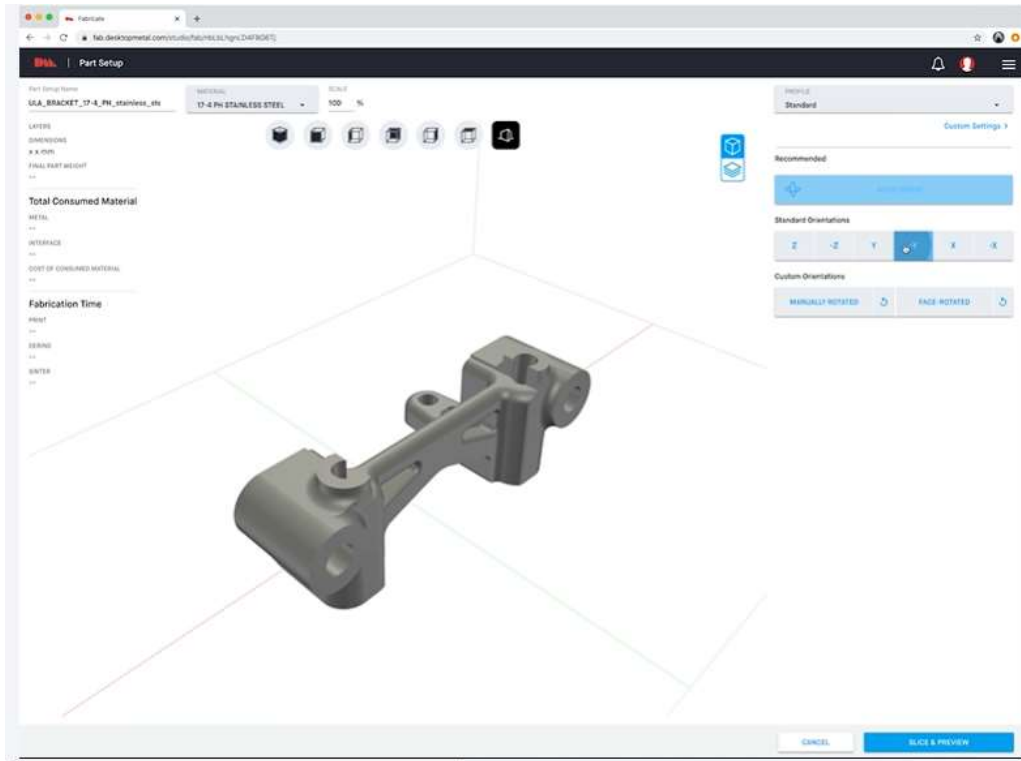


Figure 3-2: Fabricate™ software interface [37].

After importing the CAD model, software allows us to select the material, like stainless steels as 17-4 PH and 316L, H13 tool steel, AISI 4140, Copper and Nickel based superalloy 625 [37]. We can scale the object with respect to the model size in this software. Layer height is 50 μm with high resolution printhead and 100-220 μm with standard resolution printhead [37] the difference lies in the nozzle diameter: 0.40 mm for standard resolution and 0.25 mm for high resolution. the software calculates the approximative total processing time, surface quality and metallic material consumption with also considering supports from selected parameters and the chosen orientation (out of 6 standard combinations). Real-time trade-off analysis can be performed for material consumption and surface quality, like it is possible to minimize the mass consumption as the software can automatically adjust the part orientation, layer thickness and supports, it is also possible to select a custom part orientation, different from the standard ones. In software we have toolpath preview which shows the raft and the structure of each layer of building part, which means the infill pattern, the outer and inner walls, and the supports as well. There is a possibility to set manually each individual printing parameter such as velocity of the extrusion head and many others through advanced menu. After printing set up was done, Fabricate™ displays the final part weight, the number of layers, its dimensions after printing, material consumption and fabrication time partitioned in the different steps.

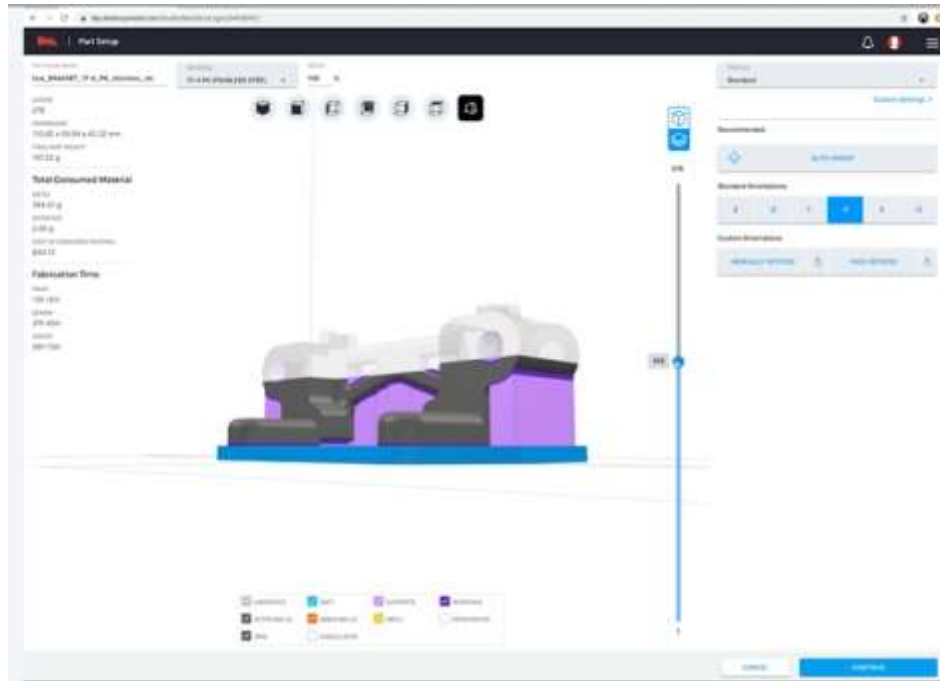


Figure 3-3 Toolpath preview [37].

Finally, the part is located on the platform. We can add more number of parts if required for printing simultaneously in that case software displays the maximum number of the parts which can be added to the selection and their positioning by considering the printer capacity (6.5 kg [37]). Later this assembly is sent to the machine and the 3D printing process starts.

Before starting the material extrusion, the chamber is heated up to 50 °C [37], the extrusion nozzles to 200 °C and the print bed to 65 °C, under the plastic sheet platform vacuum is created to get a planar surface. Printer feedstocks are supplied in form of bars, contained in cartridges. We have two independent extrusion heads: one dedicated to printing bound metal rods and the other for adding ceramic interface medium. For the interface media(ceramic), the printhead nozzle diameter is fixed to 0.40 mm [37] not as metal one. Metal print head can be changeable for different metals to prevent contamination of materials. The raft is printed first, followed by the part and its supports, with a build rate of 16 cm³h⁻¹ [37], this value corresponds to full regime printing, but in practice because of rods refill, the actual build rate is 5-8 cm³h⁻¹. The final part produced is called green part.



Figure 3-4 Changing Material Cartridge and print head [37].



Figure 3-5 Feed stock in form rods (metal powder and binder in form of rods) and Cartridge [37]

3.3 Debinder:



Figure 3-6 Desktop Metal™ debinder [37].

After the green part produced debinding step is required before sintering. DM™ debind process is solvent based. In Studio System+™ debinder unit is a 102 x 74 x 57 cm box, with a low emission design, safe and suitable for an office environment, made of a stainless steel basket with adjustable trays (3 levels) [37]. To dissolve binder main component (wax), green parts are immersed in a debind fluid. Open-pore channels are formed throughout the part in preparation for sintering. Here also everything starts from the Fabricate™ software, where the parts can be selected, added and proper shelving is chosen and software sends information to the machine, and the solvent based debind process will start. Regularly solvent type debinding requires harsh chemicals (odorous and flammable) to remove the main component, which is often a wax, so it necessitates ventilation, so operators are required to wear protective devices during handling, from exposing to open chemicals and wet parts. Desktop Metal™ debinding machine is completely sealed with nonflammable solvent, thus eliminating the need for a fume hood or external ventilation. With only single-chamber processing, the parts enter and exit from the debinder as dry and all the debind fluid is drained during operation, so there is no necessary to wear a mask [37]. The debinding chamber is a 30 x 20 x 20 cm box, maximum fluid volume in processing tank is 17.4 L while a maximum of 22.5 L solvent can be stored inside the storage tank [37]. It has automatic fluid distillation and

recycling so there is no need to refill between each cycle. This guarantees a quasi-continuous use of the unit with easy management.

Binder during the debinding process following each cycle is collected in a disposable waste canister by performing distillation [37]. Distillation is performed by heating the wax and solvent mixture through a heating plate located under the waste canister.



Figure 3-7 Loading debinder with green parts [38].

Desktop Metal™ defines a refill of 1L of solvent every 10 cycles. This value is taken as average, Additive Italia experience is that the amount of solvent consumed during each cycle is depends on total mass to be debinded. The solvent loss is not well explained; may be referred to small amount of solvent evaporation and non-optimal distillation. On-board UI alerts users if the job requires more fluid than is available. Once the canister is full, it automatically reminds the user to dispose of the canister and guides the user through replacement.

The solvent used in Additive Italia process is the DM™ proprietary debind fluid, which contains an organic chlorinated chemical as main component. The safety data sheet of the product states the non-flammability of the solvent mixture. The main component of the mixture is present with a concentration > 90 % and it is a colorless, light liquid with a sweetish odor, forming different azeotropic mixtures both with water and ethanol. Below table shows some of its main properties [23].

Melting point	~ -49.5 °C
Boiling point at 1 atm	~ 48.5 °C
Density at 20 °C	~ 1.26 g·cm ⁻³
Vapor pressure at 0 °C	~ 15.1 kPa
Vapor pressure at 20 °C	~ 35.3 kPa
Heat of evaporation (boiling point)	~ 29 kJ·mol ⁻¹
Critical temperature	~ 243 °C
Critical pressure	~ 5.5 MPa
Flash point	~ 4 °C
Autoignition temperature	~ 459 °C
Octanol/water partition coefficient as log P _{ow}	2.09
Relative vapor density	(air = 1): 3.34

Table 3-1 Main properties of the principal component of the solvent used in the debinding process [23].

Compared to water the solvent is a low boiling chemical with a higher volatility, also it has a positive $\log P_{ow}$, which describes its hydrophobic and lipophilic behaviors and therefore an easiness to be absorbed by the wax material. The debinder solvent is sold by aluminum cans with capacity of 1L [23].

3.4 Furnace:



Figure 3-8 Studio System+™ furnace by Desktop Metal™ [37]

Desktop Metal™ furnace is 161.8 x 138.0 x 75.4 cm sized to fit a doorway and it is the first office-friendly sintering unit available on the market. After debinding step, the part is called brown part and it is ready for the sintering cycle. Brown part is heated to relatively high temperatures in the furnace, so that the polymeric part of the binder is removed, and later the metal particles join, resulting densified part. Depending on the material the part may shrink about 17 to 22 %, during densification [37].

The furnace has an adjustable shelving stackable graphite retort box which designed for batch processing. The graphite retorts allow an optimal thermal conductivity, offering uniform heating. Sintering is performed under inert atmosphere and the graphite retorts provide gas channels, which allow gas flow throughout all layers and improves thermal uniformity [37].

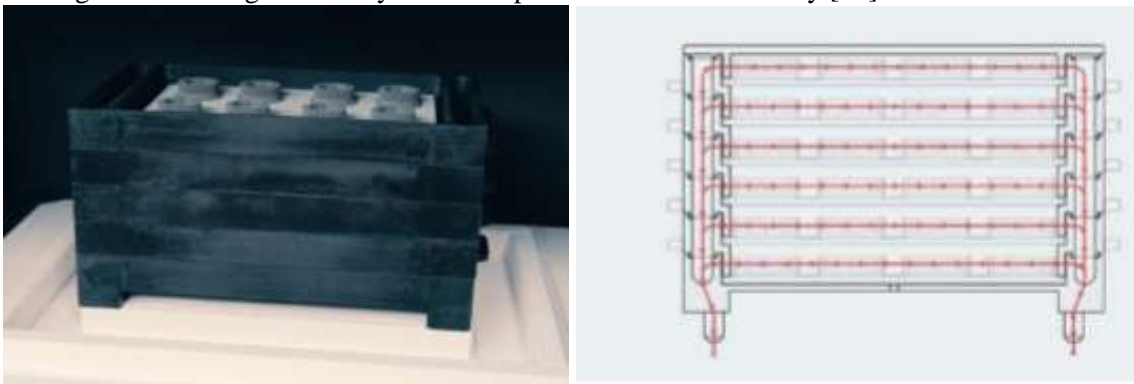


Figure 3-9 Stackable graphite retort box with adjustable shelving and gas channeling [37].

Last step of the process starts from the Fabricate™ software same as printing and debinding. From the software menu we can select the brown parts that just finished the debinding phase, then it

suggests best positioning for parts to place on the stackable graphite retort to achieve the best metallurgical quality possible, then placed manually on the retort by following the program instructions, then the sintering cycle starts. Temperature and pressure evolutions are not accessible during the process from the display on the furnace throughout sintering.

Additive Italia performs the sintering process under argon and hydrogen mixed atmosphere, which are externally supplied by two 900L gas cylinders. However, Additive Italia remark that each sintering cycle requires approximately 750L of gas.

In the cylinders volumetric composition of the gases is 2.66 - 3 % v/v hydrogen and remaining volume is argon. It replaces oxygen inside the chamber to provide inert environment. Argon is usually used for the most reactive alloys. Argon is used instead of nitrogen to avoid nitrogen pick up [37]. Little amount of hydrogen is necessary for the presence of oxygen traces, which prevents metal oxidation by reacting with oxygen to give water.



Figure 3-10 Desktop Metal™ gas cylinder [23].

Software automates and auto-generates the thermal cycle by the itself, creates optimized and tuned for each build and material, to ensure repeatable shrinkage and densification. It is divided into two heating ramps: the first one for binder removal and the second one for part sintering. The rest of the binder in the part is converted to vapor during the initial thermal cycle. Vacuum pump in the furnace sucks the binder vapors from the chamber into a binder trap, where it cools and condense. In this way polymeric part of the binder is collected and sent to disposal. The remaining removal of binder ensures correct metallurgy, regular shrinkage and avoids contamination [37].



Figure 3-11 Binder trap for collecting and removing remaining binder of the part [23].

Heating is performed through SiC elements by generating an average heat load of 2.37 kW. In Desktop Metal™ furnace maximum temperature of 1400 °C can be reached. In normal furnaces

they reach only a maximum temperature of 1300 °C, which limits to 94 % of densification for many steels. Because of higher temperature densification can reach higher values of up to 96 to 99.8 %. The retort surrounded by heating elements from all sides. Better thermal uniformity is provided by placement of these heating elements combined with the stacking retort, they also improve the sintering volume. Uniformity is around +/- 5 °C to sintering temperature [37].

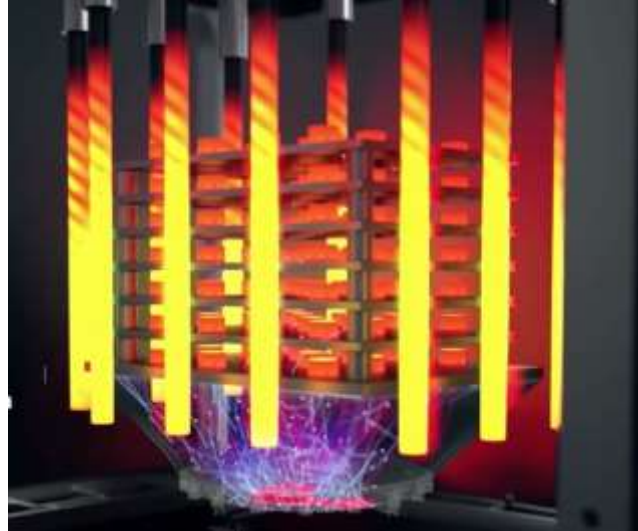


Figure 3-12 Furnace heating system with the SiC heating elements positioned on 4 sides [39].

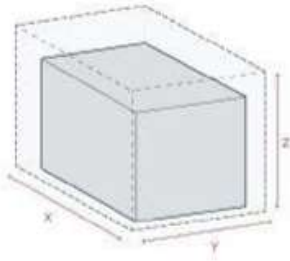
Parts printed using supports, supports are separated by ceramic interface media from the part are do not bond to the metal. This material is disintegrated during sintering due to this the supports can be removed easily from the part. In laser type machines they require rigid supports to aid heat dissipation and resist shrinkage, so they are more difficult to remove and more time require for machining.

3.5 BMD™ guidelines:

BMD™ can build complex structures and geometries, BMD™ part has strength and accuracy which are ideal for prototyping, jigs & fixtures, tooling applications, and low-volume production [36]. BMD™ can also be used to optimize the parts that are already existing and conventionally produced, which can increase their performances and capture benefits from the specific features of this 3D printing technique. It will not make any sense to 3D print simple geometries or parts produced in high volumes due to cost per part but recent innovations reducing this gap. Part geometry, economics, and performance are important factors tied with fabrication.

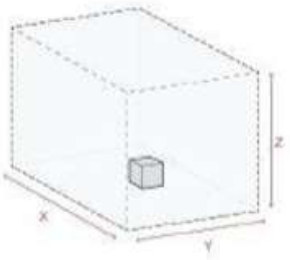
Design guidelines provided by DM™ must be considered and it is recommended to eliminate parts which are not appropriate based on size and/or geometry that cannot be modified by following the BMD™ design guidelines. BMD™ design guidelines are shown in following table.

Standard print head 400 μm	High res. Print head 250 μm
-------------------------------	--------------------------------



Maximum part size

X: 240 mm	X: 60 mm
Y: 150 mm	Y: 60 mm
Z: 155 mm	Z: 60 mm



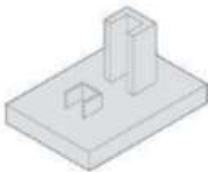
Minimum part size

X / Y / Z: 6 mm X / Y / Z: 3 mm

The minimum part size considers the number of bottom layers, top layers, and wall lines required for a successful part.

Minimum wall thickness

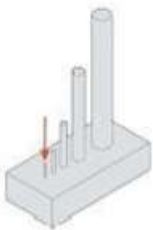
1 mm	0.6 mm
------	--------



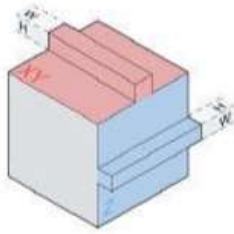
The minimum wall thickness considers structural integrity during printing, debinding, and sintering. Wall thickness must be at least two toolpaths wide.

Minimum pin diameter

3 mm	1.5 mm
------	--------

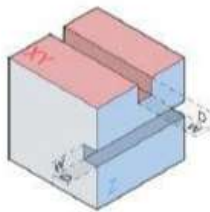


Pins should obey the aspect ratio guideline of 8:1.



Minimum embossed feature

XY	XY
W: 0.45 mm	W: 0.3 mm
H: 0.50 mm	H: 0.3 mm
Z	Z
W: 0.25 mm	W: 0.15 mm
H: 0.50 mm	H: 0.30 mm

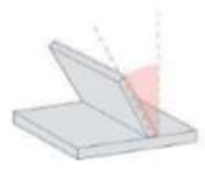


Minimum engraved feature

XY	XY
W: 0.25mm	W: 0.3 mm
H: 0.50 mm	H: 0.3 mm
Z	Z
W: 0.50 mm	W: 0.15 mm
H: 0.45 mm	H: 0.30 mm

Minimum unsupported overhang angle

40° 40°



Overhangs greater than 40° from vertical will require supports, but sintering tolerances must be considered as well. A good practice is to avoid cantilevered masses and small features that cause the entire part to sit on top of support.

Minimum clearance

0.3 mm

0.2 mm

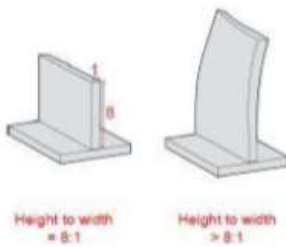


In the fabrication of a moving assembly, components joints should have 0.3mm of clearance.

Aspect ratio

8:1

8:1

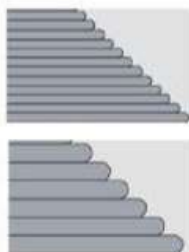


Unsupported tall, thin features are challenging for debind and sintering processes and should be limited when possible. The ratio of height to width for tall walls or pillars should not exceed 8:1. Tall cylinders and walls are the least stable geometries.

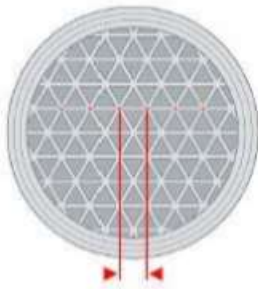
Layer height

150 - 200 μm

50 μm



Larger layer heights allow for faster print times, but there is a trade-off between print time and surface quality. Parts with fine features are better suited to a finer layer height to ensure that small features are accurately printed. Larger parts can make use of the coarse profile to ensure fast print times

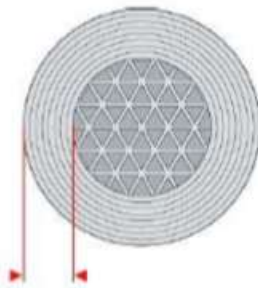


Infill line spacing

2.8 mm

1.75 mm

The default setting for infill line spacing is 2.8 mm for the standard print head and 1.75 mm for the high-res printhead.



Maximum shell thickness

4 mm Part with
infill

4 mm Part with
infill

Together, the part's walls, top layers, and bottom layers comprise the part shell. The limit to shell thickness is the

10 mm Part
without infill

10 mm Part
without infill

Table 3-2 BMD™ guidelines for Studio System+™ 3D printing machine [40].

Complex structures provided by BMD™ also includes parts with fully enclosed, fine voids. Internal lattice structures can be printed within the part except for extremely small geometries. With the powder bed AM methods closed cell infill is not possible, such as selective laser melting, which are restricted to open-cell lattices for removing unbound powder from the void spaces. The infill affects both printing and debind time. The time required to debind a part is directly related to cross sectional thickness, which can be reduced by printing with infill. Infill also reduces the weight of a part while maintaining the outer design of the part [36].



Figure 3-13 Left side shows Cross sectional thickness based on wall thickness and internal infill [40] and Right side shows Example of internal infill of a part. Courtesy of Additive Italia Srl.

Combination of outside shell and infill-based structures provide better rigidity at minimal weight. The shape of the infill geometry has a significant impact on both the effective modulus and the degree of anisotropy of structural properties. Triangular infill offers several benefits over hexagonal or square infill geometries and it results in a constant elastic modulus in the X-Y plane, ranging from 18-28 % of the solid material's elastic modulus [40]. BMD™ can be applied to any sinterable powder that can be compounded with thermoplastic media. Up to now, DM™ has reported the production of parts with different materials such as 17-4 stainless steel, 316 stainless steel and H13 tool steel. Materials under development are Alloy 625, AISI 4140 and copper.

Chapter4 Computational fluid dynamics (CFD)

4.1 Introduction

In this chapter basics of Computational Fluid Dynamics which are related to thesis are discussed. Turbulence and its models weren't discussed in this chapter.

Computational fluid dynamics (CFD) is a branch of fluid mechanics that analyze and solve problems involving fluid flows, using numerical analysis and data structures. Computers are used for performing the calculations for simulation of free-stream flow of the fluid, and the interaction between fluid (liquids and gases) and surfaces defined by boundary conditions.

Modern day CFD development started with advancement of digital computer in the early 1951. Initially the basic tools used in the solution of partial differential equations are Finite Difference Methods (FDM) and Finite Element Methods (FEM) for Structural and Fluid dynamics problems. First paper was presented about using FDM for the solution of stress analysis of masonry dam in 1910 by Richardson at Royal society of London. First FEM work was published in the *Aeronautical Science Journal* in 1956 by Turner, Clough, Martin, and Topp about aircraft stress analysis. Later this methods extensively developed in heat transfer, fluid dynamics etc. [41]. Later several researchers were used FEM and FDM in CFD for different applications and developed several methods [41]. Finite Volume Methods (FVM) has grown more popularity recently due to their simple data structure, its formulation relates to both FDM and FEM. Flowfield-dependent variation (FDV) [Chung 1999] has relation with both FEM and FDM [41].

4.2 Conservation laws

In CFD problem is solved by solving governing equations. Governing equations of the fluid flow represent mathematical statements of the conservation laws of physics.

- Law of Conservation of Mass.
- Law of Conservation of Momentum (Newton's second law: the change of momentum equals the sum of forces on a fluid particle).
- Law of Conservation of energy (Thermodynamics First law: rate of change of energy equals the sum of rate of heat addition to and work done on fluid particle).

Law of conservation of energy wasn't discussed in following sections because of not used in thesis work.

Consider a small fluid element with sides δx , δy and δz which is shown in following figure.

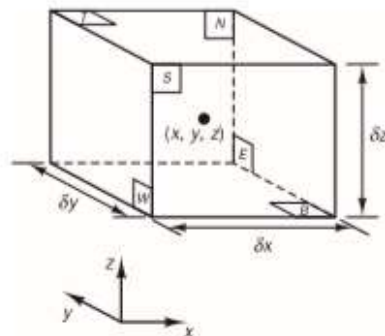


Figure 4-1 Fluid element [42].

The six faces are named as N, S, E, W, T and B, which means for North, South, East, West, Top and Bottom and flow positive directions along the coordinate axes. The center of the element is at position (x, y, z) . All fluid properties are functions of space and time so we need to write $\rho(x, y, z, t)$, $p(x, y, z, t)$, $T(x, y, z, t)$ and $u(x, y, z, t)$ for the density, pressure, temperature and the velocity vector respectively. The density at the center (x, y, z) of a fluid element at time t is denoted by ρ and x-derivative of pressure at (x, y, z) and time t by $\frac{\partial p}{\partial x}$, the element considered is very small so fluid properties at the faces can be expressed by means of the first two terms of a Taylor series expansion [42]. For example, the pressure at the W and E faces, with a distance of $\frac{1}{2}\delta x$ from the center of element can be written as

$$p - \frac{\partial p}{\partial x} \left(\frac{1}{2}\delta x\right)$$

And

$$p + \frac{\partial p}{\partial x} \left(\frac{1}{2}\delta x\right)$$

4.2.1 Mass conversion in three dimensional:

According to law of conservation of mass is that mass can neither be created nor destroyed. So, in infinitesimal fluid element rate of increase of mass into fluid element must be equal to Net rate of flow of mass in fluid element [42].

The rate of increase of mass in the fluid element is:

$$\frac{\partial}{\partial t} (\rho \delta x \delta y \delta z) = \frac{\partial \rho}{\partial t} (\delta x \delta y \delta z)$$

The mass flow rate across a face of the element is given by the product of density, area, and the velocity component normal to the face. In Figure 4-2 rate of flow of mass into the element and exiting element across its boundaries can be seen.

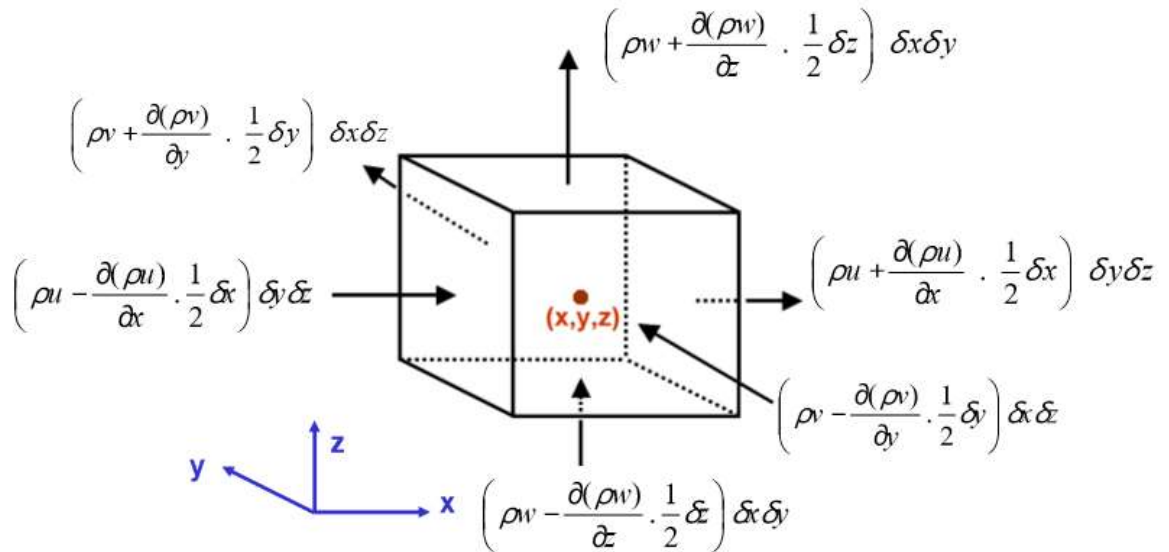


Figure 4-2 Mass flow in and out of a fluid element [43].

By solving the inflow and outflow of mass in the fluid element from figure we will get

$$\frac{\partial \rho}{\partial t} + \frac{\partial(\rho u)}{\partial x} + \frac{\partial(\rho v)}{\partial y} + \frac{\partial(\rho w)}{\partial z} = 0$$

Or

$$\frac{\partial \rho}{\partial t} + \text{div}(\rho \mathbf{u}) = 0$$

The above equation is the unsteady three-dimensional mass conservation or continuity equation at a point in a compressible fluid. The first term on the left-hand side of the equation is the rate of change of density while second term is net flow of mass out of the element across its boundaries and is called the convective term [42]. For an incompressible fluid (i.e. a liquid) the density is constant, and equation will become as

$$\frac{\partial u}{\partial x} + \frac{\partial v}{\partial y} + \frac{\partial w}{\partial z} = 0$$

4.2.2 Momentum equation in three dimensional:

Law of conservation of momentum states that the total momentum of an isolated system remains constant. So, rate of increase of momentum of fluid particle must be equal to sum of forces on fluid particle. The rates of increase of x, y, and z momentum per unit volume of a fluid particle are

$$\rho \frac{Du}{Dt} \quad \rho \frac{Dv}{Dt} \quad \rho \frac{Dw}{Dt}$$

Two types of forces on fluid particle are distinguished as surface forces (pressure forces, viscous forces) and body forces (centrifugal force, Coriolis force, electromagnetic force). In the momentum equations surface forces and body forces are separated body forces as source terms.

The stresses of a fluid element is defined in terms of the pressure and the nine viscous stress components shown in Figure 4-3. The pressure (as normal stress), viscous stresses is denoted by p , τ . The suffix notation τ_{ij} is given to indicate the direction of the viscous stresses, in τ_{ij} suffix says that the stress component acts in the j -direction on a surface normal to the i -direction.

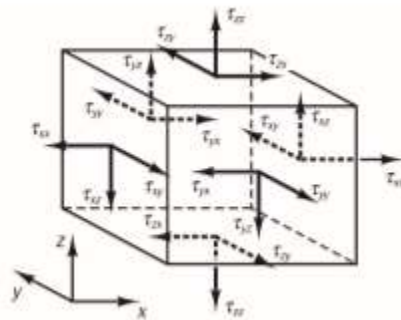


Figure 4-3 Stress components on three faces of fluid element [42].

Initially in x direction stress components are considered and solved these stress components are shown in following figure. The net force in the x-direction is the sum of the force components acting in that direction on the fluid element.

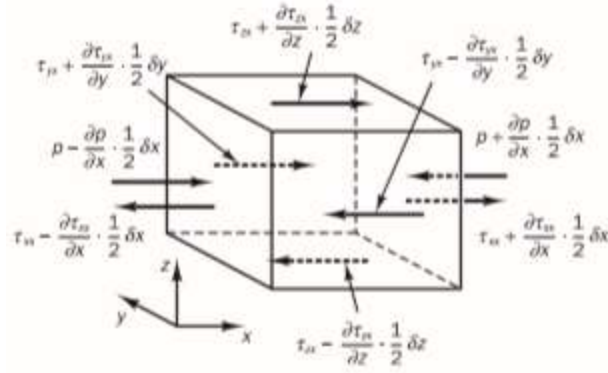


Figure 4-4 Stress components in the x-direction [42].

The x-component of the momentum equation is obtained by setting the rate of change of x-momentum of the fluid particle equal to the total force in the x-direction on the element due to surface stresses plus the rate of increase of x-momentum due to sources:

$$\rho \frac{Du}{Dt} = \frac{\partial(-p+\tau_{xx})}{\partial x} + \frac{\partial\tau_{yx}}{\partial y} + \frac{\partial\tau_{zx}}{\partial z} + S_{Mx}$$

Similarly, y-component and z-component of the momentum equations respectively is given by

$$\rho \frac{Dv}{Dt} = \frac{\partial\tau_{xy}}{\partial x} + \frac{\partial(-p+\tau_{yy})}{\partial y} + \frac{\partial\tau_{zy}}{\partial z} + S_{My}$$

$$\rho \frac{Dw}{Dt} = \frac{\partial\tau_{xz}}{\partial x} + \frac{\partial\tau_{yz}}{\partial y} + \frac{\partial(-p+\tau_{zz})}{\partial z} + S_{Mz}$$

Sign associated with the pressure is opposite to the normal viscous stress, due to sign convention takes tensile stress to be the positive, here pressure is a compressive normal stress so minus sign. The effect of surface stresses is accounted for explicitly: the source terms S_{Mx} , S_{My} and S_{Mz} include contributions due to body forces only. For example, the body force due to gravity would be modelled by $S_{Mx} = 0$, $S_{My} = 0$ and $S_{Mz} = -\rho g$ [42].

4.3 Navier-Stokes equations for a Newtonian fluid

The governing equations for mass and momentum conservation contain unknowns the viscous stress components τ_{ij} . A model for the viscous stresses τ_{ij} introduced for obtaining the useful forms of the conservation equations for fluid flows. In various fluid flows the viscous stresses are expressed as functions of the local deformation rate or strain rate. In three-dimensional flows the local rate of deformation is composed of the linear deformation rate and the volumetric deformation rate [42].

The rate of linear deformation of a fluid element has nine components in three dimensions, six of which are independent in isotropic fluids (Schlichting, 1979) denoted by the symbol s_{ij} . The suffix system is similar to stress components [42].

There are three linear elongating deformation components:

$$s_{xx} = \frac{\partial u}{\partial x} \quad s_{yy} = \frac{\partial v}{\partial y} \quad s_{zz} = \frac{\partial w}{\partial z}$$

The six shearing linear deformation components are:

$$s_{xy} = s_{yx} = \frac{1}{2} \left(\frac{\partial u}{\partial y} + \frac{\partial v}{\partial x} \right) \quad s_{xz} = s_{zx} = \frac{1}{2} \left(\frac{\partial u}{\partial z} + \frac{\partial w}{\partial x} \right) \quad s_{yz} = s_{zy} = \frac{1}{2} \left(\frac{\partial v}{\partial z} + \frac{\partial w}{\partial y} \right)$$

The volumetric deformation is given by:

$$\text{div } \mathbf{u} = \frac{\partial u}{\partial x} + \frac{\partial v}{\partial y} + \frac{\partial w}{\partial z}$$

In a Newtonian fluid the viscous stresses are proportional to the rates of deformation. The three-dimensional form of Newton's law of viscosity for compressible flows involves two constants of proportionality:

1. Dynamic viscosity μ , to relate stresses to linear deformations
2. Viscosity λ , to relate stresses to the volumetric deformation.

The nine viscous stress components in which six are independent, they are:

$$\begin{aligned} \tau_{xx} &= 2\mu \frac{\partial u}{\partial x} + \lambda \text{div } \mathbf{u} & \tau_{yy} &= 2\mu \frac{\partial v}{\partial y} + \lambda \text{div } \mathbf{u} & \tau_{zz} &= 2\mu \frac{\partial w}{\partial z} + \lambda \text{div } \mathbf{u} \\ \tau_{xy} = \tau_{yx} &= \mu \left(\frac{\partial u}{\partial y} + \frac{\partial v}{\partial x} \right) & \tau_{xz} = \tau_{zx} &= \mu \left(\frac{\partial u}{\partial z} + \frac{\partial w}{\partial x} \right) & \tau_{yz} = \tau_{zy} &= \mu \left(\frac{\partial v}{\partial z} + \frac{\partial w}{\partial y} \right) \end{aligned}$$

Viscosity λ is not known much due to its effect is small in practice. For gases, a good approximation obtained by taking the value $\lambda = -\frac{2}{3}\mu$ (Schlichting, 1979). Liquids are incompressible so the mass conservation equation is $\text{div } \mathbf{u} = 0$ and the viscous stresses are twice the local rate of linear deformation times the dynamic viscosity. Substitution of the above shear stresses into moments equation it yields the so-called Navier–Stokes equations, named after the two nineteenth-century scientists who derived them independently [42]:

x-component:

$$\rho \frac{Du}{Dt} = -\frac{\partial p}{\partial x} + \frac{\partial}{\partial x} \left(2\mu \frac{\partial u}{\partial x} + \lambda \text{div } \mathbf{u} \right) + \frac{\partial}{\partial y} \left[\mu \left(\frac{\partial u}{\partial y} + \frac{\partial v}{\partial x} \right) \right] + \frac{\partial}{\partial z} \left[\mu \left(\frac{\partial u}{\partial z} + \frac{\partial w}{\partial x} \right) \right] + S_{Mx}$$

y-component:

$$\rho \frac{Dv}{Dt} = -\frac{\partial p}{\partial x} + \frac{\partial}{\partial y} \left(2\mu \frac{\partial v}{\partial y} + \lambda \text{div } \mathbf{u} \right) + \frac{\partial}{\partial x} \left[\mu \left(\frac{\partial u}{\partial y} + \frac{\partial v}{\partial x} \right) \right] + \frac{\partial}{\partial z} \left[\mu \left(\frac{\partial v}{\partial z} + \frac{\partial w}{\partial y} \right) \right] + S_{My}$$

z-component:

$$\rho \frac{Dw}{Dt} = -\frac{\partial p}{\partial x} + \frac{\partial}{\partial z} \left(2\mu \frac{\partial w}{\partial z} + \lambda \text{div } \mathbf{u} \right) + \frac{\partial}{\partial x} \left[\mu \left(\frac{\partial u}{\partial z} + \frac{\partial w}{\partial x} \right) \right] + \frac{\partial}{\partial y} \left[\mu \left(\frac{\partial v}{\partial z} + \frac{\partial w}{\partial y} \right) \right] + S_{Mz}$$

Rearranging the viscous stresses terms for x component:

$$\begin{aligned} \frac{\partial}{\partial x} \left(2\mu \frac{\partial u}{\partial x} + \lambda \text{div } \mathbf{u} \right) + \frac{\partial}{\partial y} \left[\mu \left(\frac{\partial u}{\partial y} + \frac{\partial v}{\partial x} \right) \right] + \frac{\partial}{\partial z} \left[\mu \left(\frac{\partial u}{\partial z} + \frac{\partial w}{\partial x} \right) \right] = \\ \frac{\partial}{\partial x} \left(\mu \frac{\partial u}{\partial x} \right) + \frac{\partial}{\partial y} \left(\mu \frac{\partial v}{\partial y} \right) + \frac{\partial}{\partial z} \left(\mu \frac{\partial w}{\partial z} \right) + \left[\frac{\partial}{\partial x} \left(\mu \frac{\partial u}{\partial x} \right) + \frac{\partial}{\partial y} \left(\mu \frac{\partial v}{\partial x} \right) + \frac{\partial}{\partial z} \left(\mu \frac{\partial w}{\partial x} \right) + \frac{\partial}{\partial x} \left(\lambda \text{div } \mathbf{u} \right) \right] \\ = \text{div } (\mu \text{grad } \mathbf{u}) + [S_{Mx}] \end{aligned}$$

The viscous stresses in the y- and z-component equations can be written in a similar manner.

$$S_M = S_M + [S_M]$$

The Navier–Stokes equations for the development of the finite volume method can be written as:

$$\rho \frac{Du}{Dt} = -\frac{\partial p}{\partial x} + \text{div } (\mu \text{grad } \mathbf{u}) + [S_{Mx}]$$

$$\rho \frac{Dv}{Dt} = -\frac{\partial p}{\partial x} + \text{div } (\mu \text{grad } \mathbf{v}) + [S_{My}]$$

$$\rho \frac{Dw}{Dt} = -\frac{\partial p}{\partial x} + \text{div } (\mu \text{grad } \mathbf{w}) + [S_{Mz}]$$

4.4 Discretization

Analytical methods, which are applicable for simplified flow problems only. The space where the flow which is to be computed is called the physical space and it is divided into a large number of geometrical elements called grid cells(mesh). Grid generation by placing first grid points (also called nodes or vertices) in the physical space and then connecting them by using straight lines called s grid lines. In two dimensional grids are like triangles or quadrilaterals, and in three dimensions like tetrahedra, hexahedra, prisms, or pyramids. The most important requirement for grid generation tool that is there shouldn't be any holes between the grid cells and also that the grid cells do not overlap on each other. There exist basically two types of grids which are structured and unstructured grids.

- Structured grids: each grid point (vertex, node) can be uniquely identified. It is shown in figure 4-4 where each grid point is uniquely identified by the indices i, j, k and the corresponding Cartesian coordinates $x_{i,j,k}$, $y_{i,j,k}$, and $z_{i,j,k}$.

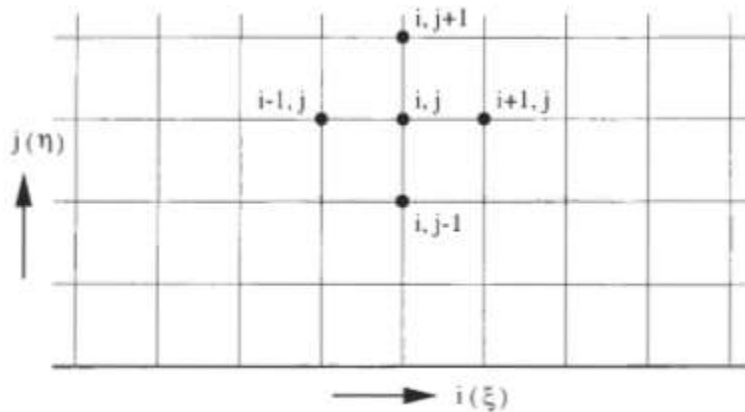


Figure 4-5 Structured grid [44].

- Unstructured grids: grid cells and grid points do not have any particular ordering, i.e., neighboring cells or grid points cannot be identified directly by their indices. In past grid cells were triangles in 2D and tetrahedra in 3D for this type but today it consist of a mix of quadrilaterals and triangles in 2D and of hexahedra, tetrahedra, prisms and pyramids in 3D, in order to resolve the boundary layers properly.

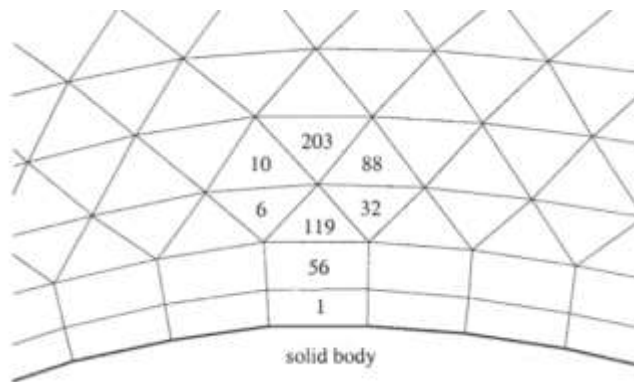


Figure 4-6 Unstructured grid, numbers are marked to individual cells to shows that it doesn't have any particular order as in structured [44].

4.4.1 Finite Volume Method:

The finite volume method utilizes the conservation laws directly (the integral formulation of the Navier-Stokes equations). It was first used by McDonald [44] for the simulation of 2-D inviscid flows. The finite volume method discretizes the governing equations by first dividing the physical space into a number of control volumes. There are many possibilities for defining the shape and position of the control volume with respect to the grid.

The two basic approaches can be distinguished as:

- Cell-centered scheme: the flow quantities are stored at the centroids of the grid cells. So, the control volumes are identical to the grid cells.
- Cell-vertex scheme: the flow variables are stored at the grid points. The control volume can be either union of all cells sharing the grid point, or some volume centered around the grid point.

In first case overlapping of control volumes, in the second case of dual control volumes.

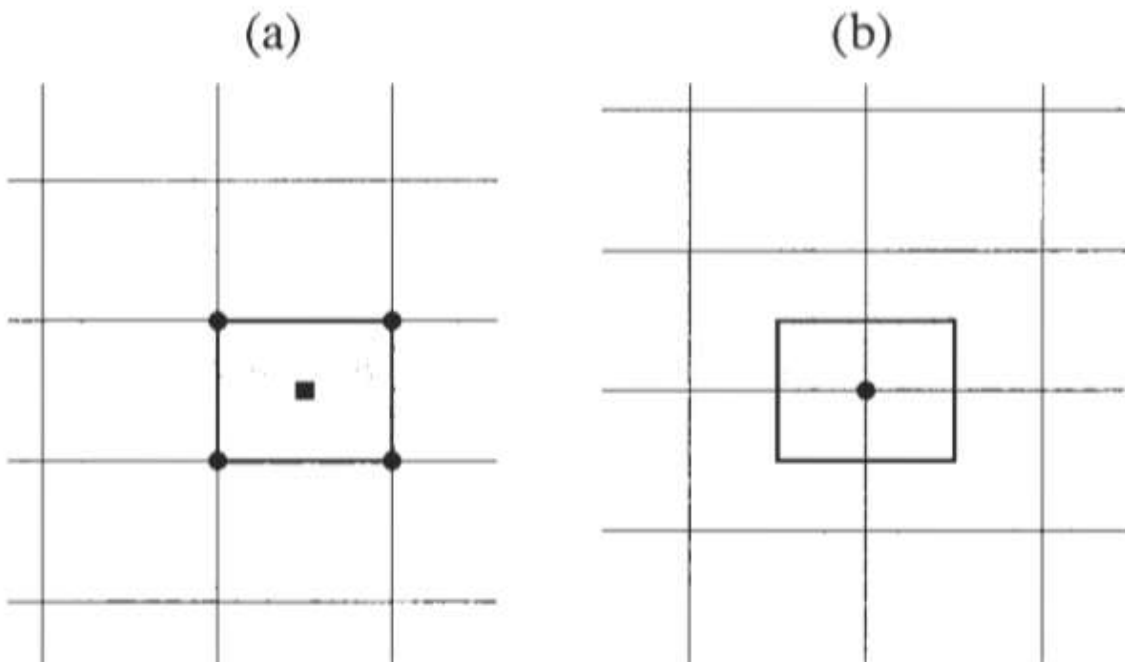


Figure 4-7 Control volume of cell-centered (a) and cell-vertex (b) scheme [44].

The main advantage of the finite volume method is that the spatial discretization is carried out directly in the physical space. So, there will be no problems with any transformation between coordinate systems and it is very flexible so, it can be easily implemented on structured and on unstructured grids. This leads the finite volume method suitable for the treatment of flows in complex geometries [44].

4.5 Mesh Quality:

Doing an appropriate mesh is so important for a CFD simulation because it has a tremendous impact on simulation results. Although there is no specific rule for meshing, however it should meet some quality requirements, there are some parameters like skewness, aspect ratio, orthogonality.

4.5.1 Cell aspect ratio:

The Cell aspect ratio can be defined as the ratio of longest edge length to shortest edge length of a mesh cell. It should be equal to 1 for an ideal mesh. (Note: It is less important in boundary layer mesh). The aspect ratio is a measure of the stretching of a cell. It can also be computed as the ratio of the maximum value to the minimum value of any of the following distances: the distances between the cell centroid and face centroids, and the distances between the cell centroid and nodes [45].

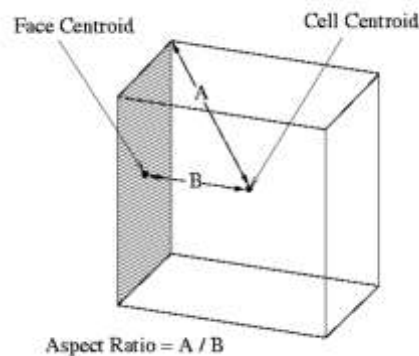


Figure 4-8 Calculating the Aspect Ratio for a Mesh cell [45].

4.5.2 Skewness:

It is one of the key quality parameter for a mesh. It can be measured by using the distance between the intersection of the line connecting two cell centers with their common face and center of that face. According to the definition of skewness, a value of 0 indicates an equilateral cell (best) and a value of 1 indicates a completely degenerate cell (worst). Highly skewed faces and cells are not acceptable because the equations being solved by assume that the cells are relatively equilateral or equiangular [45].

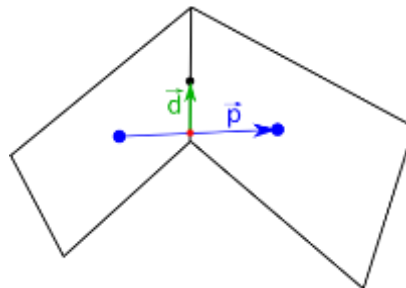


Figure 4-9 Skewness [46].

4.5.3 Mesh orthogonality:

The mesh orthogonality can be measured by using the angle between the connecting lines of two cell centers and the normal of their common face. The orthogonality measure ranges from 0 to 1. Value should be always near to the 1 for best quality.

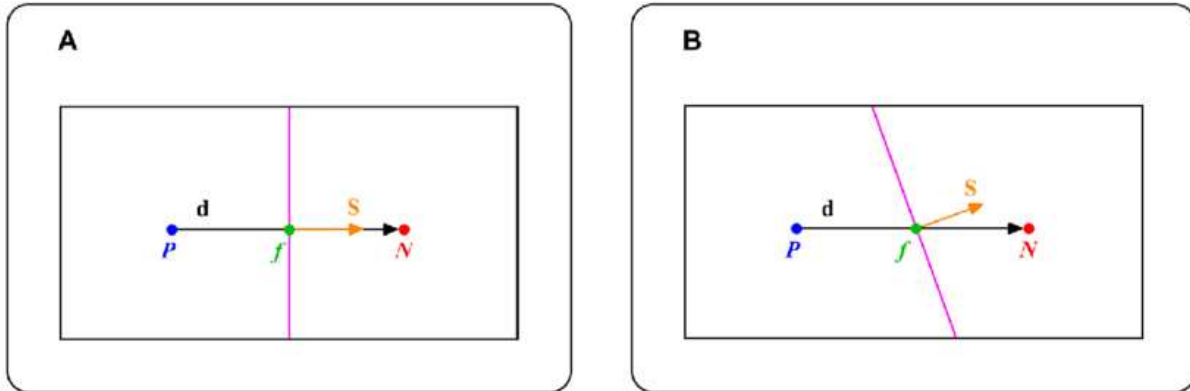


Figure 4-10 A) Vector d and S , on an orthogonal mesh. B) Vector d and S , on a non-orthogonal mesh [47].

Chapter5 Analysis of the component - Propeller blade

5.1 Introduction

In this chapter propeller blade loads identification, stresses in the blade, geometric constraints, roughness constraints etc. are discussed.

The propeller blade CAD design was provided by EWOL, which is a part of a 17-inch boat propeller, here 17-inch represents propeller diameter and modified version of blade's 3D design is shown in figure 5-1. Design is modified for ease of analysis. The propeller is righthand propeller which means from looking backside (aft side) of the ship the propeller rotates clockwise, and ship moves forward in direction.

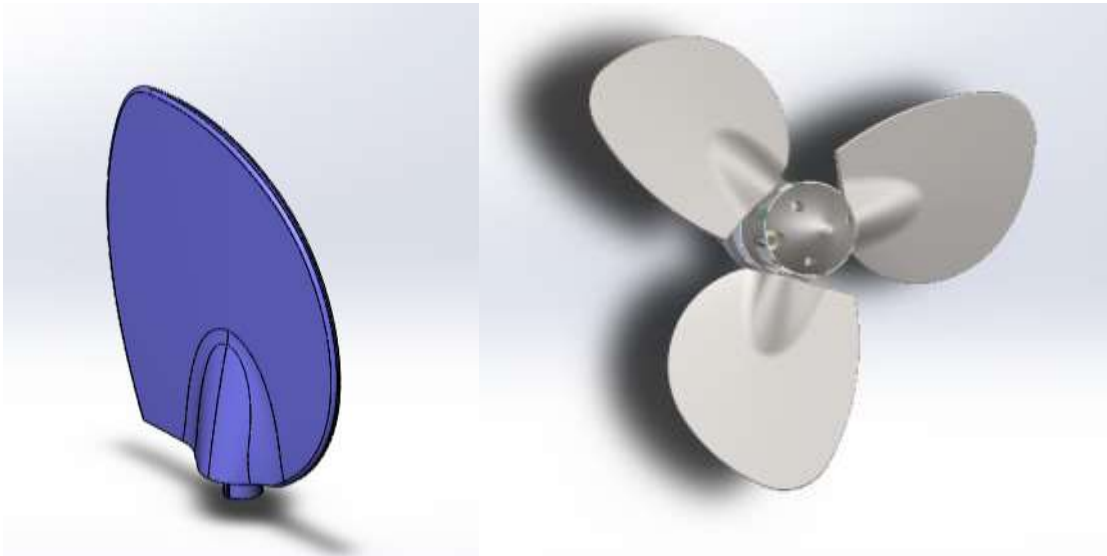


Figure 5-1 Left side shows modified 17” propeller’s blade 3D design and Right side shows 17” propeller assembly 3D design Courtesy by EWOL Srl.

5.2 Identifications of loads subjected by 17” propeller’s blade (CFD analysis):

Ansys Fluent has been chosen for identification of the loads subjected by the blade. Due to pressure difference on the blade surfaces thrust is produced. One side blade will have high pressure and other side lower pressure due to movement of fluid over the blade. So, to identify these pressure Ansys fluent (CFD Tool) has been chosen.

Problem: Boat propeller speed is about 1300 rpm, blade angle is taken 20 deg because it is maximum allowed angle of rotation for blade, boat speed 8 knots/h (4.11m/s,14.8kmph), these values taken as reference to find thrust and pressure on blade. But at same propeller speed (rpm), we took different inlet water velocity (0.5m/s ,1m/s, 2m/s,3m/s) for better understanding of thrust produced by propeller.

To get the pressure data problem approached by following this steps:

1. Pre-Analysis
2. Geometry
3. Mesh
4. Model setup
5. Numerical solution

6. Numerical Results
7. Verification & Validation

5.2.1 Analysis at propeller-speed:1300rpm ,20deg blade orientation

In this section propeller blade analysis done at propeller speed 1300rpm, 20 deg blade orientation with different inlet velocities.

5.2.1.1 At inlet-velocity:4.11m/s

At first analysis was done for 4.11 m/s inlet velocity and procedure for analysis also established in this section. This inlet velocity is chosen because of ship's maximum speed is 4.11 m/s, as per using relative velocity concept propeller with zero velocity and inlet water velocity taken as 4.11 m/s.

5.2.1.1.1 Pre-Analysis:

Mathematical Model: The governing equations are the continuity and Navier-Stokes equations. These equations are written in a frame of reference rotating with the blade. This has the advantage of making our simulation not require a moving mesh to account for the rotation of the blade.

The equations that we will use look as follows:

- a. Conservation of mass:

$$\frac{\partial \rho}{\partial t} + \nabla \cdot \rho \vec{v}_r = 0$$

- b. Conservation of Momentum (Navier-Stokes):

$$\nabla \cdot (\rho \vec{v}_r \vec{v}_r) + \rho (2\vec{\omega} * \vec{v}_r + \vec{\omega} * \vec{\omega} * \vec{r}) = -\nabla p + \nabla \cdot \bar{\bar{\tau}}_r$$

Where \vec{v}_r is the relative velocity (the velocity viewed from the moving frame) and $\vec{\omega}$ is the angular velocity.

Boundary Conditions: The propeller is in symmetry in general so the propeller is divided into 3 equal parts as the circle divided into 3 parts each into 120 deg of total 360deg so it make us easy to do analysis and we can perform analysis in fluent from taking propeller's blade by periodic conditions.

Sea Water conditions considered are Temperature 21⁰C, Density $\rho=1.02813$ (g/cm³), Kinematic Viscosity $\nu=1.07854e-6$ (m²/sec)

The flow condition is considered as laminar flow which was said by EWOL representative Ing. Moroni and he mentioned propeller speed is about 1300 rpm, blade angle is taken 20 deg because it is maximum allowed angle of rotation for blade, boat speed 8 knots/h (4.11m/s,14.8kmph), these values taken as reference to find thrust and pressure on blade.

FLUENT converts these differential equations into a set of algebraic equations. Inverting these algebraic equations gives the value of (u, v, w, p) at the cell centers. Everything else is derived from the cell center values (post-processing). As fluent works on basis of Finite Volume method.

Hand-Calculations for Expecting Results: One simple hand-calculation that we can do before even starting simulation is to find theoretical water velocity at the tip of the blade. We can then later compare our answer with what we get from our simulation to verify.

The velocity v, on the blade tip should follow the formula:

$$v = r * \omega$$

r= distance of the tip from the center of the hub.

ω =angular velocity.

Plugging in our angular velocity of 1300 rpm and using the blade length of 0.4318 meters distance from the center of hub, we get

$$v = -\left\{1300 * 2 * \left(\frac{\pi}{60}\right) \hat{k}\right\} * (-0.4318\hat{i})$$

$$v = 28.95 \frac{m}{s} \hat{j}$$

EWOL Srl provided experimental data of thrust's at different speed of propeller at 18° blade angle for 16'' and 22'' size propellers for estimation of the thrust because 17'' propeller is in development process. Those values are shown in following graphs

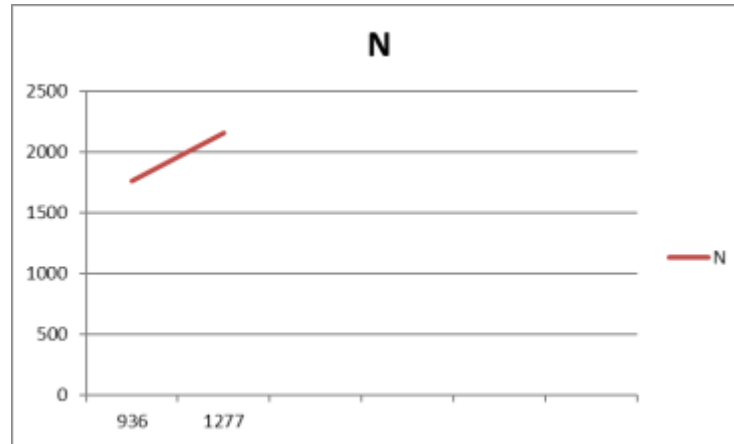


Figure 5-2 Experimental data of thrust's at different speed of propeller at 18° blade angle for 16'' size propeller, x-axis represents rpm and y-axis represents thrust produced in Newtons courtesy by EWOL Srl.

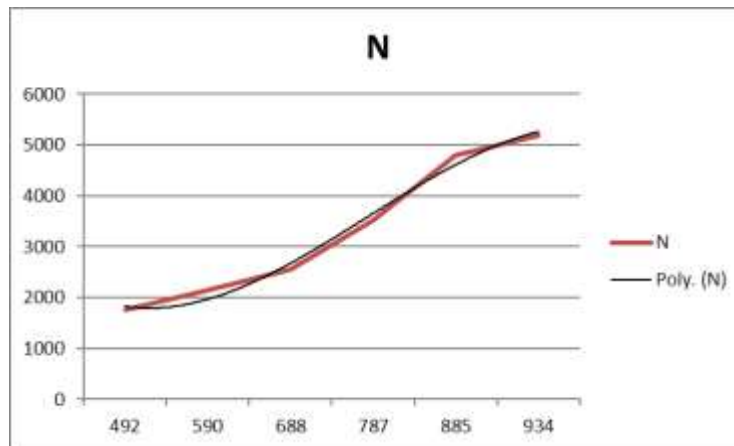


Figure 5-3 Experimental data of thrust's at different speed of propeller at 18° blade angle for 22'' size propeller, x-axis represents rpm and y-axis represents thrust produced in Newtons courtesy by EWOL Srl.

For 17'' propeller thrust values are estimated by simple average method from given aforementioned data by EWOL at 18 deg orientation of blade. Thrust values at 1000 rpm is 2621.5N and at 1300 rpm is 2966.4 N.

5.2.1.1.2 Geometry

Initially in Ansys Workbench the Fluent in analysis system taken as stand-alone project. the blade design provided by EWOL Srl is imported into the geometry (Design modeler) of fluent system.

Then the blade is rotated $-ve 90^{\circ}$ about Z-axis later rotated $+ve 20^{\circ}$ about x-axis (clockwise rotation represents positive), translated 0.12 m in $-ve$ x-axis direction so, these rotation and translation brings our blade into the position that represents blade alignment/assembly to the propeller. Then the fluid domain is created around the blade by using skin tool from two 2D sketches and Boolean operation(subtraction) in which blade is tool body and other one as target body, these operation is used to make it as a single domain. The final geometry is shown in the figure 5-4. In figure one side of the of domain is smaller section for inlet and larger one for outlet for having better understanding of flow after the blade. Here period1 and period 2 represents interface faces of one third section with remaining section. These naming's shown in figure helps for identifications while assigning boundary conditions.

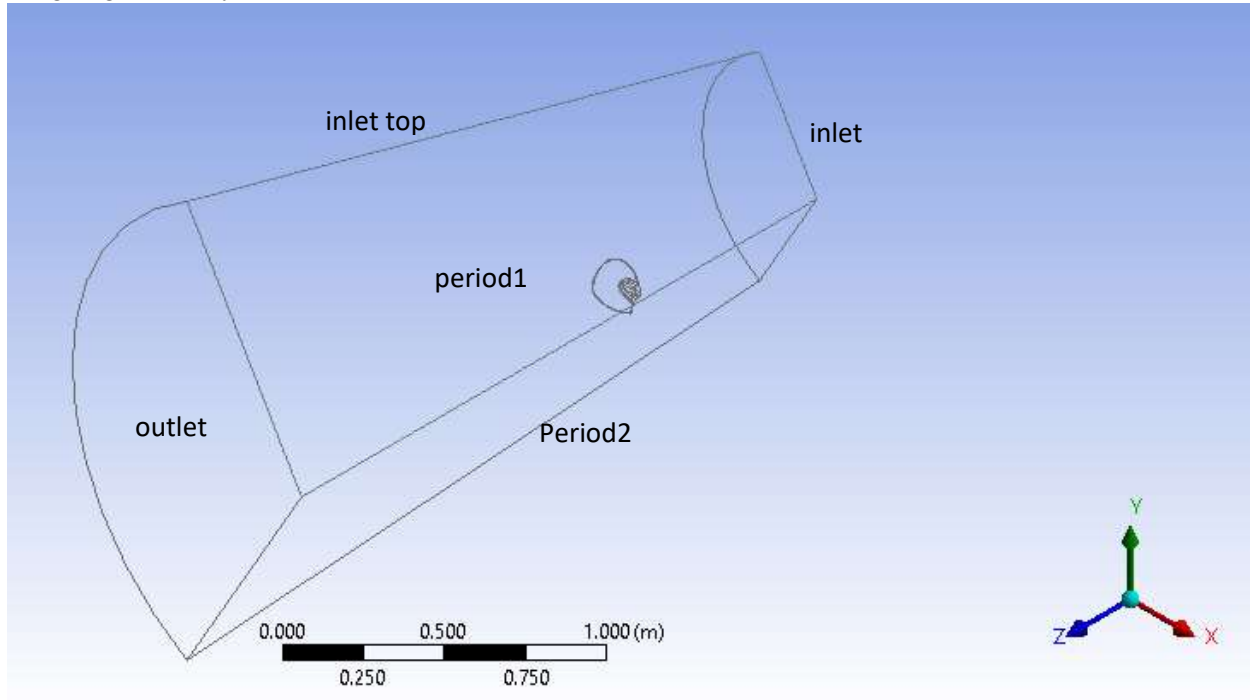


Figure 5-4 Wireframe representation of fluid domain and blade in geometry model and the names of each faces.

5.2.1.1.3 Mesh:

Initially coarse mesh was created in a way to have understanding in the flow and thrust. Initially started by naming various faces of our geometry for later use in FLUENT and to make surface body referencing much easier when creating our mesh.

Create named selections: Inlet, Inlet-Top, Outlet, Blade, Period 1 (one of the quadrilateral surfaces), Period 2 (the other quadrilateral surface), Fluid (for overall domain other than blade). Some of these names are shown in figure 5-4.

Tetragonal irregular mesh has been chosen as it producing better results as shown from different studies [48]

Initially rough mesh created and later these summary of steps followed for creating mesh:

1. Insert Match Control
 - Select the two trapezoid faces for the high and low geometry selection
 - Choose axis of rotation to be global coordinate
 - Match control is for the nodes to match up for the periodic sides.
2. Insert face sizing

- Use the name selection, blade surface.
 - Input sizing of 5 mm.
 - Behavior should be hard.
3. Insert local inflation around the blade
 - Geometry is the whole body
 - For boundary, select named selection and choose the blade (click enter)
 - Keep default settings for the rest
 4. Add a sphere of influence
 - First, create a new coordinate system.
 - Define it by named selections and choose the blade surface.
 - Insert body sizing
 - Geometry, the whole body
 - Type: sphere of influence
 - Sphere center: Coordinate System
 - Radius: 500 mm
 - Element size: 10 mm
 5. Click Generate

These different operations are used to get the better quality in the mesh, where skewness and orthogonality are metrics for measuring quality of mesh, which will influence the result of the analysis. In this we got 2453118 elements. Average skewness is 0.205 and average orthogonality 0.793 are in good shape compared to shown in figure 5-5.

Skewness:

Outstanding	Very Good	Good	Sufficient	Bad	Inappropriate
0-0.25	0.25-0.50	0.50-0.80	0.80-0.95	0.95-0.98	0.98-1.00

Orthogonal quality:

Inappropriate	Bad	Sufficient	Good	Very Good	Outstanding
0-0.001	0.001-0.15	0.15-0.20	0.20-0.70	0.70-0.95	0.95-1.00

Figure 5-5: Quality Range index for Skewness and Orthogonal quality [49].

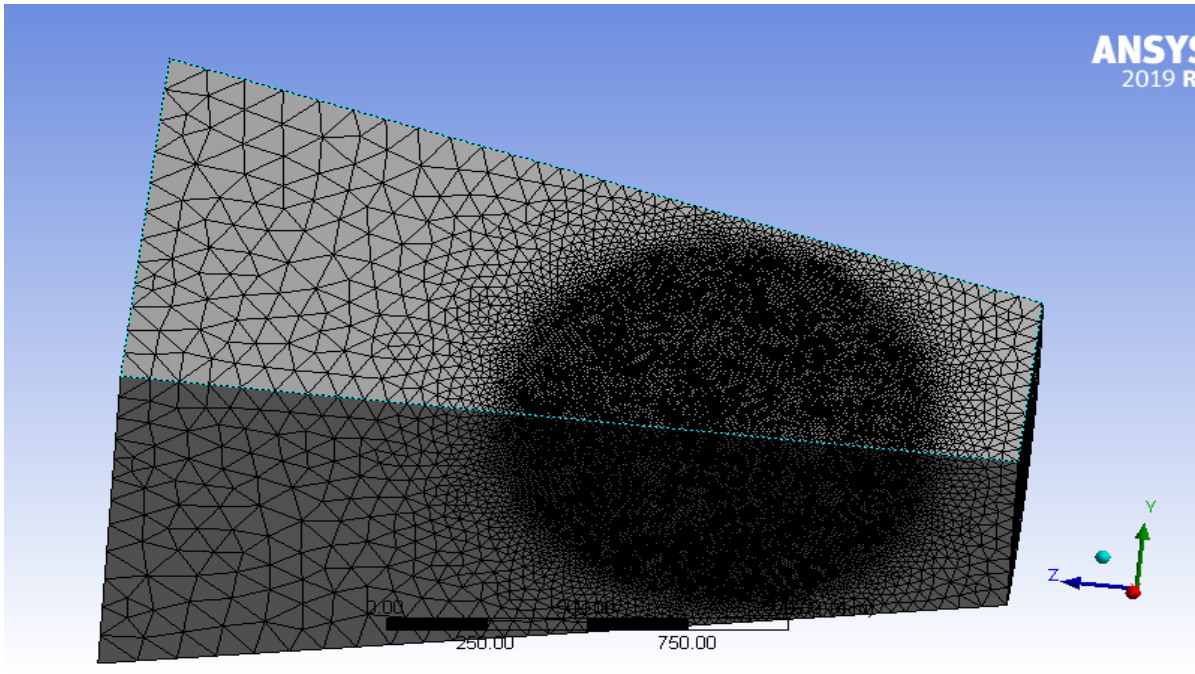


Figure 5-6 Created Mesh for fluid domain.

5.2.1.1.4 Model setup:

Finite volume method is used by the Ansys Fluent. Parallel processing is used to have fast results compare to series. Used 2 cores for parallel processing which is due to limitations computation power. Next each section is shown and discussed for settings to set for running the simulation in same order as in Fluent.

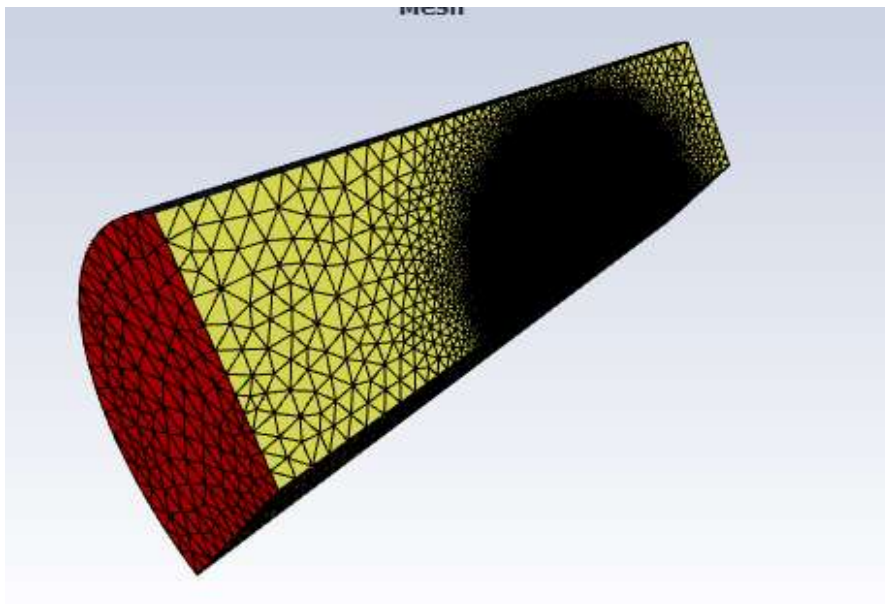


Figure 5-7 Mesh domain as shown in Fluent after launch of the window.

- I. **General:** In this section solver settings can be set and mesh quality can be checked and scale of the model which can be seen in the figure 5-8. In this case settings are set to steady and pressure based which can be seen in same figure.

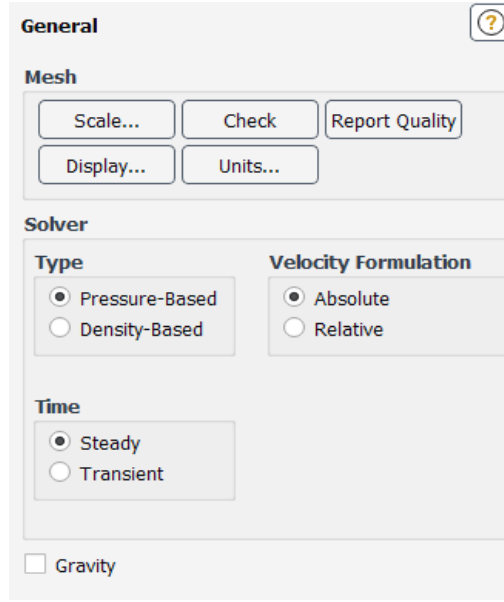


Figure 5-8 Solver settings used in this case study in Fluent.

- II. **Model:** In this section flow condition like laminar or turbulent, phase change settings, energy dependence etc. can be set which are shown in the figure 5-9 which also shows settings for our study.

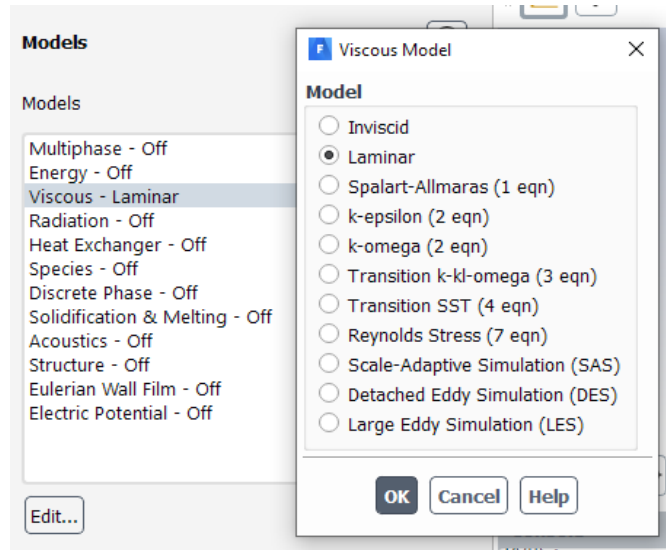


Figure 5-9 Shows Model settings for governing equations.

- III. **Materials:** In this section material properties can be created. In our case new material created under the name of seawater which can be seen in the figure 5-10.

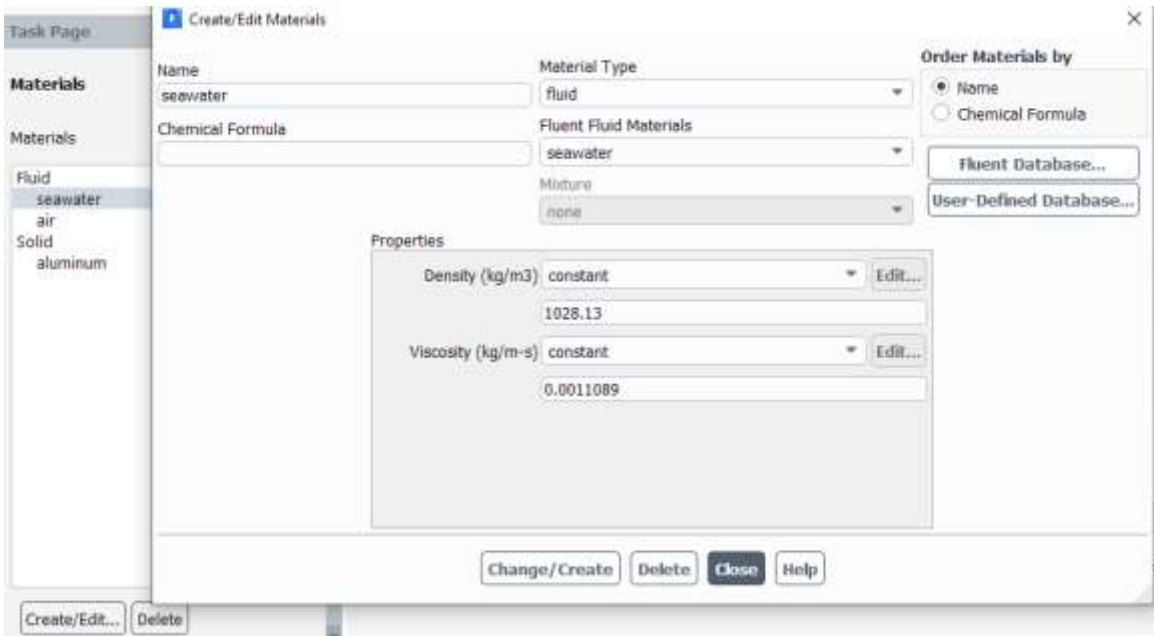


Figure 5-10 Material seawater created with properties as mentioned initially.

- IV. **Cell Zone Conditions:** In this section fluid domain conditions like frame motion etc, and material properties can be assigned which are created initially (settings like the fluid properties like material, any motion). In our case we have blade which is rotating at 1300 rpm, so by using frame motion we provided rotation to fluid in relative method to have rotation condition for blade.

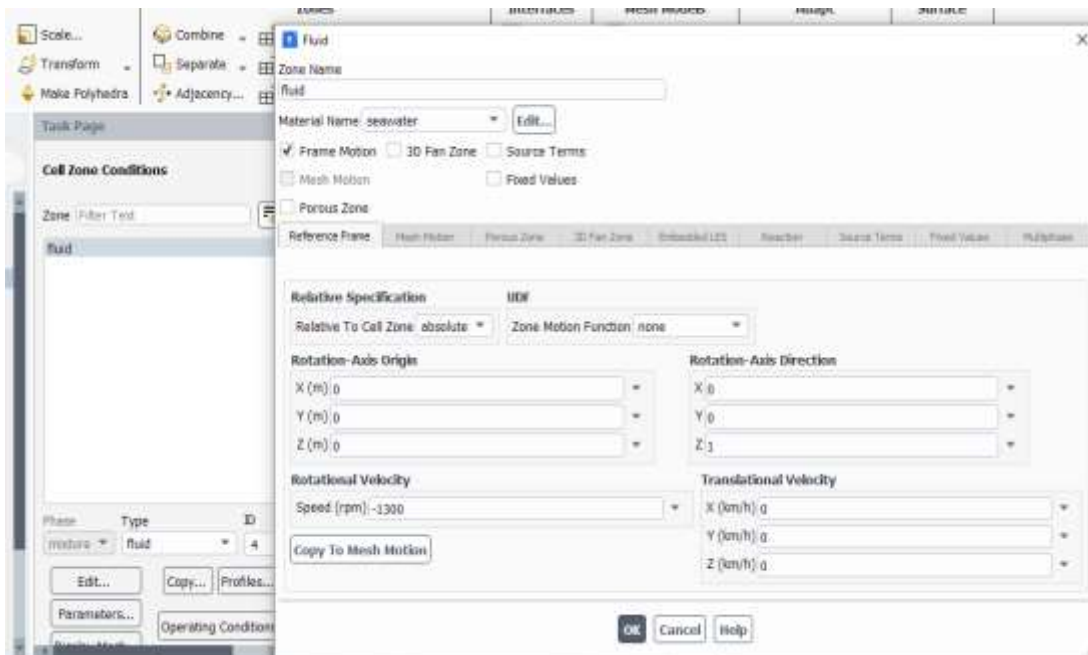


Figure 5-11 Assigned Cell zone condition settings with frame motion

V. **Boundry Conditions:** In this section boundry conditions can be assigned, in our case study boundry condition settings are shown in following figure

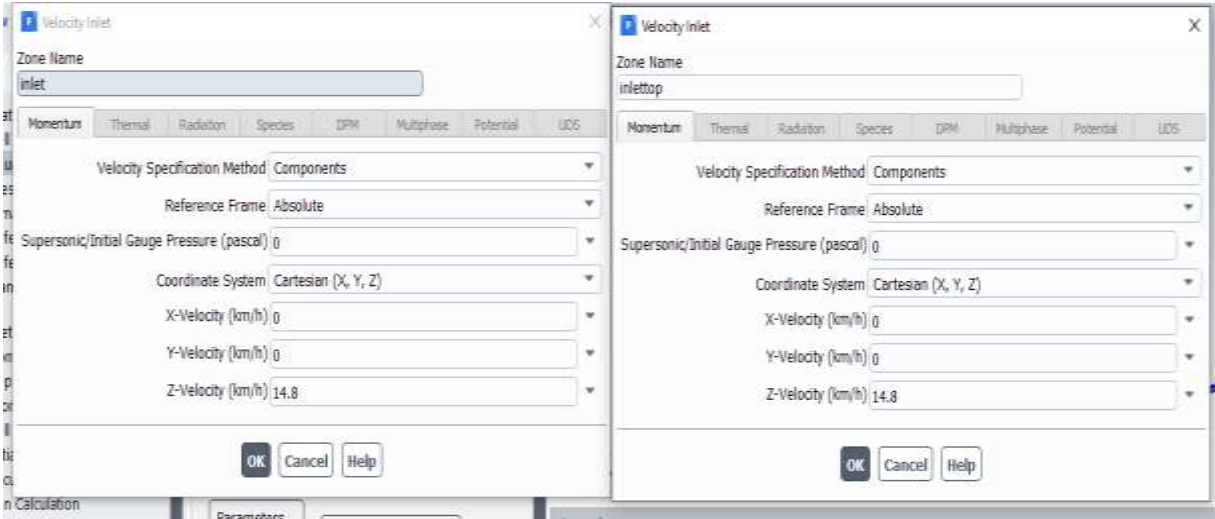


Figure 5-12 Defined inlet velocity conditions for the inlet and inlet top faces.

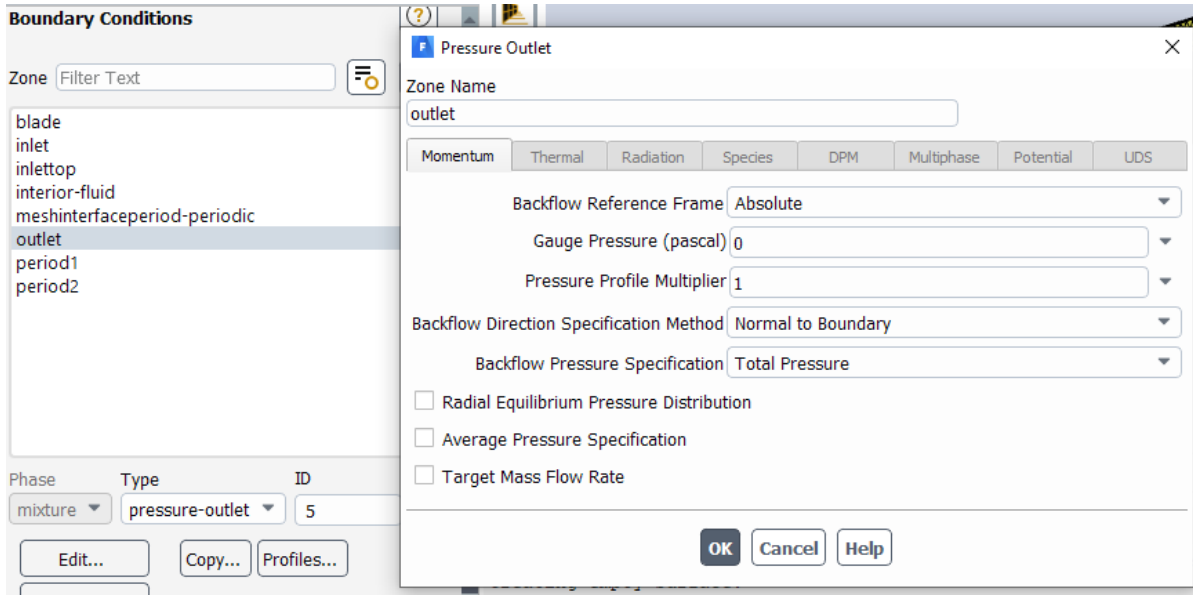


Figure 5-13 Assigned outlet settings.

Change the boundary type for "period 1" and "period 2" to interface (they are originally labeled as wall).

Mesh Interfaces: Mesh interface should be created to define rotation of frames here period1 and period2 faces are part of fluid they are not walls. We need to define mesh interface by manually as shown in figure 5-14. We defined periodicity so it automatically understands symmetry. The order

in which the interface zones is selected matters because of how the offset is computed. So, the first interface zone is period 1 and second interface zone is period 2. Otherwise, error may occur:

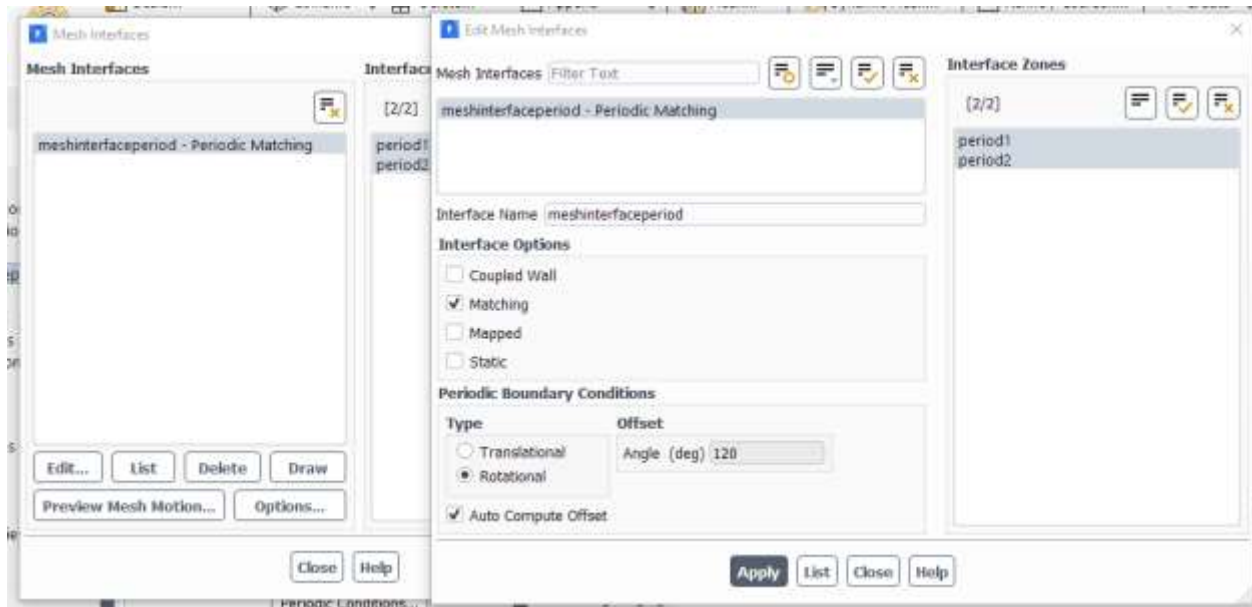


Figure 5-14 Assigned Meshinterface settings.

5.2.1.1.5 Numerical Solution:

Here, in this section we tell FLUENT which solution method to use, how many iterations to perform, how to initialize to solution and what to visualize during the calculation. Finally, we run the calculation.

- I. **SolutionMethod:** In this section we can assign different solution methods. Second order is considered for pressure and momentum to have the best output.

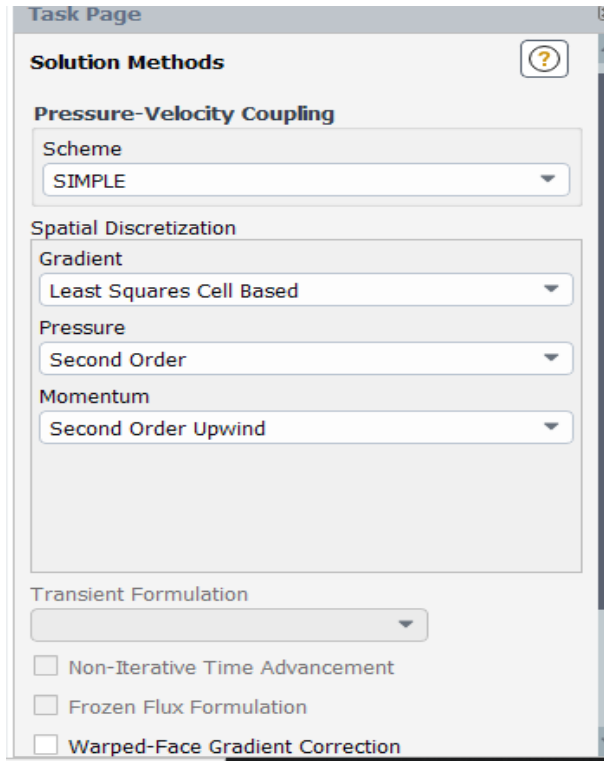


Figure 5-15 Assigned solution methods settings

- II. **Monitors:** Here convergence criterion and residual values can be changed. Residual absolute criteria changed to $1e-6$

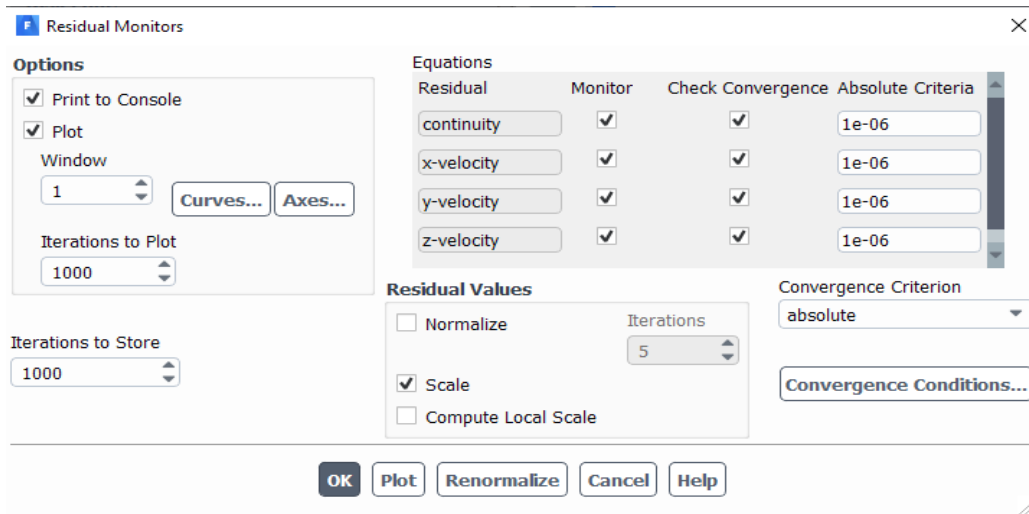


Figure 5-16 : Residual Monitors.

- III. **Initialization:** This is helps to initialization the problem with guess values. So, here standard type initialization method with inlet conditions as guess values has been chosen.

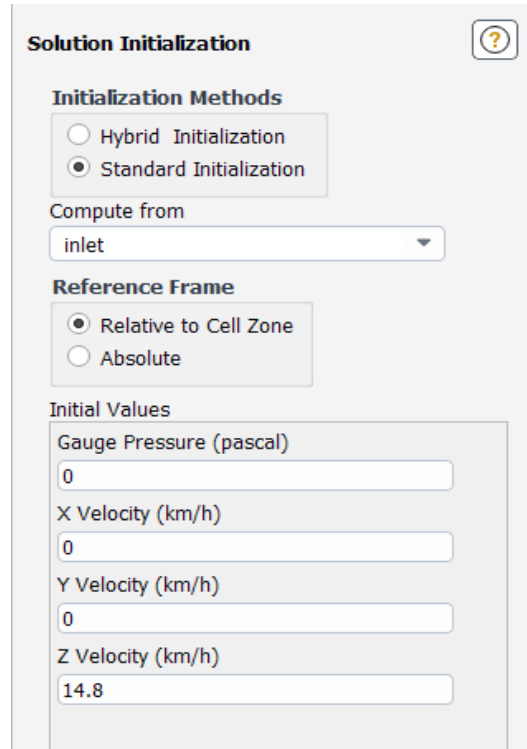


Figure 5-17 Assigned initializing settings.

After the initialization the calculation was run with 6000 iterations which took around 16 hours of computation time.

5.2.1.1.6 Numerical Results:

In this section both FLUENT and CFD-Post were used to view various results. Various results are shown in the following figures.

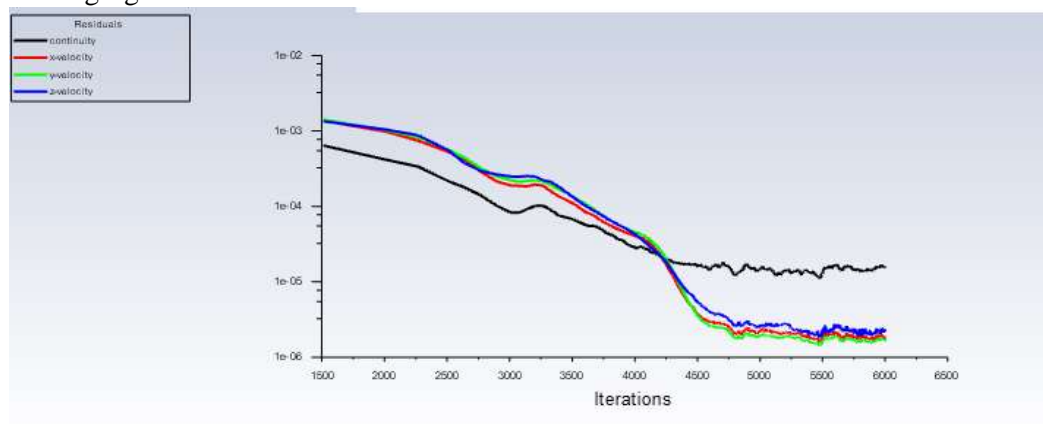


Figure 5-18 : Residuals graph (propeller-speed:1300rpm, inlet-velocity:4.11m/s,20deg blade orientation).

Residuals not reached $1e-6$ but at iteration 6000: continuity (mass residual) is $1.5885e-05$, x-velocity is $1.7918e-06$, y-velocity is $1.6601e-06$, z-velocity is $2.2115e-06$. Mass imbalance is -0.002kg/s . Thrust is 657 N

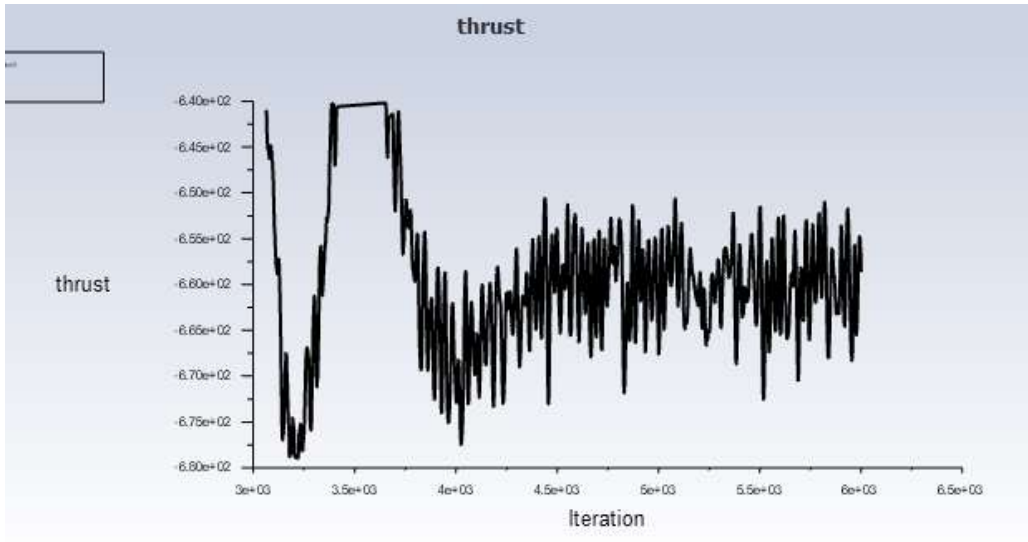


Figure 5-19 Thrust vs iterations Graph.

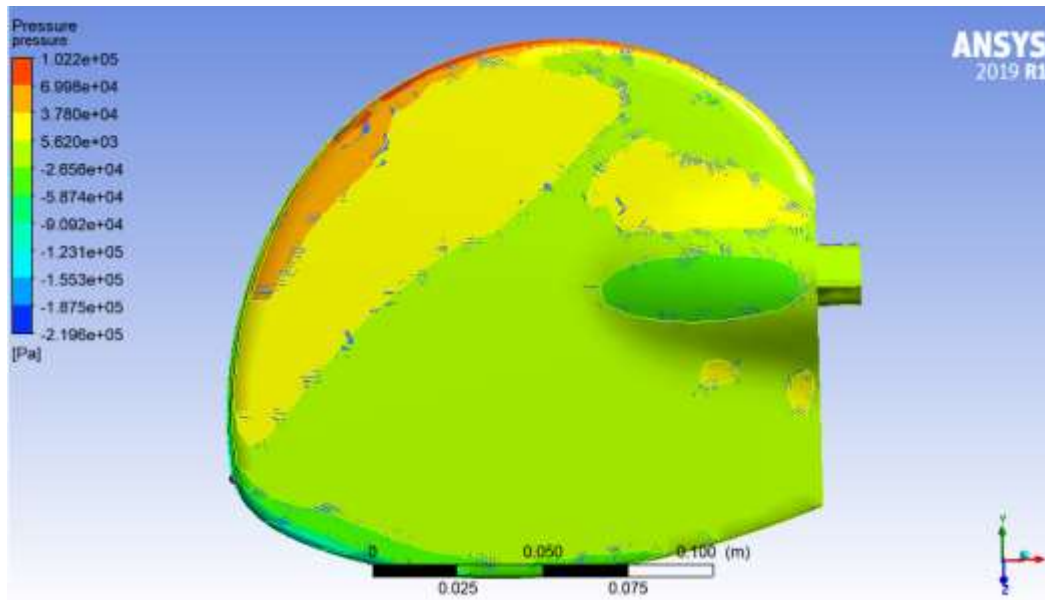


Figure 5-20 Pressure field map on front side of blade

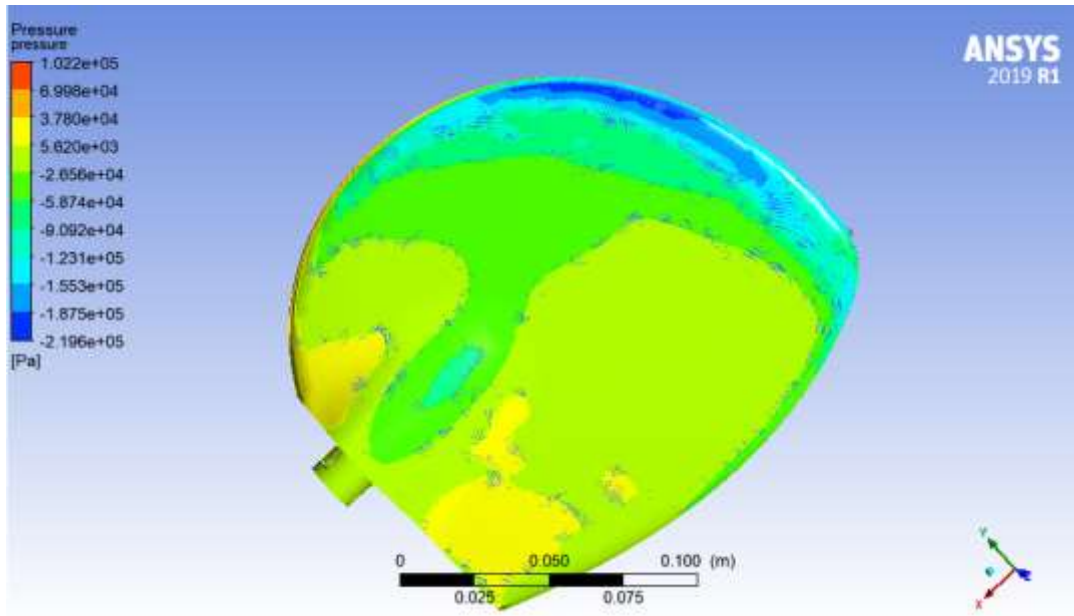


Figure 5-21 Pressure field map on back side of blade.

Velocity at tip of the blade is 29.75m/s as shown in below figure.

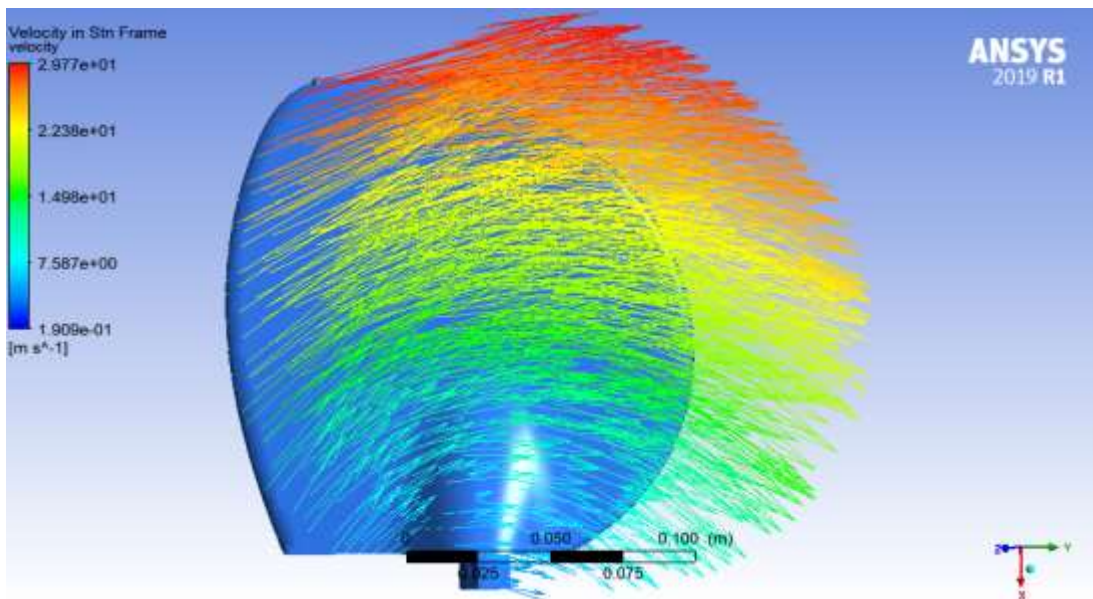


Figure 5-22 velocity vectors from the blade.

5.2.1.1.7 Verification & Validation:

In this section our results are verified

- Mass imbalance also less but not as less as negligible. Mass imbalance should be zero but due to error in discretization it will not be zero.
- Velocity at tip of the blade should be 28.95m/s from the hands-on calculations initially done in pre analysis step and we got 29.77m/s which is near to required and shown in figure 5-22.

- The pressure map shown on the frontside, backside of the blade in figures 5-20 and figure 5-21 respectively shows high pressure and low-pressure sides respectively which leads to motion in -ve Z axis direction which means forward motion of the ship, so, this shows the basic validation of physics.
- Mesh is refined to get the change of variation in the results produced or to get the better result.

a) Refined Mesh:

Now the mesh is refined to elements 2,792,615 by reducing to half of elements length. Mesh metrics are average skewness is 0.209 and average orthogonality 0.789 are in good shape compared to shown in figure 5-5. The same setup and conditions were used as aforementioned steps in Model setup and Numerical solution.

After the initialization the calculation was run with 6200 iterations which took around 20hours of computation time.

Numerical Results, Verification & Validation:

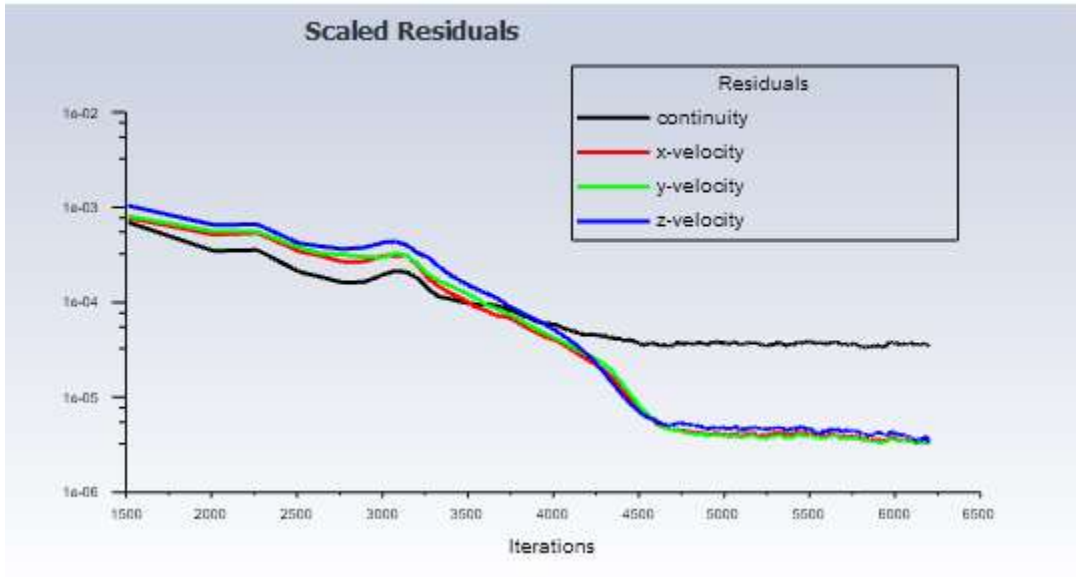


Figure 5-23 Residual graph of refined mesh.

At iteration 6200, continuity is 3.5478×10^{-5} , x-velocity is 3.3163×10^{-6} , y-velocity is 3.3138×10^{-6} , z-velocity is 3.6008×10^{-6} . Here the residuals not reached 1×10^{-6} . But mass imbalance 0.0014398 kg/s . Thrust at 6200 iteration is 689 N.

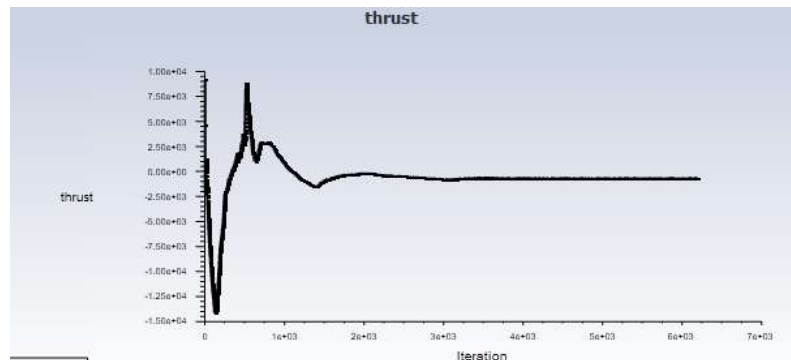


Figure 5-24 Thrust vs iterations graph.

In thrust vs iterations graph it can be observed that graph became flat without much deviation.

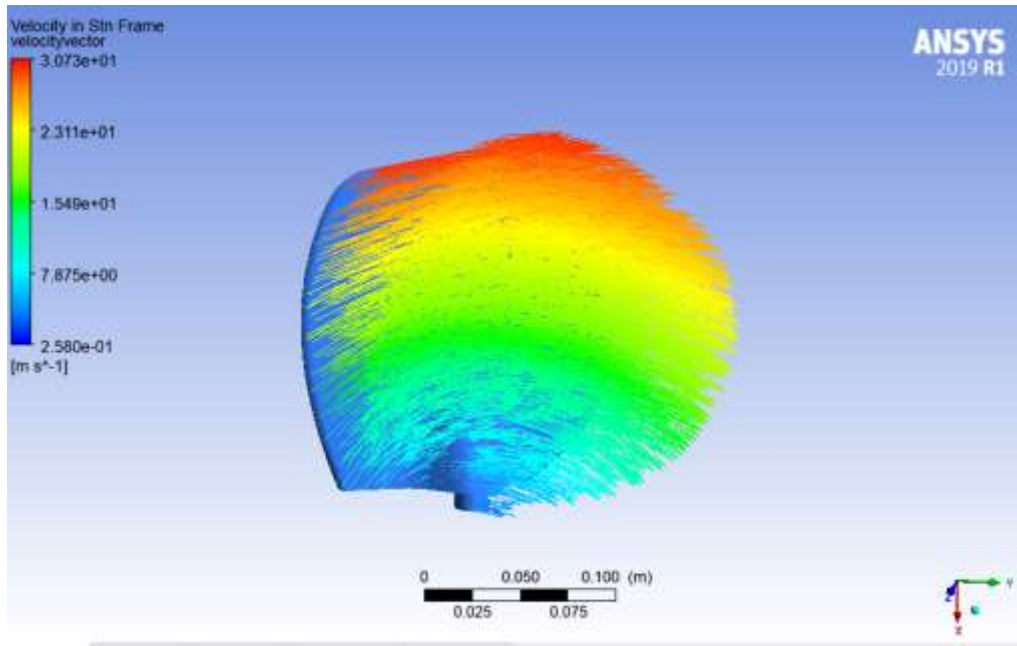


Figure 5-25 velocity vectors of blade.

Here we have 30.73m/s and theoretical is 28.95 m/s.

So, after refining the mesh there is change in Thrust value, so again mesh is refined to check change.

b) Fine Mesh:

Tried to refine mesh by reducing the element length by half, but number elements created are not able to transfer to fluent because computation power limitations and system started crashing. So, after number of trail and errors mesh refined to elements of 3145898 quality. Mesh metrics are average skewness is 0.208 and average orthogonality 0.790 are in good shape compared to shown in figure 5-5. This refined mesh was able to transfer into fluent. So, the same setup and conditions were used as aforementioned steps in Model setup and Numerical solution, calculations are made for 10000 iterations which took around 30hrs of computation time.

Numerical Results, Verification & Validation:

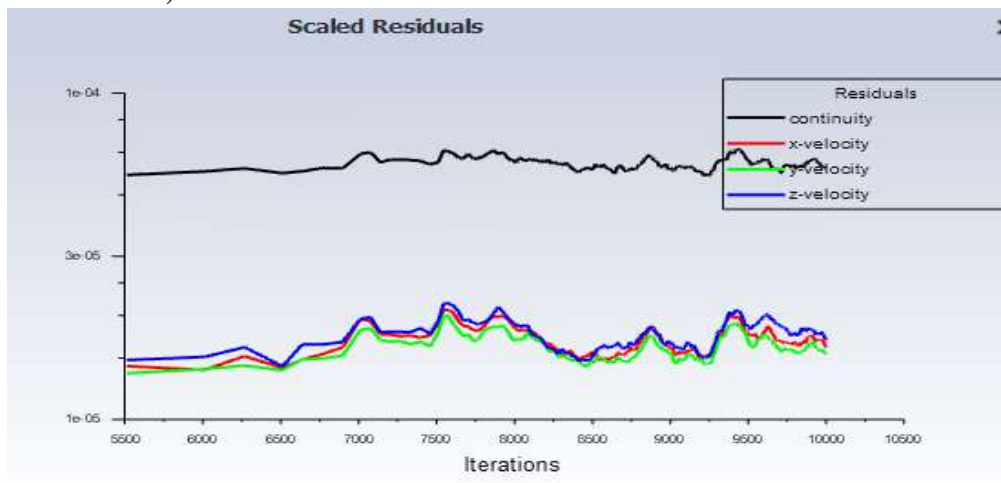


Figure 5-26 Residuals graph of fine mesh

At iteration 10000, continuity is 5.9229×10^{-5} , x-velocity is 1.6631×10^{-5} , y-velocity is 1.5837×10^{-5} , z-velocity is 1.7581×10^{-5} , Mass imbalance is -0.01377858 Kg/s. Here residuals are started to oscillate without decreasing after 5000 iterations which can be observed in graph, so further iterations have not performed. Thrust 708 N at 10000th iteration. In thrust vs iterations graph it can be observed that graph became flat without much deviation.

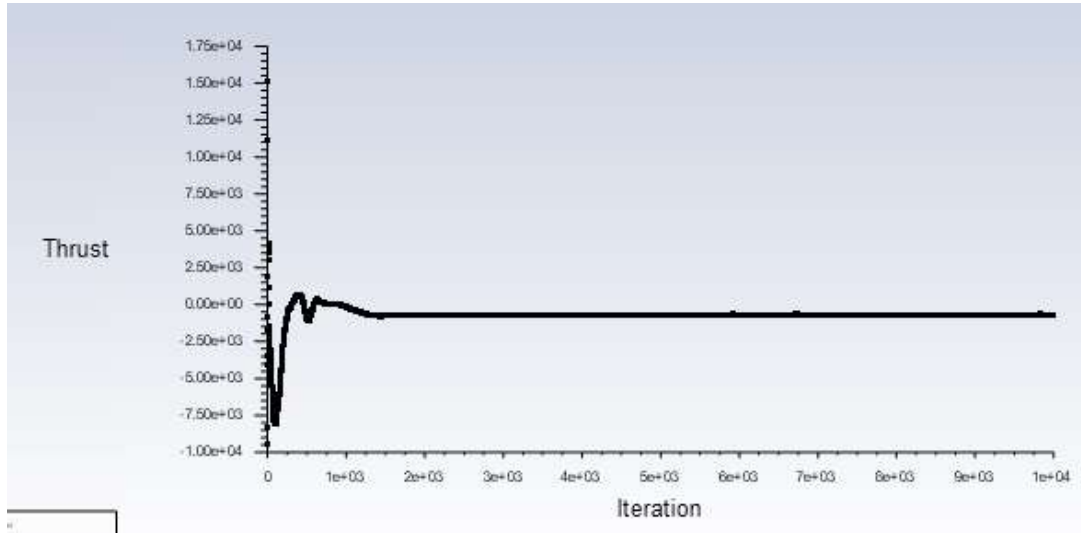


Figure 5-27 Thrust Vs iterations graph

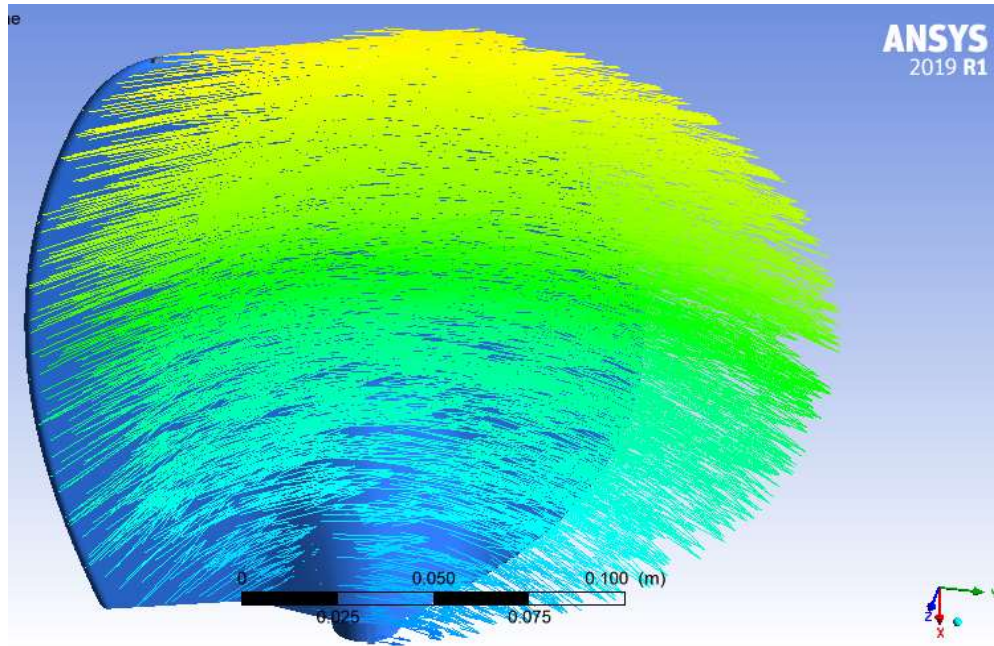


Figure 5-28 velocity vectors of Blade.

By using the probe tip velocity was observed which is at 29.8 m/s, theoretical value is 28.95 m/s. Pressure map also observed, and it is satisfactory. So, results obtained are accepted for this analysis.

5.2.1.2 At different inlet velocities:

To observe the change in thrust values due to difference in the inlet velocities at constant rpm of propeller. Same fine mesh was used. So, at each speed of 0.5m/s, 1m/s, 2m/s,3m/s CFD analysis was performed with same setup settings except velocity which are mentioned in previous sections. Each analysis done for 10000 iterations which took around 30hours for each inlet velocity.

So, after changing the inlet conditions the thrust value observed at each velocity is shown figure 5-29 as a graph. Residuals are oscillated without decreasing for or reaching below $1e-6$ as same as mentioned in previous case. At low velocity 0.5 m/s after water leaving the blade wake fields are produced for this issue different solution methods are also tried but they do not make any calculations because of limitations in computational power.

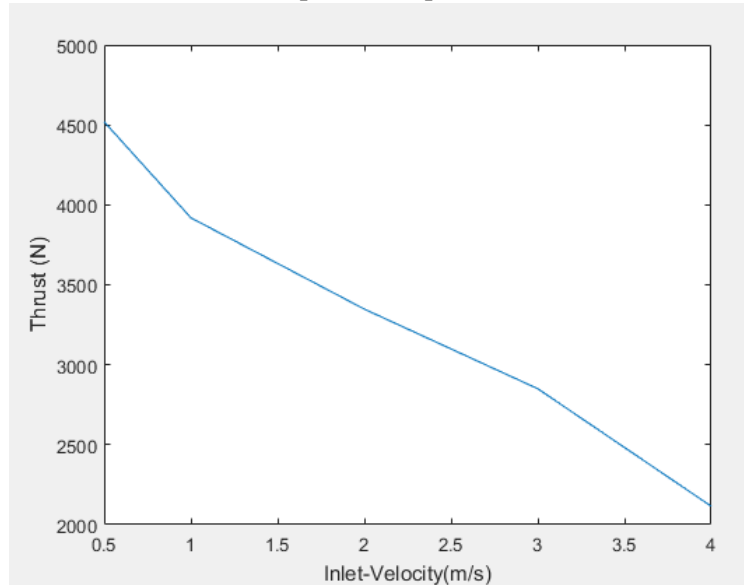


Figure 5-29 Graph for Thrust Vs inlet velocities at 1300 rpm and 20deg orientation of blade.

At 0.5 m/s observed more thrust so at that condition pressure data is exported to excel file with coordinates to use in further process as static analysis.

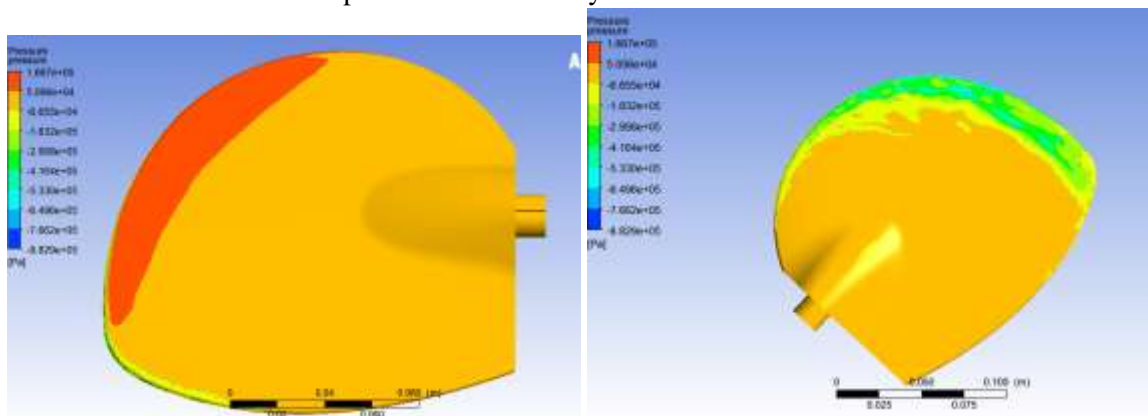


Figure 5-30 Left side shows Pressure field map on front side of blade and Right side shows Pressure field map on back side of blade at 1300rpm,20 deg orientation, inlet velocity 0.5 m/s.

5.2.2 At 18 deg Blade orientation with different propeller speed:

EWOL provided the Thrust values for 22” propeller and 16” propeller at 18deg orientation to understand our values at different rpms and they said inlet velocity is zero but performing the calculations at zero inlet velocity is not helpful. So, performed the analysis at 1m/s at 1300rpm and 1000rpm with 18deg orientation for 17” propeller about 10000 iterations. In this fine mesh is used and followed the aforementioned steps and setup with these conditions. A graph is drawn to understand. So, Blue line in graph shows thrust values by CFD analysis for 17” propeller at 1m/s, Green line shows the estimated values by Average method from given data by EWOL for 17” propeller.

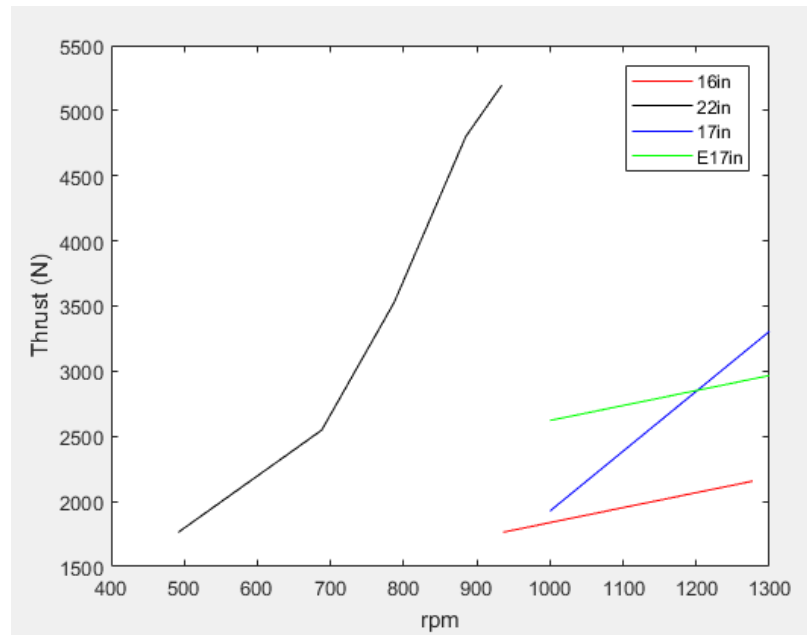


Figure 5-31 Graph between Thrust and rpm for different types of propellers. Black for 22” propeller, Red for 16” propeller (Both velocities zero as mentioned by EWOL). Blue line in graph shows thrust values by CFD analysis for 17” propeller at inlet velocity at 1m/s, Green line shows the estimated values by Average method from given data by EWOL for 17” propeller. For all propellers 18 deg is the blade orientation.

EWOL Srl provided information about where they installed propellers. 22” propeller was installed for a boat model named BAVARIA CRUISER 56 [50] which has displacement of 18,596 kg which represents weight of water displaced by boat. For this type of boat thrust provided by 22” propeller was sufficient in range of 2000N – 5500N can be seen in graph in figure 5-31. 17” propeller planned to install in boats SUN ODYSSEY 34 (JEANNEAU) and OCEANIS 34 (BENETEAU) which has displacement of 4700 kg [51] and 5700 kg [52], respectively. So, by comparing displacements with BAVARIA CRUISER 56 and SUN ODYSSEY 34 (JEANNEAU) or OCEANIS 34 (BENETEAU) and thrust provided range’s it can be understandable that 17” propeller’s thrust range provided by CFD analysis is good enough for propelling the two boat models.

5.3 Static analysis of blade:

Initially at 0.5 m/s pressure load data was extracted for identifying stresses developed in the blade. Data has been exported as an excel file with coordinates. Software tool chosen for this analysis was nTopology, because of further usage in lattice structure creation for blade. It is FEM based software tool.

5.3.1 Setup and Analysis:

Cad body of the blade is imported into the nTopology later converted it into implicit body which is helpful for performing the analysis.

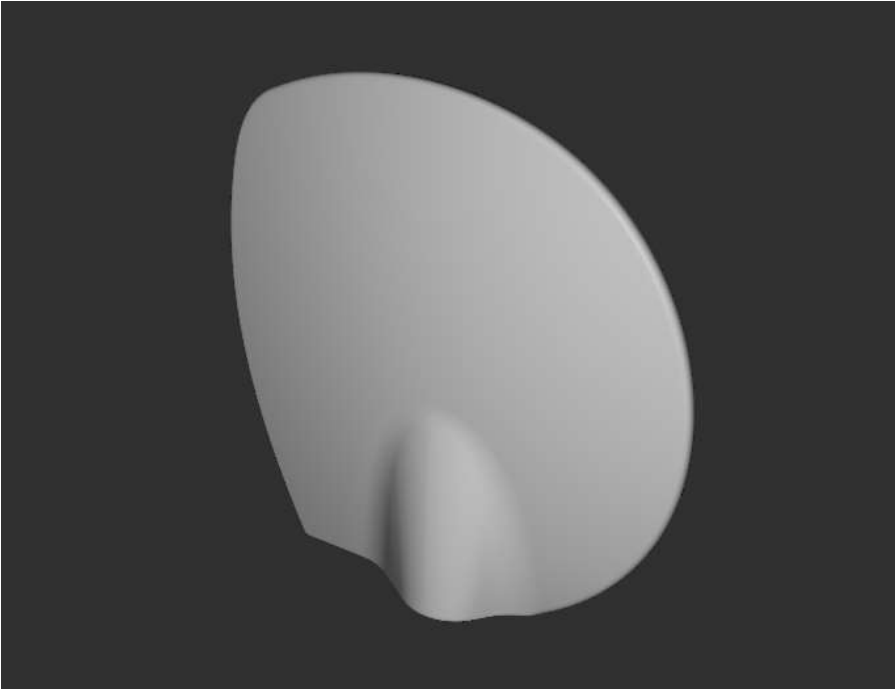


Figure 5-32 Imported Cad body from nTopology (implicit body).

For utilizing pressure data from Ansys Fluent our body should be in same alignment as in Fluent. For this we can approach two methods one we can import aligned body from Ansys geometry, or we can adjust it in nTopology, here imported cad design was used. Then pressure data with coordinates is applied to cad body.

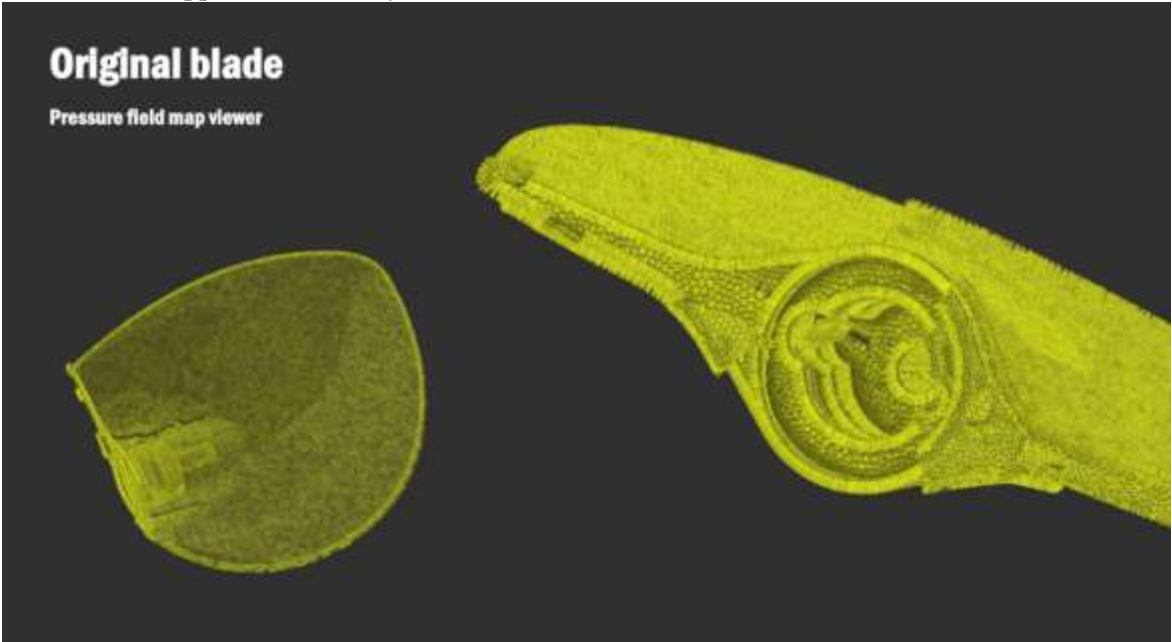


Figure 5-33 Pressure field view on blade from nTopology.

The blade is meshed with tetrahedral elements with edge length of 1 mm total number of elements are 1,315,127. Less than 1mm didn't made possible because of limitations in computation power. Both linear and quadratic geometric order was chosen for analysis for better understanding. Material chosen for analysis and for manufacturing was 17-4PH stainless steel.

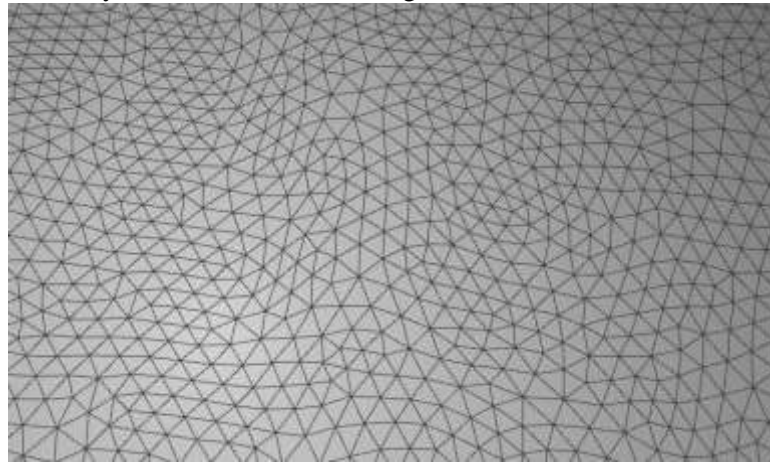


Figure 5-34: Shows tetrahedral(triangle elements) elements on blade.

Blade was fixed at bottom as a constraint, where it will be coupled to hub via screw type fitting.it can be observed from figure 5-35.

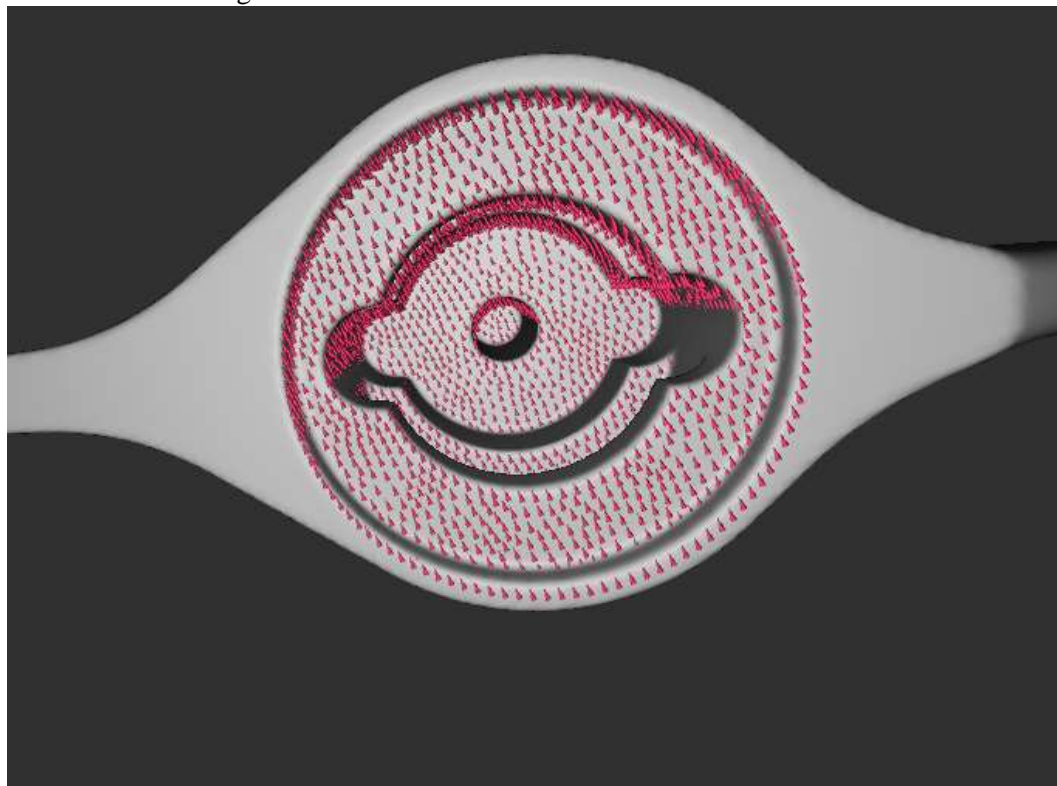


Figure 5-35 Fixed constraint position for blade at coupling interface.

Now static analysis was performed for both linear and quadratic geometric orders after aforementioned initial setups.

5.3.2 Results:

Results of static analysis can be seen directly in same platform without any additional requirement. Von Mises stresses are observed to identify the most stress points in the blade.

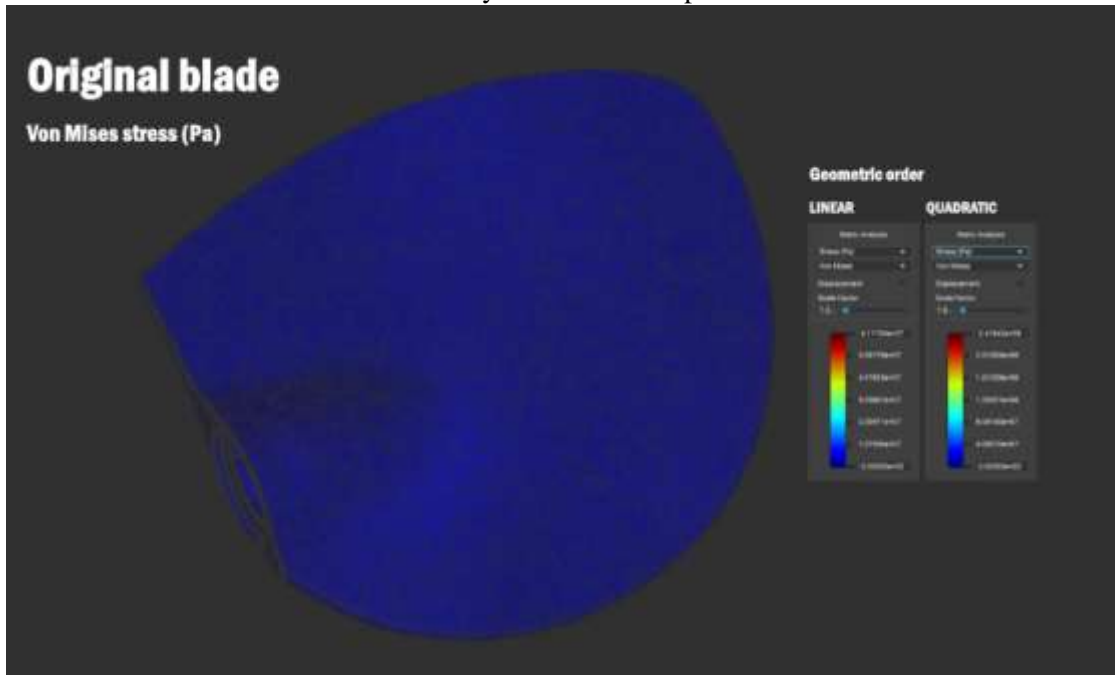


Figure 5-36: Von Mises stress for both linear and quadratic geometric orders.

Linear geometric order analysis has given maximum stress of 61.7 MPa which is under the limit and way less. This result is due to the linear type shape functions. Quadratic type shape functions give better result compared to linear but not exact solution. From quadratic analysis maximum stress is 241.8 MPa. Highest stress points and distribution can be seen from the following figure.

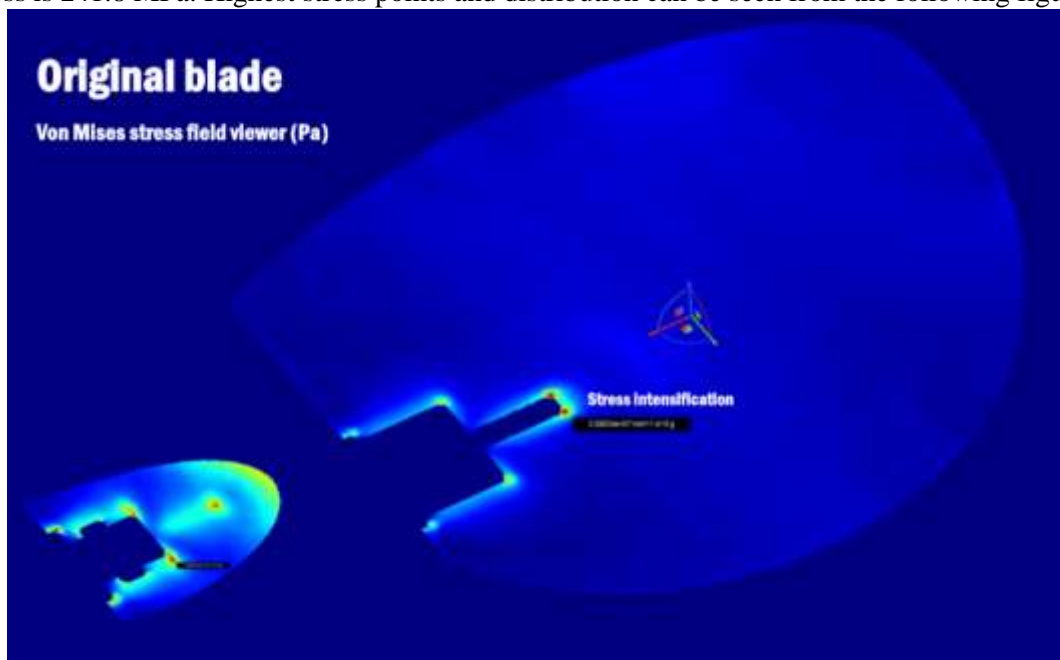


Figure 5-37 Most stressed locations from blade with 2 plane cross section views.

Here from the figure it can be observed that most stressed points are due to geometric discontinuities (sharp edges) at the coupling interface of the blade. These can be neglected because they can be avoided while manufacturing by making them round shape and this occurred due to cad design without any fillets. In this software there is a drawback like it doesn't have any probe to look for stress at particular point. After clear observation, the most stressed part of the blade is at its center of gravity and just above of the coupling interface (above bulged area of the blade), the stress variation in that region is between 90MPa to 120MPa. As this occurred like cantilever beam. Remaining region of the blade has low stress values.

5.4 Constraints to be maintained for optimization and AM:

Geometric Constraints:

- One of the main constraint for performing the optimization is coupling interface, it should be preserved because it connects blade to the hub.



Figure 5-38 Coupling Interface which should be preserved.

- Profile of blade or whole outer structure design of the blade should be preserved because it has hydrodynamic profile which causes the pressure difference on both sides of the blade which ultimately provides the thrust for motion of the ship. The profile of the blade is similar to airfoil profile of an aircraft wing or aircraft propeller. So, if the profile or outer structure of blade disturbed the whole design value changes and its behavior also.

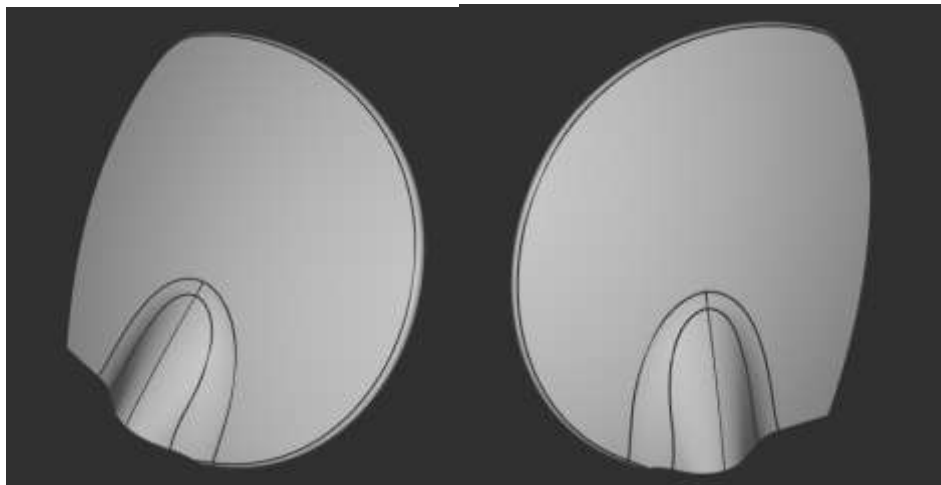


Figure 5-39 Outer design of the blade on both side which should be preserved.

So inner volume of the blade is the design space where changes can be allowed to make. The final part surface roughness shouldn't be too rough but there is no requirement of fine finish also, surface after the printing process by studio system is well enough for acceptance, if required extra finishing can be done.

5.5 17-4PH Stainless steel characteristics:

Precipitation hardening (PH) stainless steels are made by strengthening throughout an age or precipitation hardening thermal treatment is carried, which is a strengthening process where hard precipitate particles are formed in the host metal and these precipitates restrict dislocation slip [53]. These steels are strengthened due to formation of intermetallic copper-rich precipitates in a martensitic matrix that delay the dislocation motion. Normally the martensitic PH stainless steels have high martensite finish temperature M_f (above room temperature), this allows transformation from austenite to martensite to completely occur at room temperature. Typically martensite start temperature, M_s , and finish temperature, M_f , are 132 °C and 32 °C for 17-4 PH stainless steel [54]. 17-4 PH (AISI630) stainless steel (Cr 15–17.5, Ni 3–5, Cu 3–5, Mn <1, Si, Nb 0.15–0.45, balance Fe in % w/w), due to its high stress-corrosion resistance and high fracture toughness compared to semi-austenitic PH stainless steel, so, it is one of the most widely used PH martensitic stainless steels [23].

Material extrusion additive manufacturing is similar as the Metal Injection Molding cycle. So, the characterization of the MIM 17-4 PH steel provides suitable reference to material processed via MEAM. Microstructure of sintered material consists of three main constituents: pores, martensite, and δ -ferrite shown in following figure.

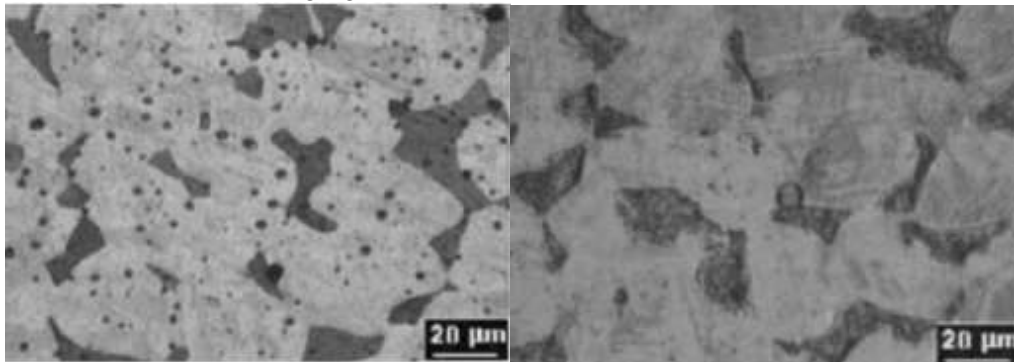


Figure 5-40 Left side shows Microstructures of water atomized 17-4 PH sample in the as-sintered condition and Right side shows gas atomized 17-4 PH sample in the as-sintered condition [23].

Some of the studies shows the presence of retained austenite, generated due to cooling from δ -ferrite. Phase proportions, other constituents in material presence are affected by powder characteristics, sintering atmosphere, sintering temperature, and heat treatment. Which will affect the mechanical and corrosion behavior of the sintered material. It is difficult to separate the effect of a single parameter on the sintered material behavior [23].

Cycles of sintering involves heating and holding to allow binder burnout and impurity removal. Optimal holding temperature is near 600 °C for final polymer removal and near 1000 °C for impurity reduction. The heating rate approach to the peak temperature ranges 2 to 10 °C·min⁻¹. When the heating rate drops to 2 °C·min⁻¹, then almost all shrinkage occurs prior to the isothermal hold [23]. When 1320-1350 °C is reached, the density is high and further gains with extended holds are small. This implies that, upon reaching the ideal sintering temperature range, only a few minutes of hold are required. Most of the densification occurs during heating [23].

Desktop Metal™ already certified the 17-4 PH stainless steel properties. Those properties are ensured if the material is processed without any modification in the processing parameters which are calculated by the integrated software. Desktop Metal™ certified chemical composition, tensile properties, hardness, and relative density. Certified mechanical properties of the material processed by Studio System+™ technology are can be noticed from Tables 5-1,5-2, they are close to the wrought material properties and fit the minimal properties of the as-sintered material.

Composition %	
C	0.07 (max)
Cr	15.5 - 17.5
Ni	3 - 5
Cu	3 - 5
Mn	1.0 (max)
Nb + Ta	0.15 - 0.45

Table 5-1 Chemical composition of 17-4PH certified by Desktop Metal™ [55]

Mechanical properties'				
	standard	Studio System™ as-sintered	ASTM B883 as-sintered (min)	Wrought ³ for reference
Yield strength (MPa)	ASTM E8M	660	650	980
Ultimate tensile strength (MPa)	ASTM E8M	1042	795	1060
Elongation at break	ASTM E8M	8.5%	4%	8%
Young's modulus (GPa)	ASTM E8M	195	190 (typ)	200
Hardness (HRC)	ASTM E18	37	-	35
Density (relative)	ASTM B311	98%	-	100%

Table 5-2 Mechanical properties certified by Desktop Metal™ [55].

Additive Italia Srl also certified the material Bound metal deposition technology. All the samples were printed using the Desktop Metal™ Studio System+™ 3D printer with a nozzle diameter of 400 μm. The integrated software Fabricate was used to set the printing parameters: layer thickness 0.150 mm, print speed 30 mm·s⁻¹, walls (inner and outer) printing speed 25 mm·s⁻¹, printing surface temperature 175 °C and build plate temperature 65 °C [23]. The solvent-based debinding was performed with a chlorinated organic solvent, same for all the samples. The sintering cycle is performed under a vacuum/controlled atmosphere. The thermal cycle is completely automated and auto-generated by the software itself, optimized for the 17-4 PH stainless steel, therefore all the samples are sintered with the same temperature ramp and atmosphere [23].

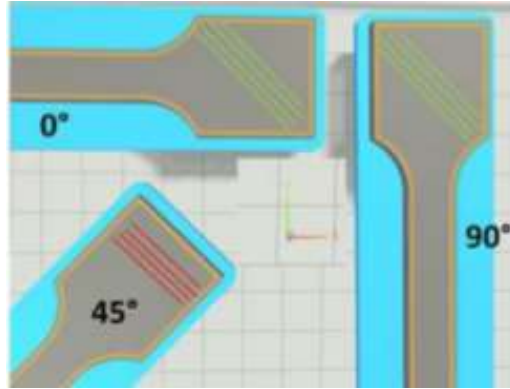


Figure 5-41 Infill layers patterns for samples courtesy by Add-it.

Different tests are performed; Archimedes immersion test used for measuring solid density and porosity, Hardness tests etc. From Archimedes test samples shown 98.25%, 98.42%, 98.36% density [23] which is similar to desktop metal certified one. From hardness tests results average value 25 HRC. From tensile test, ultimate tensile strength average value is 797 MPa, Yield strength is 748MPa, ϵ_b is the elongation at break average value is 12.76% [23].

Chapter6 Optimization and 3Dprinting of Blade

In this chapter optimization of the blade by satisfying the constraints, loads and printing of the final optimized part is discussed. In generally, it is possible to optimize the topology by using the loads or stress field, some software's can handle this type of work for optimizing, after optimization we can add or remove mass like modifying structure for manufacturing and for providing better structural rigidity. Most of them also have lattice structure-based optimization which is open structure type, where almost all of them can't create lattice structure for internal volume of a body by keeping outside surface with some thickness. In this case study we need to utilize the pressure data to identify the stress conditions due to changes made in the blade, and also required to have multiple design options for infill creation. nTopology is a software specially designed for optimization requirements, it has better options for creation of infill for a body better than others, but this software also can't produce internal lattice structure by keeping outer surface and by using also load data. We can import the pressure data and static analysis also can be done. Due to better options nTopology was chosen.

6.1 Optimization:

Main objective of the optimization is to reduce the mass of the blade without compromising in the structural rigidity and stability. Original weight of the blade is 1.3kg. Here few conditions should be considered before performing optimization. Geometrical constraints for the blade already mentioned in previous chapter. In some cases, while propeller in operation there is chance of having collision with sea debris like plants, plastic etc., at the edges of the blade. So, blade should have sufficient thickness and rigidness at the edges. Outer surface of the blade should have sufficient thickness to have the original hydrodynamic profile as not to alter any travelling length of the water particle on the blade surface or creating any weak upper surface strength on the infill so it can leads to failure of the body. It is also better to create the pathway or channels for removing the powder from the inside of the blade as in future it is going to be manufactured in Desktop Metal™ machines which are Shop system (for low-mid volume production) and Production system (for large volume production), these machines works using binder jetting technology. So due to this reason it is not useful to create small matrix type or mesh type infill.

For creating the internal lattice structure this steps were followed:

- i. Creating a shell structure of the blade with thickness of 1.5mm and preserving it.
- ii. Creating lattice structure by using blade.
- iii. Merging the shell structure with lattice structure to have the final desired design.
- iv. Performing the static analysis to identify the stresses.

6.1.1 First design:

With considering the above constraints one lattice structure was created which has vertical ribs type structure like columns which is later merged with initially created shell body using Boolean tool option. This structure can be observed in figure 6-1. This type of lattice structure provides easy removal of powder.

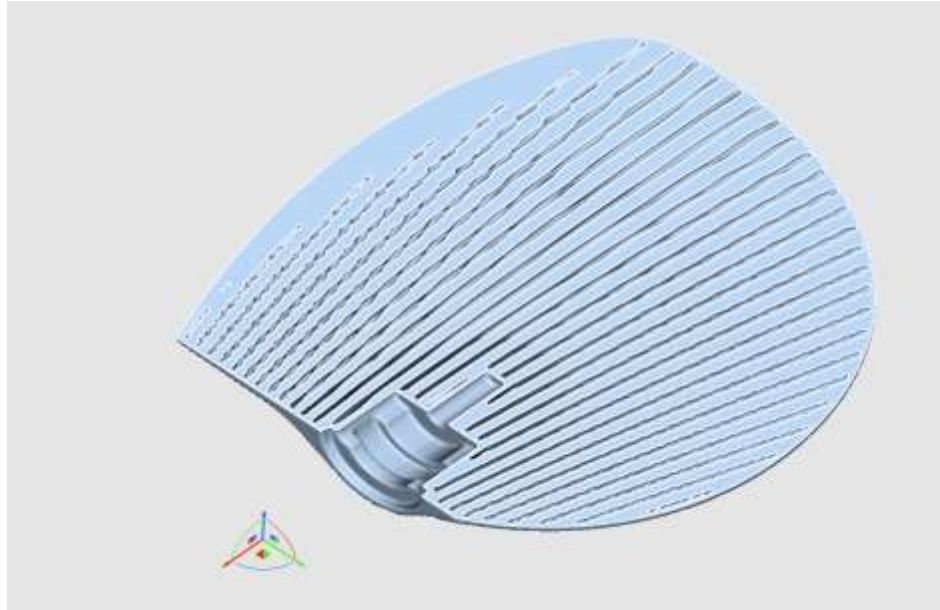


Figure 6-1 Column type lattice structure in the blade.

In future it was planned to manufacture the blade with 316L stainless steel also other than 17-4PH stainless steel which is used for this case study. Desktop Metal™ also certified the 316L steel, it has 165MPa yield strength [56]. So, stresses should be under the limit. After having the aforementioned design static analysis should be performed to identify the stresses developed in the blade. So, by using the pressure data from the CFD analysis static analysis performed with tetrahedral mesh elements with 1 mm edge length and quadratic geometric order (Shape functions). Results are shown in figure 6-2.

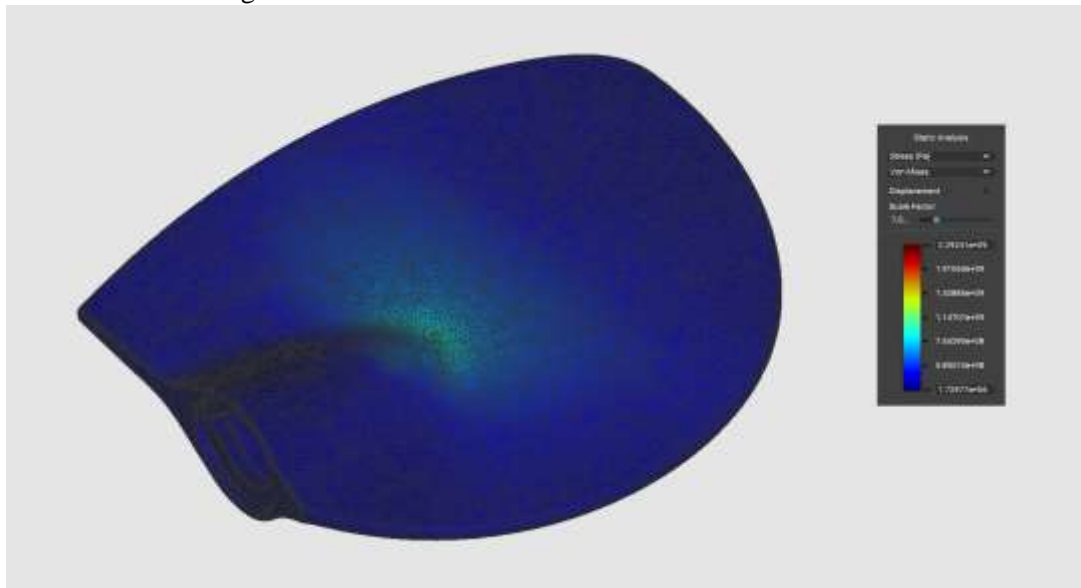


Figure 6-2 static analysis results.

Here the results are high can be observed from the figure 6-2, which are more than 1000MPa, so it is more than limit. So, another optimization was performed.

6.1.2 Second design:

TPMS (triply periodic minimal surface) diamond lattice structure was created which is later merged with initially created shell body using Boolean tool option. Study's also shown TPMS has better mechanical properties [57]. TPMS structure can be observed in figure 6-3.

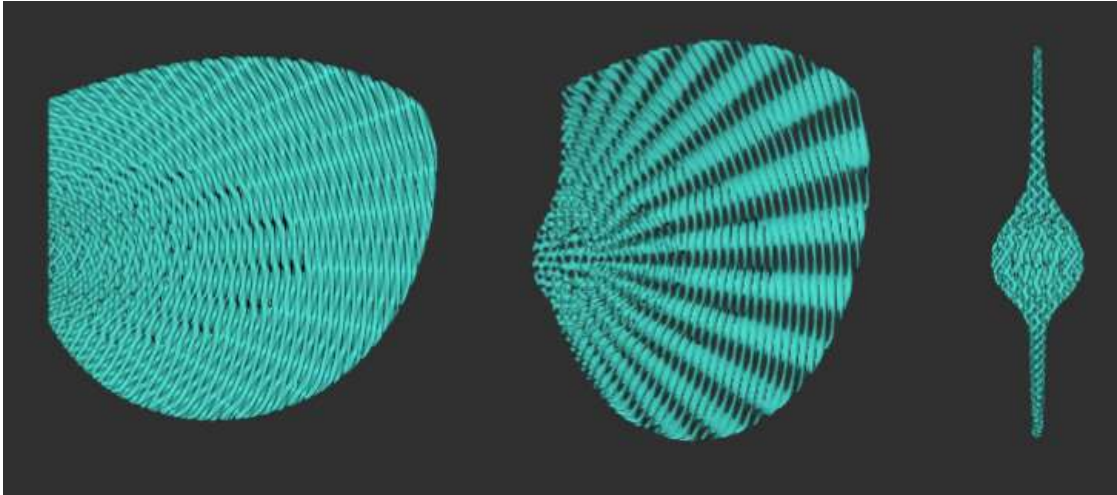


Figure 6-3 TPMS lattice structure created with blade structure.

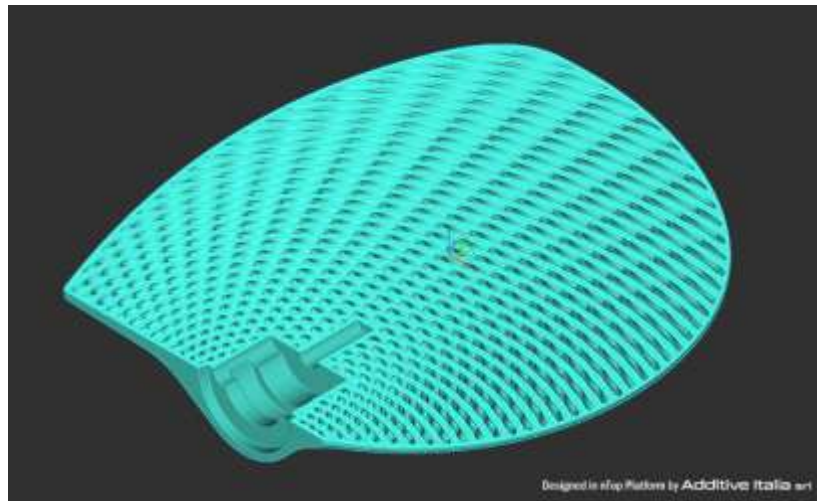


Figure 6-4 TPMS lattice structure merged with shell.

After this design using the pressure data from the CFD analysis static analysis was performed with tetrahedral mesh elements with 1 mm edge length and quadratic geometric order (Shape functions). Results are shown in figure 6-5. In the figure it can be observed that stresses are more than limit. From the analysis it was observed that more stresses are at coupling interface.

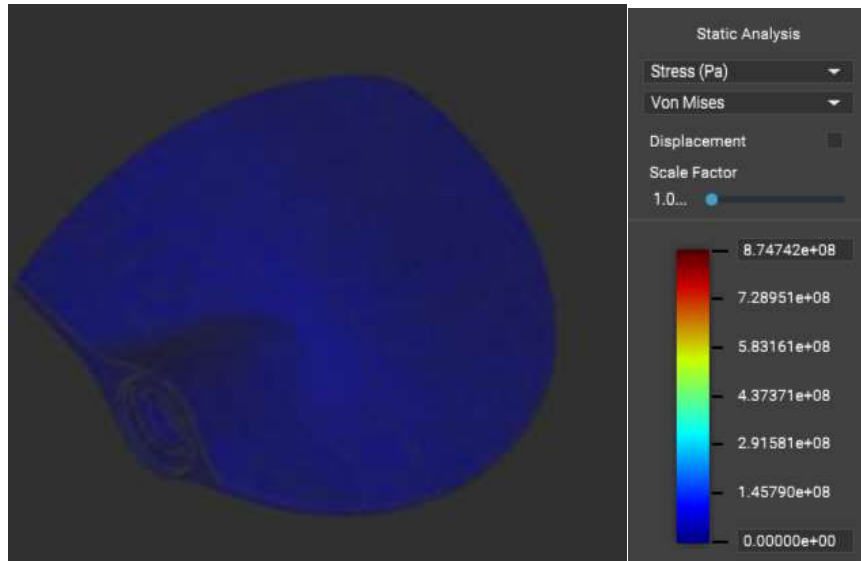


Figure 6-5 Static analysis results of TPMS lattice structure.

Final weight achieved from this design was 977.25gms.

6.1.3 Final design:

Due to more stresses at coupling interface reinforcement was added around the coupling interface and depowdering channel was added to it. This final design shown in figure 6-6.

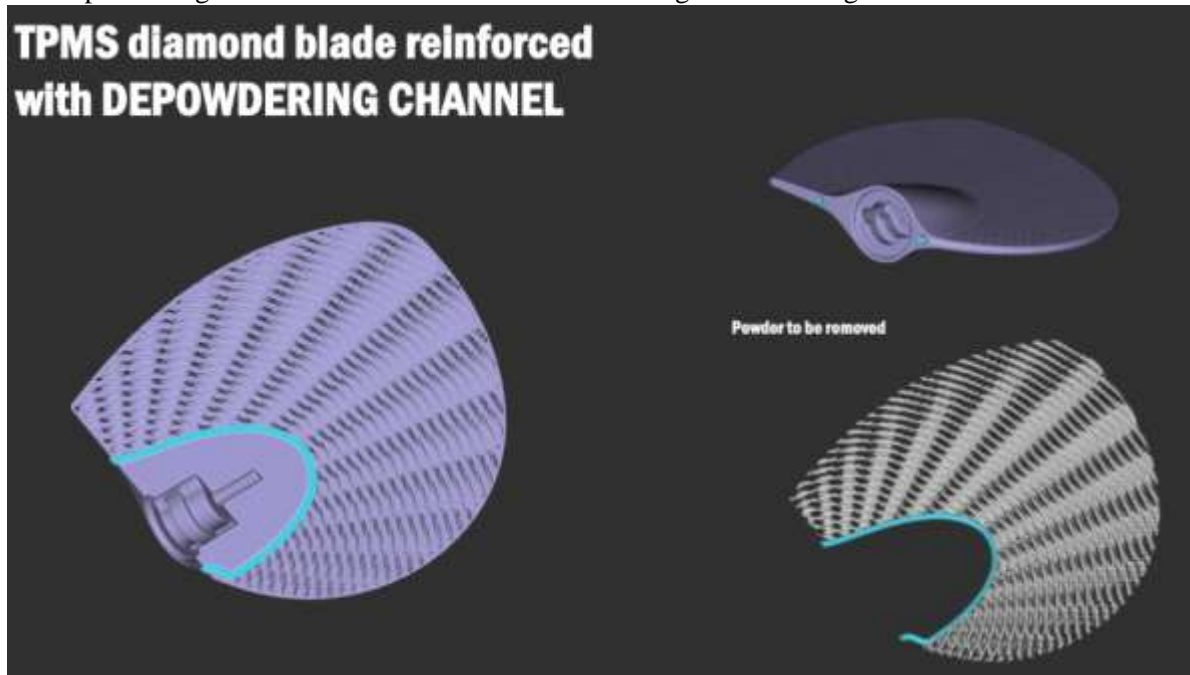


Figure 6-6 TPMS lattice structured blade with depowdering channel and reinforced around.

After this design using the pressure data from the CFD analysis static analysis was performed with tetrahedral mesh elements with 1 mm edge length and quadratic geometric order (Shape functions). Results are shown in figure 6-7.

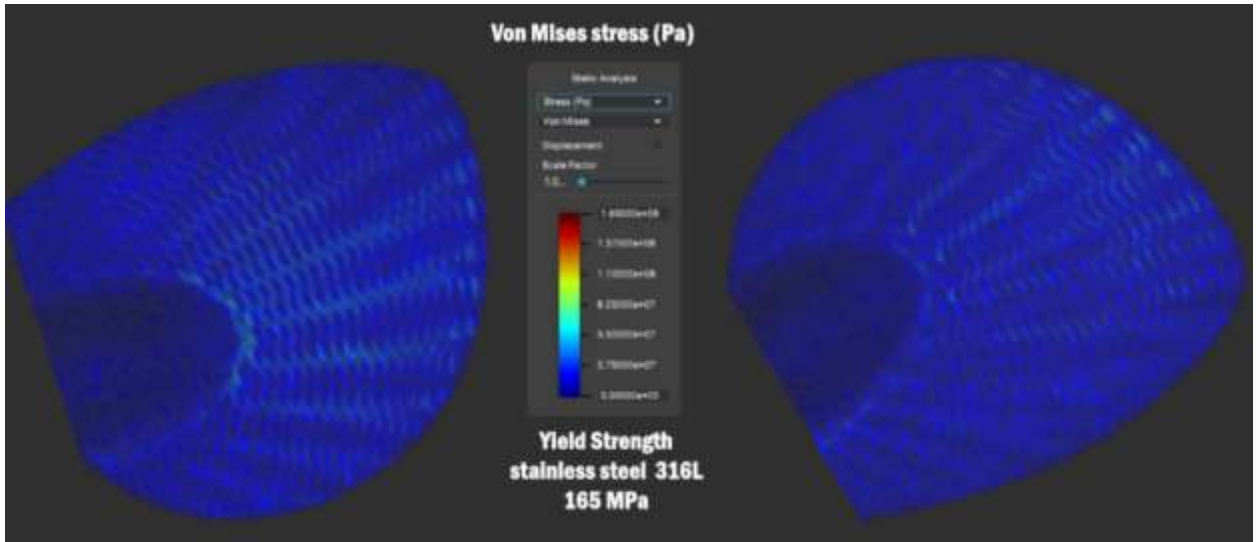


Figure 6-7 static analysis for TPMS reinforced with depowdering channel.

So due to addition of reinforcement stress are at the limit, here from analysis maximum stress value is 165 MPa which is equal to certified one for 316L stainless steel which is less for 17-4PH steel. Maximum stresses are observed at the geometrical discontinuities. In this study 17-4PH is used so it can be negligible.

Final weight achieved from this design was 1.03Kg. Weight of the increased due to addition of reinforcement compared to previous design.

6.2 AM the Blade:

As mentioned earlier in chapter 3 about Desktop Metal's Bound Metal Deposition™ Studio System+™ and its workflow and technology are explained. Here two versions of blade models are printed for optimizing the printing parameters for first version second design was printed while working on the final optimized design.

From Desktop Fabricate™ software it is required to select parameters from the software to perform the printing which called as selecting printing profile. For selecting a printing profile Desktop metal provided a clear standards:

Depending on the requirement it is possible to choose from a list of pre-configured print profiles. Each profile defines a default shell thickness, infill spacing, and layer height. These factors have an impact on the resulting part density, fabrication time, and surface quality. Before selecting a profile, the final part density planning to achieve should be considered. At present there are four categories those are shown in table 6-1.

	Wall thickness**	Infill spacing***	Layer height	Shell density****
Standard (400µm nozzle)	1.44 mm	2.8 mm	150µm	~96%
Coarse (400µm nozzle)	1.44 mm	2.8 mm	220µm	~95%
Dense mode (400µm nozzle)	1.92 mm	2.62 mm	150µm	~98%
Ultra-fine (250µm nozzle)*	0.9 mm	1.75 mm	50µm	~97%

Table 6-1 Print profiles & settings [58].

* The ultra-fine profile is only compatible with the high-resolution (250µm) nozzle.

** Width of material making up the walls in the shell of the part.

*** The default spacing between each line of infill. Note: by default, infill represents about 45% of the part's overall density.

**** Approximate as-sintered density of the shell of the part (which does not contain infill). The density values depend on the material. The density values shown here reflect approximate data for 17-4 PH stainless steel.

In general, profiles are selected based on the desired density of the sintered part, but these profiles also impact the print speed and the resulting surface quality this shown in following table 6-2.

	Shell density	Print speed	Surface quality
Standard (400µm nozzle)	~96%	Fast	Better
Coarse (400µm nozzle)	~95%	Fastest	Good
Dense mode (400µm nozzle)	~98%	Average	Average
Ultra-fine¹ (250µm nozzle)	~97%	Slow	Best

Table 6-2 Impact on print speed & surface quality [58].

Guidelines for selecting the right print profile:

Parts printed in standard profile will take a bit longer time to fabricate than those printed using the coarse profile, but they will have a better surface quality due to the smaller layer height. Standard profile is for a good balance between fabrication time and surface quality. Coarse profile is for a faster print speed of large parts.

Parts printed in dense mode will have a higher as-sintered density and default shell thickness but take longer time to print and lower surface quality than standard or coarse profiles. Dense mode is for very small parts (smaller than 8.6 mm) and testing purposes [58].

The ultra-fine profile pairs with the high-resolution (250 µm) print head to print small parts with intricate design features. The shell thickness and relative amount of infill present is the same as the standard and coarse profiles, but the smaller nozzle size produces infill lines that are thinner and printed closer together. This increases print stability while a smaller layer height (50 µm) reduces the porosity throughout the part, it is for small parts with fine features. Part size should be less than 25mm x 25mm x 25mm for best results [58].

6.2.1 Version1:

After getting the optimized design, the design was converted to STL file and it was transferred to Desktop Fabricate™ software for the final steps. After importing the STL file it is oriented like a flat position as shown in figure 6-8 but blade tip is inclined to platform little bit. Later supports were provided automatically by the software. 316L stainless steel material was chosen for printing. Coarse printing profile was chosen due to large size compared to platform and for better printing speed and later our software filled required parameters automatically as mentioned in table 6-1. Layer height is pre-determined which is 0.22 mm and software sliced the part in to 232 layers.

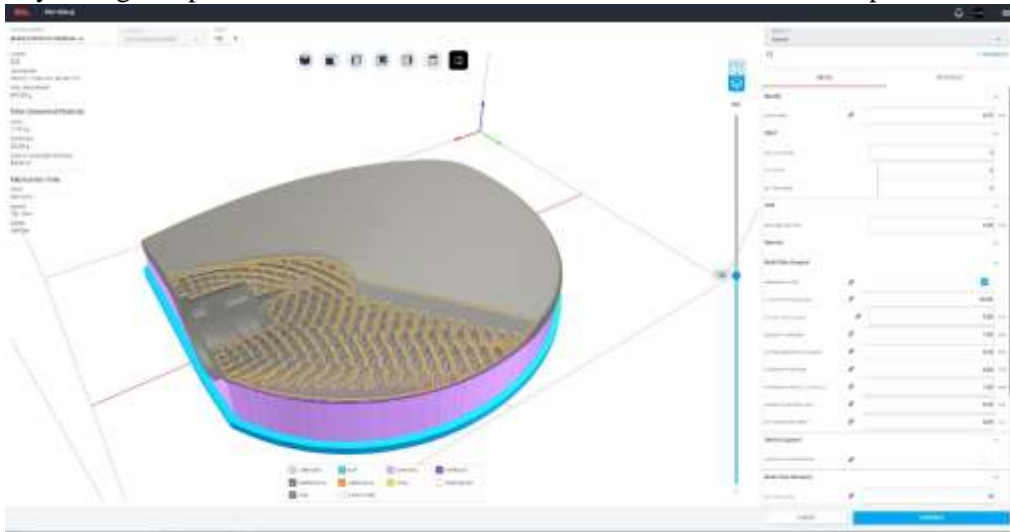


Figure 6-8 Toolpath preview of blade courtesy by Add Italia.

After finishing the setup fabricate software a window with final parameters and printing time estimation which is shown figure 6-9. Estimated printing time is 56h 51m. Estimated debinding time is 13h 59m. Estimated sintering time is 44h 3m.



Figure 6-9 Final estimated parameters courtesy by Add Italia.

Later this sliced part file is uploaded to the printing machine then printing machine starts printing of the part. Real printing time was 78h36m this change may be due to software not considering the load time of feedstock metal rods into the printhead.



Figure 6-10 Left side shows blade while printing and Right side shows final printed part called as green part courtesy by Add Italia.

After printing the part (green part) later it was loaded into to debinding machine for removing the binder, after this process part is called as brown part. Brown part is uploaded to sintering machine for final sintering process to remove the remaining binder and for densification.

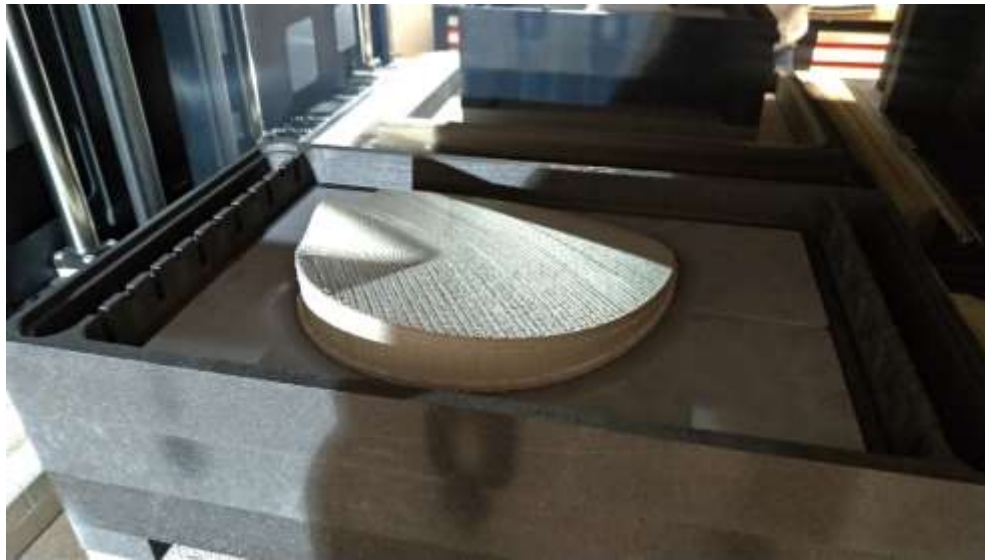


Figure 6-11 part after sintering process courtesy by Add Italia.

After sintering process, the ceramic interface will become powder so blade and supports can be separated easily. Final part and supports are shown in following figures.



Figure 6-12 separated supporting structures of blade courtesy by Add Italia.



Figure 6-13 Final blade part courtesy by Add Italia.

After the completion of printing process and post processing, the part is observed, some cracks are observed at the side of connection between blade and supports which can be seen from the figure 6-14. It was assumed that due to imbalance of center of mass of the blade cracks are arise. So, this is taken into consideration for next version printing.



Figure 6-14 Cracks on the blade courtesy by Add Italia.

6.2.2 Version2:

After getting the final optimized design, three holes are added to it which are essential for performing tests on the blade then the design was converted to STL file and it was transferred to Desktop Fabricate™ software for the final steps. After importing the STL file and by consider results from previous printing it is oriented in inclined position as shown in figure 6-15 which was like center of mass and more mass is near to the printing platform. Conical supports were provided to the blade which reduces the mass of the supports compared to normal supports and with providing inclination for the blade, these supports are under experimental stage, Conical support details are provided by the Desktop Metal [59]. 17-4PH stainless steel material was chosen for printing. Coarse printing profile was chosen due to large size compared to platform and for better printing speed and later our software filled required parameters automatically as mentioned in table 6-1. Layer height is pre-determined which is 0.22 mm and software sliced the part in to 240 layers.

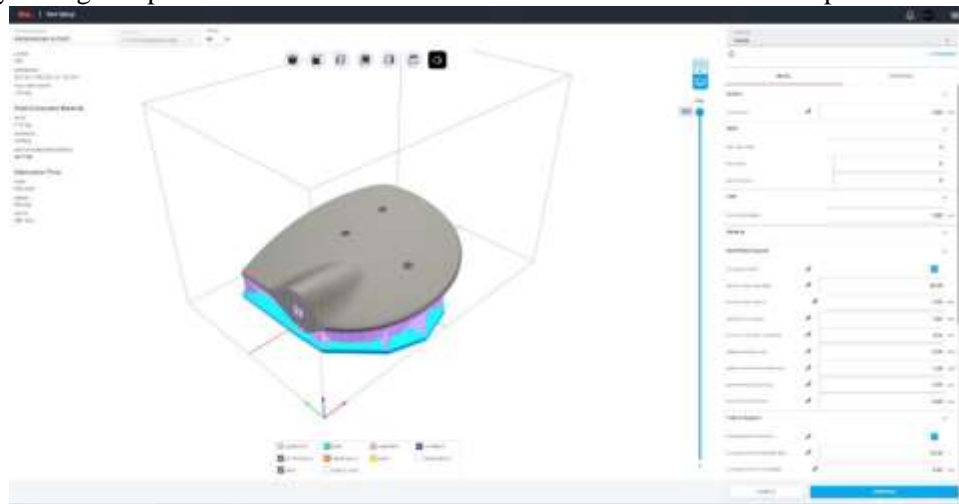


Figure 6-15 Blade with supports and parameters courtesy by Add Italia.

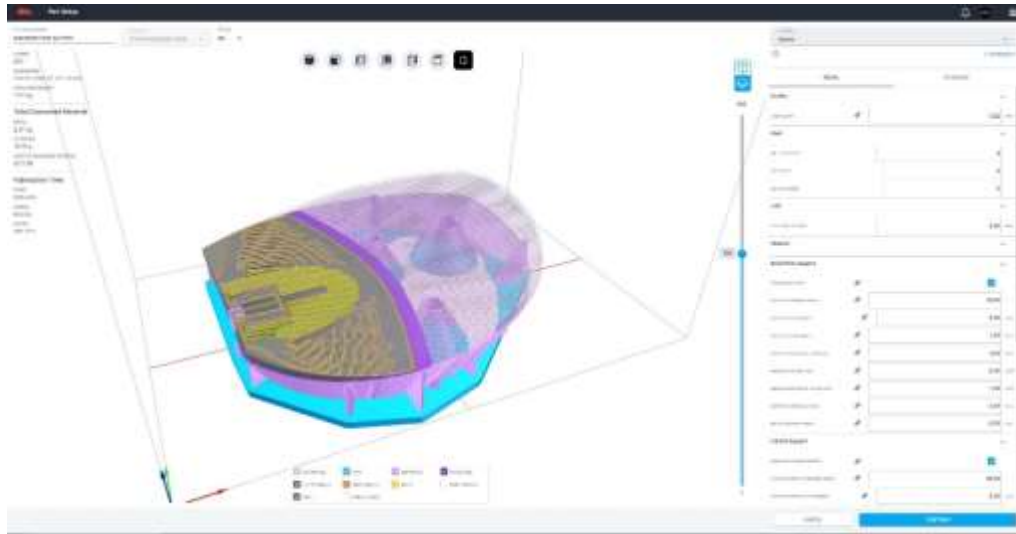


Figure 6-16 Tool Path preview courtesy by Add Italia.

After finishing the setup fabricate software a window with final parameters and printing time estimation which is shown figure 6-17. Estimated printing time is 69h 42m. Estimated debinding time is 61h. Estimated sintering time is 48h 12m.

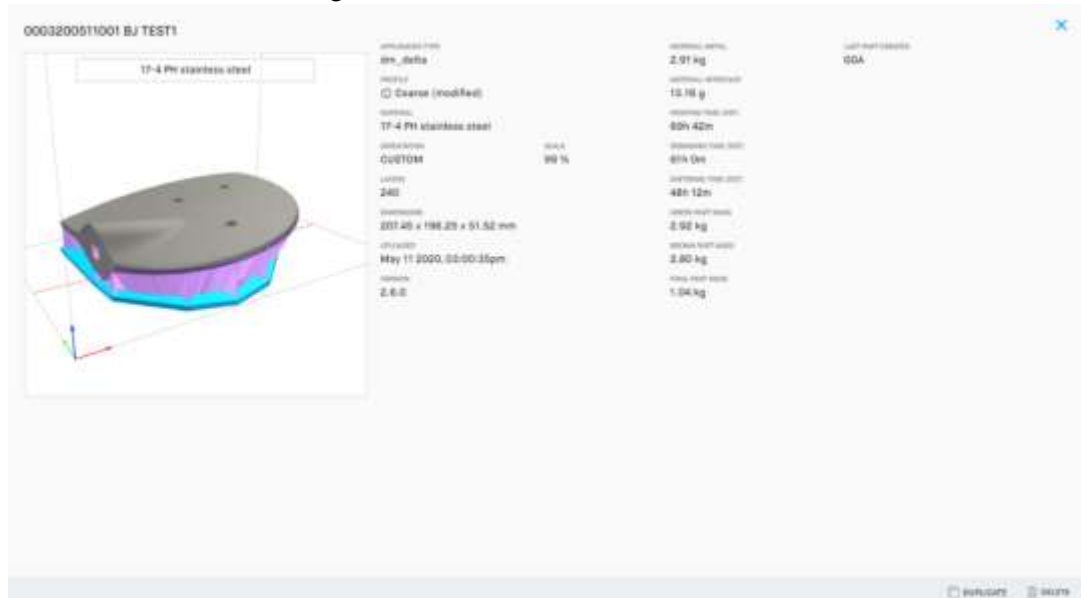


Figure 6-17 Final estimated parameters courtesy by Add Italia.

Later this sliced part file is uploaded to the printing machine then printing machine starts printing of the part. Real printing time was 92h46m this change may be due to software not considering the load time of feedstock metal rods into the printhead.



Figure 6-18 Printed part courtesy by Add Italia.

After printing the part (green part) later it was loaded into to debinding machine for removing the binder, after this process part is called as brown part. Brown part is uploaded to sintering machine for final sintering process to remove the remaining binder and for densification.



Figure 6-19 Part after sintering process with supports courtesy by Add Italia.

After sintering process, the ceramic interface will become powder so blade and supports can be separated easily. Final part and supports are shown in following figures.



Figure 6-20 Final part after removing the supports courtesy by Add Italia.

After the completion of printing process and post processing, the part was observed, some cracks are observed at the side of blade where connection between its surface and supports which can be seen from the figure 6-21. Even cracks can be seen in the supports also.



Figure 6-21 Cracks occurred on the final part courtesy by Add Italia.



Figure 6-22 Cracks on support structures courtesy by Add Italia.

Selection of conical supports may be the cause of cracks in the blade. But these supports are the only way to tilt the blade and reducing the mass of the supporting structures simultaneously.

Conclusion:

The main aim of the thesis work is to utilize the additive manufacturing for the production of Sail boat propeller blade while simultaneously utilizing advantages provided by additive manufacturing like optimizing the mass of blade without compromising its structural properties as it can manufacture complex parts. The method which is used for blade printing is Bound Metal Deposition™ (BMD) by using machine Studio system by Desktop Metal™, in future it is planned for printing blade by using Shop system and Production system by Desktop Metal™ which are binder jetting machines.

The propeller blade design was provided by EWOL Srl, which is a part of a 17-inch Sailboat propeller. For performing optimization loads acting on the blade should be identified for understanding the stresses acting on the blade. So, the loads acting on the blade were identified by using Ansys Fluent at 20deg orientation and 1300 rpm with different inlet velocity conditions. As well as at other inlet, propeller speed, and 18 deg orientation conditions loads also identified. Flow condition taken was laminar for flow for all the above conditions as per EWOL Srl instructions and to have better understanding. Loads are verified by using data from EWOL Srl and boats they are planning to install the propeller. The loads obtained are pressure acting on the blade this data is extracted in to excel format as pressure vs pressure acting coordinate points on the blade. Then static analysis was performed on the original blade design to understand the stresses produced by the obtained pressure data (highest thrust produced pressure data was used). This analysis was performed using nTopology software as it was used for optimization process also. The performed analysis shown good results for both materials (316L stainless steel and 17-4PH stainless steel). These materials are intended to use for printing the blade. Then the optimization was performed to reduces the mass in way by creating lattice structure inside the blade. Directly by using loads it is not possible to perform the optimization, so by merging lattice structure and shell of the blade the optimization was performed, and later stress analysis was performed to check whether stresses are under the limit. Optimization also done by considering the future production methods so for removing powder the flow channels are provided for the blade. The final mass is 1.014 Kg obtained from the optimization which is 300gms less compared to original blade. Then this blade design was printed in two different versions to obtain better printing parameters. Initially the blade printed in normal orientation with normal supports later debinding and sintering was performed but cracks are obtained on the at the side of connection between blade and supports which can be seen from the figure 6-14. It was assumed that due to imbalance of center of mass of the blade cracks are arise. So, this is taken into consideration for next version printing then blade is inclined towards platform at the higher mass section (center of mass) by using Conical supports which also helpful in reducing the mass of the supports simultaneously, these supports are in experimental stage. After the completion of printing process and post processing, the part was observed, some cracks are observed at the side of blade where connection between its surface and supports which can be seen from the figure 6-21. Even cracks can be seen in the supports also. Selection of conical supports may be the cause of cracks in the blade. But these supports are the only way to tilt the blade and reducing the mass of the supporting structures simultaneously.

Recommendations for future work on this topic is to perform the investigation for the cause of cracks occurred on the blade. Next performing the numerical study on fatigue, turbulence effects on the blade. Performing the Thrust, static, fatigue experimental analysis on the blade.

As it can be seen that additive manufacturing is efficient way of using materials compared to traditional manufacturing. So, this thesis study shows that the manufacturing of blade by AM is

possible while simultaneously reducing the mass of the blade without compromising structural properties.

References

- Anish, "Propeller, Types of Propellers and Construction of Propellers," 2020. [Online]. Available: <https://www.marineinsight.com/naval-architecture/propeller-types-of-propellers-and-construction-of-propellers/>.
- [2] wiki, "Propeller," [Online]. Available: <https://en.wikipedia.org/wiki/Propeller>.
- [3] J. Carlton, "The early development of the screw propeller," in *Marine Propellers and Propulsion*, Elsevier Ltd, pp. 1-9.
- [4] S. K. Stein, "The Sea in World History: Exploration, Travel, and Trade," in *The Sea in World History: Exploration, Travel, and Trade*, p. 600.
- [5] wiki, "Rim-driven thruster," wikipedia, [Online]. Available: https://en.wikipedia.org/wiki/Rim-driven_thruster.
- [6] "wartsilla," wartsilla, [Online]. Available: <https://www.wartsila.com/encyclopedia/term/propeller-screw-propeller>.
- [7] S. Khasnabis, "Different Ways To Reduce Ship Propeller Vibrations And Increase Its Efficiency," marineinsight, [Online]. Available: <https://www.marineinsight.com/naval-architecture/different-ways-to-reduce-ship-propeller-vibrations-and-increase-its-efficiency/>.
- [8] S. Ghosh, "Understanding Design Of Ship Propeller," marineinsights, [Online]. Available: <https://www.marineinsight.com/naval-architecture/design-of-ship-propeller/>.
- [9] M. Paez, "FACTORS IN PROPELLER SELECTION," Rice Propulsion, [Online]. Available: <http://ricefoundries.com/assets/frontend/cartas/TNL52/TNL52.htm>.
- [10] "A Review On Materials Used For Marine Propellers," *materials today:proceedings*, vol. 18, no. 7, pp. 4482-4490, 2019.
- [11] K. S. Yonas Mitiku Degu, "Marine Propeller Manufacturing – A New Approach," *American Journal of Engineering Research*, vol. 3, no. 5, pp. 207-211 , 2014.
- [12] O.Diegel, "Advances in Additive Manufacturing and Tooling," in *Comprehensive Materials Processing*, 2014.
- [13] O. Munz, "Photo-Glyph Recording". Us Patent 2,775,758., 1956.
- [14] W. Swainson, "Method, Medium and Apparatus for Producing Three-Dimensional Figure Product". US Patent 4,041,476., 1977.
- [15] L. Richard, "Schwerel, R.E., et al Three Dimensional Photochemical Machining with Lasers," in *Applications of lasers to Industrial Chemistry*, 1984, pp. 90-97.

- [16] F. L. L. Piscitello, " Additive Manufacturing : Determinats of Adoption and Effects on Global Value Chains Participation . a Country-Level Analysis," 2017.
- [17] R. Housholder, "Molding Process". US Patent 4,247,508., 1981.
- [18] H. Kodama, "Automatic method for fabricating a three-dimensional plastic model with photo-hardening polymer," *Review of Scientific Instruments*, vol. 52, no. 11, pp. 1770-1773, 1981.
- [19] A. Herbert, "Solid Object Generation," *Applied Photographic Engineering*, pp. 185-188, August 1982.
- [20] Wiki, "RepRap project," Wikipedia, [Online]. Available: https://en.wikipedia.org/wiki/RepRap_project.
- [21] B. P. ., J. M. P. André O Laplume, "Global value chains from a 3D printing perspective," *International Business Studies* , vol. 47, pp. 595-609, 2016.
- [22] "3D PRINTING AND THE FUTURE OF SUPPLY CHAINS," November 2016. [Online]. Available: https://www.dhl.com/content/dam/downloads/g0/about_us/logistics_insights/dhl_trendreport_3d_printing.pdf.
- [23] S. L. T. Carlo Francesco, "SUSTAINABILITY EVALUATION VIA LIFE CYCLE ASSESSMENT OF A METAL COMPONENT FOR NAUTICAL APPLICATIONS PRODUCED BY ADDITVE MANUFACTURING," 2018/2019.
- [24] 3dprinting.com. [Online]. Available: <https://3dprinting.com/>.
- [25] BSI, "Additive manufacturing - General principles - Part 2: Overview of process categories and feedstock (ISO 17296-2:2015)," *BSI Standards Publication*, 2015.
- [26] "CustomPart.Net," [Online]. Available: <https://www.custompartnet.com/>.
- [27] J. F. D. G. F.P.W. Melchels, "A review on stereolithography and its applications in biomedical engineering," 2010.
- [28] WIKI, "CLIP," [Online]. Available: https://en.wikipedia.org/wiki/Continuous_Liquid_Interface_Production.
- [29] "3Dhubs," [Online]. Available: <https://www.3dhubs.com/guides/3d-printing/#technologies>.
- [30] S. C. ., S. S. ., K. S. ., C. H. Joamin Gonzalez-Gutierrez, "Additive Manufacturing of Metallic and Ceramic Components by the Material Extrusion of Highly-Filled Polymers: A Review and Future Perspective," *mdpi,materials*, 18 May 2018.
- [31] S. S. CRUMP, "APPARATUS AND METHOD FOR CREATING THREE-DIMENSIONAL OBJECT". USA Patent 5121329 , 09 06 1992.

- [32] "researchgate," [Online]. Available: https://www.researchgate.net/figure/Laser-engineered-net-shaping-LENS-process-47_fig3_327701079.
- [33] "Whiteclouds," [Online]. Available: <https://www.whiteclouds.com/3DPedia/ebf3.html>.
- [34] "ALL3DP," [Online]. Available: <https://all3dp.com/2/electron-beam-melting-ebm-3d-printing-simply-explained/>.
- [35] "iom3," [Online]. Available: <https://iom3.tandfonline.com/doi/full/10.1080/09506608.2015.1116649?src=recsys#>.
- [36] Desktopmetal, "Deep Dive: Bound," Desktopmetal, 2020. [Online]. Available: <https://www.desktopmetal.com/resources/deep-dive-bmd>.
- [37] Desktopmetal, "Studio System™," Desktopmetal, 2020. [Online]. Available: <https://www.desktopmetal.com/products/studio>.
- [38] trimech, trimech, 2020. [Online]. Available: https://blog.trimech.com/hs-hubfs/hubfs/TriMech%20Blog/Hardware/2019/04%20April%202019/Printing%20Metal%20Heatsinks%20with%20Desktop%20Metal/Heatsink_in_Desktop_Metal_Debinder.jpg?width=600&name=Heatsink_in_Desktop_Metal_Debinder.jpg.
- [39] Solidsmack, [Online]. Available: <https://www.solidsmack.com/wp-content/uploads/2017/04/desktop-metal-3d-printing-03.jpg>.
- [40] Desktopmetal, "BMD design guide Studio System," 2020, pp. 1-14.
- [41] T. Chung, "Introduction," in *Computational fluid dynamics*, Cambridge University Press, pp. 3-4.
- [42] W. M. H K Versteeg, *An Introduction to Computational Fluid Dynamics Finite Volume Method*, Pearson .
- [43] AndréBakker, "bakker," [Online]. Available: <http://www.bakker.org/dartmouth06/engs150/03-cnsrv.pdf>.
- [44] J. Blazek, *COMPUTATIONAL FLUID DYNAMICS: PRINCIPLES AND APPLICATIONS*, ELSEVIER.
- [45] ANSYS, "Mesh Quality," ANSYS, 2020. [Online]. Available: <https://www.afs.enea.it/project/neptunius/docs/fluent/html/ug/node167.htm>.
- [46] "CFD support," CFD support, 2020. [Online]. Available: <https://www.cfdsupport.com/OpenFOAM-Training-by-CFD-Support/node129.html>.
- [47] J. Guerrero, "Introduction to Computational Fluid dynamics:Governing Equation," Researchgate, 2020. [Online]. Available: https://www.researchgate.net/figure/A-Vector-d-and-S-on-an-orthogonal-mesh-B-Vector-d-and-S-on-a-non-orthogonal-mesh_fig3_280385280.

- [48] L. S. Z. Jan Kulczyk, "Analysis of screw propeller 4119 using the Fluent system," *Archives of Civil and Mechanical Engineering*, vol. 7, no. 4, pp. 129-137, 2007.
- [49] C. university, "A Hands-on Introduction to Engineering Simulations," edx, 2020. [Online]. Available: <https://courses.edx.org/>.
- [50] "bavaria-cruiser-56," [sailboatdata.com](https://sailboatdata.com/sailboat/bavaria-cruiser-56), [Online]. Available: <https://sailboatdata.com/sailboat/bavaria-cruiser-56>.
- [51] "sun-odyssey-34-jeanneau," [sailboatdata.com](https://sailboatdata.com/sailboat/sun-odyssey-34-jeanneau), [Online]. Available: <https://sailboatdata.com/sailboat/sun-odyssey-34-jeanneau>.
- [52] "oceanis-34-beneteau," [sailboatdata.com](https://sailboatdata.com/sailboat/oceanis-34-beneteau), [Online]. Available: <https://sailboatdata.com/sailboat/oceanis-34-beneteau>.
- [53] A. Mouritz, "Strengthening of metal alloys," in *Introduction to Aerospace Materials*, WoodHead Publishing, 2012, pp. 57-90.
- [54] B. LuizCarneiro, "Cyclic deformation and fatigue behavior of additively manufactured 17-4 PH stainless steel," *International Journal of Fatigue*, vol. 123, pp. 22-30, 2019.
- [55] Desktopmetal, 17-4 PH stainless steel, 2020.
- [56] Desktopmetal, "desktopmetal," 2020. [Online]. Available: https://www.desktopmetal.com/uploads/DM-0011-00-Studio_MDS_316L-v1.0.pdf.
- [57] L. S. A. P. W. T. W. A. H. I. Maskery, "Insights into the mechanical properties of several triply periodicminimal surface lattice structures made by polymer additivemanufacturing," *Polymer*, vol. 152, pp. 62-71, 2018.
- [58] Desktopmetal, Selecting a print profile, Desktopmetal.
- [59] Desktopmetal, Conical support.
- [60] [Online].